JOURNAL OF GEOPHYSICAL RESEARCH, VOL. 108, NO. E12, 5129, doi:10.1029/2002JE002015, 2003

Aeolian processes in Proctor Crater on Mars: Sedimentary history as analyzed from multiple data sets

Lori K. Fenton and Joshua L. Bandfield
Department of Geological Sciences, Arizona State University, Tempe, Arizona, USA

A. Wesley Ward
U.S. Geological Survey, Flagstaff, Arizona, USA

Received 21 November 2002; revised 9 June 2003; accepted 16 July 2003; published 4 December 2003.

[1] Proctor Crater is a 150 km diameter crater in Noachis Terra, within the southern highlands of Mars. The analysis leading to the sedimentary history incorporates several data sets including imagery, elevation, composition, and thermal inertia, mostly from the Mars Global Surveyor mission. The resulting stratigraphy reveals that the sedimentary history of Proctor Crater has involved a complex interaction of accumulating and eroding sedimentation. Aeolian features spanning much of the history of the crater interior dominate its surface, including large erosional pits, stratified beds of aeolian sediment, sand dunes, erosional and depositional streaks, dust devil tracks, and small bright bed forms that are probably granule ripples. Long ago, up to 450 m of layered sediment filled the crater basin, now exposed in eroded pits on the crater floor. These sediments are probably part of an ancient deposit of aeolian volcaniclastic material. Since then, some quantity of this material has been eroded from the top layers of the strata. Small, bright dune forms lie stratigraphically beneath the large dark dune field. Relative to the large dark dunes, the bright bed forms are immobile, although in places, their orientations are clearly influenced by the presence of the larger dunes. Their prevalence in the crater and their lack of compositional and thermal distinctiveness relative to the crater floor suggests that these features were produced locally from the eroding basin fill. Dust devil tracks form during the spring and summer, following a west-southwesterly wind. Early in the spring the dust devils are largely restricted to dark patches of sand. As the summer approaches, dust devil tracks become more plentiful and spread to the rest of the crater floor, indicating that the entire region acquires an annual deposit of dust that is revealed by seasonal dust devils. The dark dunes contain few dust devil tracks, suggesting that accumulated dust is swept away directly by saltation, rather than by the passage of dust devils. Spectral deconvolution indicates that the dark dunes have infrared spectra consistent with basalt-like materials. The average thermal inertia calculated from Thermal Emission Spectrometer bolometric temperatures is 277 ± 17 J m^{-2} s$^{-0.5}$ K^{-1}, leading to an effective grain size of 740 ± 170 μm, which is consistent with coarse sand and within the range expected for Martian sand. The coarse sand that composes the large dune field may have originated from outside the crater, saltating in from the southwest. Most of the transport pathway that delivered this sand to the dune field has since been eroded away or buried. The sand was transported to the east center of the crater floor, where beneath the present-day dunes a 50 m high mound of sand has accumulated. Dune slip faces indicate a wind regime consisting of three opposing winds. Some of these wind directions are correlated with the orientations of dust devil tracks and bright bed forms. The combination of a tall mound of sand and three opposing winds is consistent with a convergent wind regime, which produces the large reversing transverse and star dunes that dominate the dune field. The dark dunes have both active slip faces and seemingly inactive slip faces, suggesting that the dunes vary spatially in their relative activity. Nevertheless, the aeolian activity that has dominated the history of Proctor Crater still continues today. *INDEX TERMS:* 5415 Planetology: Solid Surface Planets: Erosion and weathering; 5470 Planetology: Solid Surface Planets: Surface materials and properties; 5410 Planetology: Solid Surface Planets:

0148-0227/03/2002JE002015$09.00

Composition; 5464 Planetology: Solid Surface Planets: Remote sensing; 1625 Global Change: Geomorphology and weathering (1824, 1886); *KEYWORDS:* Mars, aeolian processes, dunes and ripples, surface composition, thermal inertia, geomorphology

Citation: Fenton, L. K., J. L. Bandfield, and A. W. Ward, Aeolian processes in Proctor Crater on Mars: Sedimentary history as analyzed from multiple data sets, *J. Geophys. Res.*, *108*(E12), 5129, doi:10.1029/2002JE002015, 2003.

1. Introduction

[2] Mars has long been known as a place dominated by aeolian processes [e.g., *de Vaucouleurs*, 1954]. Evidence for the action of wind on the surface ranges from the local-scale features observed at each lander site to the massive dust storms that can obscure surface features over much of the globe. Therefore the study of material transport and landscape evolution on Mars is not complete until aeolian processes are fully understood. Of the many different types of aeolian features, dunes are unique in that their morphology provides information on the complexity of the wind regime in which they reside and the direction of net transport of a specific range of particle sizes. Thus the study of Martian sand dunes can broaden the understanding of the near-surface wind circulation patterns and the erosion, deposition, and transport of sand on the surface. In addition, knowledge of the terrain in the vicinity of a dune field is necessary to understand how dunes relate and react to their environment. This work incorporates three data sets from the Mars Global Surveyor mission to study the aeolian processes in Proctor Crater, one of several craters in Noachis Terra containing a large dark dune field.

2. Setting

2.1. Background

2.1.1. Dark Dunes

[3] The first dunes identified on Mars were found in Mariner 9 images of Proctor Crater [*McCauley et al.*, 1972; *Sagan et al.*, 1972]. Further work following this discovery quickly established the important role of aeolian processes in the modification of the Martian surface [*Smith*, 1972; *Cutts and Smith*, 1973; *Arvidson*, 1974]. Since then, the dune fields of Noachis Terra (formerly known as the Hellespontus dune fields), and especially the dunes of Proctor Crater, have become the type location for the study of dark dunes on Mars. *McCauley et al.* [1972] and *Cutts and Smith* [1973] took a close look at the Proctor dunes, noting the NNW striking ridges with a spacing of 1–2 km in the center of the dune field. *Cutts and Smith* [1973] concluded that the dunes are located in an area where the effective sand-saltating winds are balanced, with possible dominant winds from the southwest. *Breed* [1977] compared the spacing and widths of the Proctor dunes to terrestrial crescentic dunes, finding that the Martian dunes are dimensionally similar to dunes in several terrestrial dune fields. *Thomas* [1984] found that the color variations of Proctor Crater dunes, streaks, and plains are similar to but simpler than crater splotches with associated streaks in other areas on Mars. *Lancaster and Greeley* [1987] took a close look at the Noachis Terra dune fields and discovered pyramid-shaped dunes and multiple slip faces, indicative of dunes produced by a multidirectional wind regime. However, since their discovery, the dunes of Proctor Crater have generally been classified as large transverse and barchan dunes.

[4] Thermal studies have also focused on the dune fields of Noachis Terra [*Christensen*, 1983; *Edgett and Christensen*, 1991; *Edgett and Christensen*, 1994; *Herkenhoff and Vasavada*, 1999]. Because dune fields consist of a large quantity of well-sorted unconsolidated particulate material, thermal inertia measurements over such areas provide an ideal condition in which to calculate effective mean grain sizes. Furthermore, such a well-constrained situation is useful for calibrating new thermal inertia techniques. The dunes of Proctor Crater have been targeted several times, producing a thermal inertia consistent with sand.

[5] The provenance of dune sand in the Noachis area of Mars is largely unresolved. *Christensen* [1983] proposed that the intracrater dune fields on Mars were formed by entrapment of dark material in the topographic lows of craters. *Breed et al.* [1979] extended this analysis further by exploring the reasons why crescentic dunes appear to be so much more abundant than linear dunes on Mars. They considered that linear (longitudinal) dunes represent areas of active sand transport, whereas crescentic dunes represent areas of low or no current sand transport. They concluded that most crescentic dunes, like the ones in Proctor Crater, represent the final accumulation site of sand, and that any linear dunes that might have transported large quantities of sand have since been eroded away. They also propose that many Martian dunes are similar to terrestrial dunes located in closed basins, and that they may have taken millions of years or more to accumulate, like their terrestrial counterparts. While also considering the sand sources discussed above, *Thomas* [1984] suggests that intracrater dunes may have been formed from the aeolian reworking of eroded crater floor deposits, evidenced by the many large pits visible in craters with dunes and the lack of obvious transport pathways outside the craters. Earlier, *Thomas* [1982] proposed that the intracrater dune sand may have been supplied from eroding layered deposits near the south pole. Clearly a more detailed study of sand deposits is necessary to determine the origin of the intracrater dune materials.

2.1.2. Bright Dune Forms

[6] MOC narrow-angle images have revealed the presence of small, generally bright aeolian features in many areas on the Martian surface [*Malin and Edgett*, 2001]. Morphologically, these features are similar to terrestrial granule ripples, and thus they have generally been given the title ''granule ripples'' or ''ripple-like bed forms'' [*Malin and Edgett*, 2001; *Zimbleman and Wilson*, 2002; *Williams et al.*, 2002]. The difficulty with the presence of granule ripples on Mars is the well-known correlation of ripple wavelength with the size of the grains that comprise them [*Sharp*, 1963; *Greeley and Iversen*, 1985]. For example, *Sharp* [1963] found granule ripples in the Coachella

Valley, California, with wavelengths up to 3 m and surface grain sizes in the range of 2–5 mm with a few grains ranging up to 10 mm in size. He found that the granules moved through momentum transfer by the repeated impact of smaller sand-sized grains. As a result, the largest granule ripples exist where winds are strong enough that repeated impacts from sand grains can move such large granules. The bright dune forms on Mars are an order of magnitude larger than the granule ripples of the Coachella Valley. Present day winds on Mars that are strong enough to saltate sand-sized grains, much less provide enough momentum to move the cobbles that would comprise granule ripples the size observed on Mars, are rarely if ever measured by lander experiments [*Hess et al.*, 1977; *Schofield et al.*, 1997] or predicted by atmospheric model simulations [*Greeley et al.*, 1993; *Fenton and Richardson*, 2001].

[7] There is no evidence that the bright dune forms are in fact granule ripples. Instead, they may be small, bright dunes. However, if the bright dune forms are indeed formed by the movement of granules or even larger grains, then their existence must be explained given the current wind regime. It may be that they were formed in an ancient wind regime in which winds were stronger than they are today. If this is the case then the bright dune forms are indeed old, because model simulations of the past few million years show that winds do not dramatically increase in intensity simply by varying Mars's eccentricity, obliquity, or passage of perihelion [*Fenton and Richardson*, 2001]. In order to understand how these features formed it is important to take a close look at their morphology, stratigraphic relation to other features, and state of degradation.

2.1.3. Composition

[8] Dunes tend to have a composition distinct from that of their surroundings; thus, composition is a useful tool in studying sand dunes and locating sand sheets and sand sources. On the Earth, thermal infrared multispectral scanner (TIMS) and Landsat thematic mapper multispectral images have been used for at least three purposes: to identify changes in composition within dune fields [*Blount et al.*, 1990], to discover previously unrecognized or misidentified sand sources [*Ramsey et al.*, 1999], and to provide a more accurate estimate of mineral concentrations at the surface [*Bandfield et al.*, 2002].

[9] On Mars, spectra obtained from both ground-based and spacecraft interferometers have been used to identify surface mineralogy. In particular, TES has provided high-resolution spectra in the thermal infrared at a surface resolution of $3 \times \sim 6$ km, which has been used to determine the correlation of rock compositions with geological units on the surface. The most detailed work with TES data involves the deconvolution of spectra using several end-members, including both surface and atmospheric components [*Bandfield et al.*, 2000; *Smith et al.*, 2000]. In their work on global surface compositions, *Bandfield et al.* [2000] identified two spectral signatures that comprise a large percentage of the Martian surface. The first component, labeled type 1, has a shape similar to that of terrestrial Deccan Traps flood basalts that are composed predominantly of plagioclase and clinopyroxene. This is the same end-member identified in initial aerobraking TES data from Cimmeria Terra by *Christensen et al.* [2000a]. The second component identified by *Bandfield et al.* [2000], labeled type 2, matches spectra from basaltic andesites to andesites made of plagioclase, glass, and pyroxene. In general, the low albedo surfaces of Mars are composed of spectral types 1 or 2, or some mixture of the two. Areas with a mixed spectral signature may indicate either a composition intermediate between basalt and andesite or a physical mixture of the basaltic and andesitic components [*Bandfield et al.*, 2000].

[10] A reassessment of the deconvolution of TES spectra indicates that the type 2 surface component may be indicative of weathered basalt rather than andesite [*Wyatt and McSween*, 2002]. *Wyatt and McSween* [2002] reasoned that because sheet silicates such as clays have spectra similar to high-silica glass, surface type 2 may not be andesitic, but instead may be aqueously altered basalt. They performed a deconvolution of TES spectra using a library of minerals that omitted the high-silica glass found by *Bandfield et al.* [2000] to compose part of surface type 2. Their deconvolutions provided reasonable fits to the spectra, indicating that their hypothesis cannot be ruled out. Each conclusion regarding surface type 2 has contrasting but important implications for the geological history of Mars. Because at this point compositions have not been well determined, surface type 2 will be referred to as such in this work rather than as andesite or weathered basalt.

[11] It is possible that surface types 1 and 2 are composed of two or more minerals that combine to produce a spectral signature resembling that of basalt. For example, crystals of pyroxene and plagioclase exposed or eroded from a coarse-grained gabbro could have a spectrum similar to that of surface type 1. In this work, we refer to surface type 1 as "basalt" for simplicity, but it should be emphasized that this classification may be an oversimplification.

[12] Further spectral studies using TES data have identified surface compositions other than igneous rocks. *Christensen et al.* [2000b] found the distinct signature of hematite in Sinus Meridiani. This mineral is considered to be coarsely crystalline based on the spectral shape observed by TES. It is associated with layered deposits and may indicate the former presence of near-surface water. *Clark et al.* [2002] found outcrops of olivine, indicating that at least in some regions on the surface, aqueous weathering has not occurred. *Bandfield and Smith* [2003] have used spectra from multiple emission angles to better separate atmospheric and surface components in TES data. This has produced the first mineral identifications of bright regions. They found that the bright region spectra match well with fine particulate silicate minerals. In particular, the bright regions have spectra consistent with intermediate- to high-calcium plagioclase feldspar, indicating that the surfaces here have not been completely altered by chemical weathering, and minerals with either bound or adsorbed water.

[13] Using TES data analyzed with the techniques described above and further data from HST, work has progressed on identifying the composition of Martian dune sand. Early work using Viking Orbiter camera filters led to the idea that dark dune sands were composed of iron oxides, such as goethite [*Thomas and Veverka*, 1986]. Basaltic sand has been found in Cimmeria Terra in the southern highlands [*Christensen et al.*, 2000a] and in Nilosyrtis Mensae in the northern lowlands [*Rogers et al.*, 2000]. Intracrater sand in Arabia Terra has been interpreted as having a basaltic core

surrounded by an andesitic arc on the downwind side, suggesting a compositional sorting of sand based on particle size [*Wyatt et al.*, 2001]. The large northern polar erg has been studied with both Hubble Space Telescope (HST) near-infrared data and TES spectra. The HST has detected the signature of pyroxene, indicating the presence of mafic rocks [*Bell et al.*, 1996]. Analyses of TES data have shown that plagioclase feldspar and sheet silicates and/or high-Si glass are also present [*Noe Dobrea and Bell*, 2001; *Bandfield*, 2002], leading to the conclusion that the polar dunes are andesitic [*Bandfield*, 2002].

2.1.4. Thermal Inertia

[14] Thermal inertia is a measure of a material's thermal response to the diurnal heating cycle. Loose, fine-grained sediments lose heat rapidly after sunset, leading to low thermal inertia values. Increasingly consolidated sediments and coarser-grained materials (i.e., sand, gravel, boulders, and bedrock) lead to successively weaker diurnal temperature extrema from higher heat retention and therefore they produce progressively higher thermal inertia values. In ideal situations where all other factors are accounted for, thermal inertia can be used to estimate the average grain size of a particulate surface material. Typical values of thermal inertia for various grain sizes are listed in Table 1.

[15] The thermal inertia of Martian dunes has been studied in detail since the first thermal models were produced for Mars [*Christensen*, 1983; *Edgett and Christensen*, 1991; *Edgett and Christensen*, 1994; *Herkenhoff and Vasavada*, 1999]. In particular, the dune fields of the Helluspontus area in Noachis Terra have been used as a basis for comparison between different models, all of which have been based on a thermal model developed by *Kieffer et al.* [1977]. In all of these thermal studies, thermal inertia was calculated using a single measured surface temperature that was matched to a predicted temperature from a thermal model that involved thermal inertia and other various parameters such as albedo, season, and dust opacity. Methods differ mostly in how the atmosphere influences predicted and measured surface temperatures, but all produced a thermal inertia consistent with coarse-grained sand.

Table 1. Thermal Inertia and Effective Grain Size[a]

Name	Phi	Diameter, μm	Thermal Inertia, J m^{-2} s$^{-0.5}$ K^{-1}
Pebbles	−4 to −2	4–16[b]	417–580
Granules	−2 to −1	2–4[b]	353–417
Very coarse sand	−1 to 0	1–2[b]	300–353
Coarse sand	0–1	0.5–1[b]	254–300
Medium sand	1–2	250–500	215–254
Fine sand	2–3	125–250	182–215
Very fine sand	3–4	63–125	155–182
Coarse silt	4–5	31–63	131–155
Medium silt	5–6	16–31	112–131
Fine silt	6–7	8–16	95–112
Very fine silt	7–8	4–8	80–95
Clay	8+	<4	<80

[a]Using the thermal inertia relation of *Presley and Christensen* [1997a] with a surface atmospheric pressure of 5 mbar.
[b]In mm.

2.2. Study Area

2.2.1. Regional Context

[16] Proctor Crater (see Figure 1a) is one of several 50–300 km diameter impact basins in Noachis Terra, located in the ancient cratered terrain of the southern highlands of Mars. Located at 47°S, 30°E (330°W), it is one of perhaps a dozen craters west of Hellas Planitia (see inset) that contains a prominent, dark dune field. *Peterson* [1977] mapped the crater floor and the surrounding plains simply as "plains material", interpreting this unit as unconsolidated sediment deposits that in some areas may be underlain by flood lavas. Proctor Crater itself is roughly 150 km across, and the dark dune field within extends to ~65 km from southwest to northeast and ~35 km from southeast to northwest. The seasonal polar cap reaches northward beyond Proctor crater, covering the entire crater floor and walls with frost during the winter. Proctor Crater is well within the limit of the seasonal frost, which extends to 40°S [*James et al.*, 1992].

2.2.2. Prominent Features

[17] Figure 1b shows a digital elevation map (DEM) of the crater, combined with a shaded relief map, at a resolution of 400 m/pixel. The DEM was constructed from individual MOLA elevations using the Generic Mapping Tools (GMT). Several features that are barely visible in the MOC wide-angle mosaic are emphasized in the shaded relief map, which been stretched nonlinearly in color to emphasize relief within Proctor Crater (note color bar in Figure 1b). The crater floor is a fairly flat expanse, smooth at the 400 m resolution of the DEM. It is punctuated by two pits, the larger of which is located on the western side of the crater interior, covers one tenth of the crater floor, and is up to 1 km deep. The interior of the larger pit, here called the "western pit", is rugged and contains several craters. The smaller pit, called the "central pit", is located in the northern central region of the crater floor, has a much smoother floor, and is roughly 100 m deep. Figure 1b also shows the dune field rising above the flat surface as a series of ridges unresolved at the scale of the DEM. There is also a set of ~50 m high ridges ringing the center of the crater at roughly half its diameter (shown in dark violet in Figure 1b, at ~600 m), labeled here as "concentric ridges". These ridges are visible as dark rings in MOC wide-angle images in Figure 1a. The possible origin of these ridges is discussed by *Fenton* [2003].

[18] Figure 1c shows a profile crossing the crater, the location of which marked on the map as AA′ in Figure 1b. The western pit is a rough, negative feature that cuts sharply into the crater floor materials. The dune field appears as a poorly resolved accumulation of material superimposed on the crater floor. Also visible are the concentric ridges, which

Figure 1. (opposite) (a) MOC wide-angle mosaic of the study area, Proctor Crater, at a resolution of 250 m/pixel. Proctor Crater is located at 47°S, 30°E (330°W), and it is approximately 150 km across. The small red-bordered inset is a global shaded relief map from MOLA, with the study area highlighted in red. (b) MOLA DEM superimposed on a shaded relief at a resolution of 400 m/pixel. The elevation scale is stretched nonlinearly to emphasize topography on the relatively flat crater floor (see color bar). Profile AA′ is shown in Figure 1c. (c) Profile AA′ across Proctor Crater, with a vertical exaggeration of 15 times. Note that in this and all subsequent images, north is always oriented up.

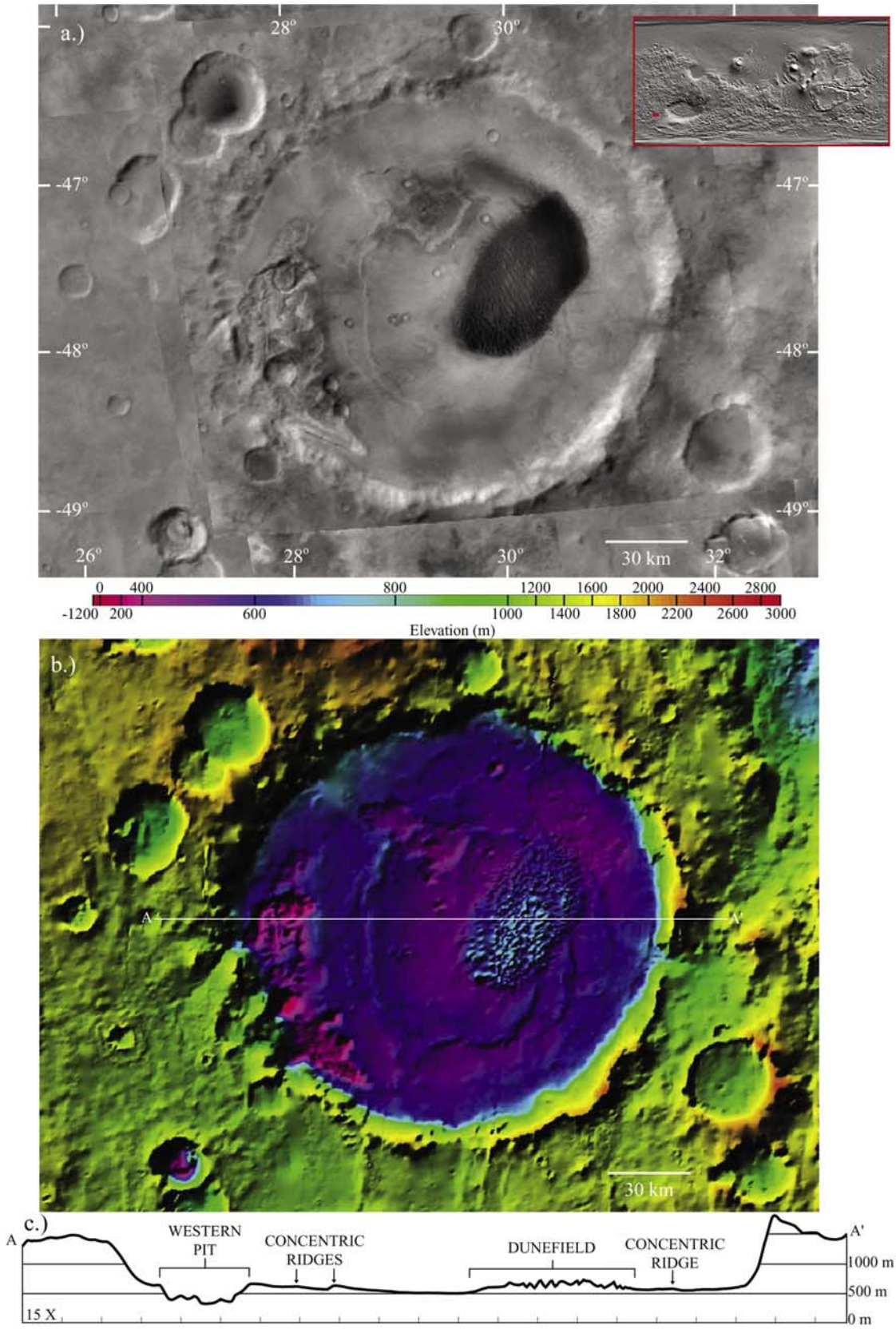
a.)
28°
30°
-47°
-48°
-49°
26°
28°
30°
32°
30 km
0 400 800 1200 1600 2000 2400 2800
-1200 200 600 1000 1400 1800 2200 2600 3000
Elevation (m)
b.)
A
A'
30 km
c.)
A
WESTERN PIT
CONCENTRIC RIDGES
DUNEFIELD
CONCENTRIC RIDGE
A'
1000 m
500 m
0 m
15 X

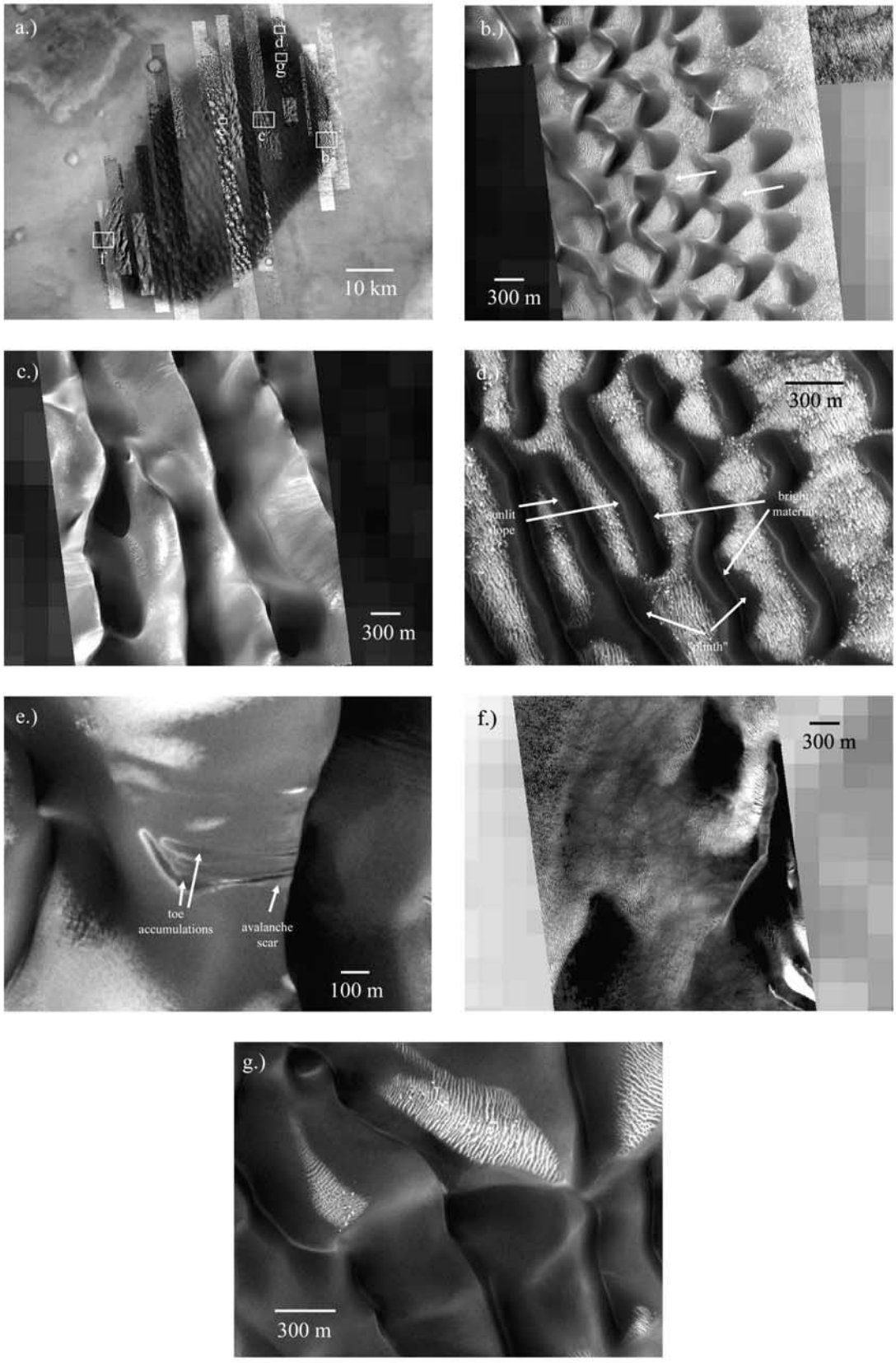
a.)
10 km
b.)
300 m
c.)
300 m
d.)
300 m
sunlit slope
bright material
"plinth"
e.)
toe accumulations
avalanche scar
100 m
f.)
300 m
g.)
300 m

appear as subtle positive features that are steeper on the slopes facing the crater walls. The remainder of the crater floor is a smooth, fairly featureless plain at the resolution of the DEM.

2.2.3. Basin Fill

[19] It is possible to use crater depth versus diameter measurements to estimate the amount of basin fill within Proctor Crater. Statistics based on MOLA DEM's by *Garvin et al.* [2000] have provided a depth versus diameter relationship for pristine craters of various sizes. For a crater with a diameter (D) larger than 100 km, the original depth (d) is estimated at:

$$d = 1.27D^{0.12}. \quad (1)$$

Thus the estimated unmodified depth of Proctor Crater is 2.31 km. The highest remaining elevation of its now largely degraded rim is 2360 m, placing the original crater floor at a lower limit of 50 m. The current crater floor elevation is roughly 500 m, implying that at most a net value of 450 m of material has accumulated in Proctor Crater since its formation.

3. Methods

3.1. GIS

[20] Data products from the Mars Global Surveyor mission were incorporated into a Geographic Information System (GIS) in order to study Proctor Crater. The software used was ArcView GIS Version 3.1, created by ESRI (Environmental Systems Research Institute), to build a GIS of Proctor Crater. Our base map is a 250 m/pixel MOC WA (Mars Orbiter Camera wide-angle) image mosaic that has been processed, corrected for gain and radiometric variations, and mapped into a sinusoidal projection using Integrated Software for Imagers and Spectrometers (ISIS) developed by the U. S. Geological Survey. We added in a digital elevation model (DEM) that we constructed from MOLA (Mars Orbiter Laser Altimeter) elevation points at a horizontal resolution of 400 m/pixel using Generic Mapping Tools (GMT) software. Inaccuracies in camera pointing information led to spatial offsets in the positioning information of the WA mosaic, and so we used the MOLA DEM as a reference to adjust the position of the WA mosaic in the GIS by hand. Mars Orbiter Camera narrow-angle (MOC NA) images from the mission phases Aerobraking 1 through Extended Subphase 11 were processed and projected to match the WA mosaic using ISIS software, and each image was added to the Proctor Crater GIS as a separate layer (theme) and at full resolution. Similar camera pointing errors led to hand positioning of each NA image on the WA mosaic. On top of these images we plotted five data sets derived from TES (Thermal Emission Spectrometer). These include bolometric thermal inertia [*Mellon et al.*, 2000], compositional end-member concentrations [*Bandfield et al.*, 2000], daytime and nighttime bolometric temperatures, and bolometric albedo. Also included were all available Viking Orbiter images of Proctor Crater, although the resolution of these proved to be no better than the MOC WA images.

[21] Once the data were assimilated into the GIS, several parameters were mapped or measured using data from the Aerobraking through Mapping mission phases. Data from the Extended mission phase have since been added to the GIS and have been inspected for consistency with the previous measurements. Among the features mapped over each NA image in Proctor Crater are dune slip face brinks and orientations, dust devil tracks and orientations, bright dune form location and orientation, boulder density, small craters, and the locations of NA images. This additional information allows for a new assessment of dune morphology, sediment volume, and wind regime using all available information. The results of each of these measurements are described below.

3.2. Measurement of Slip Face Orientations

[22] Dune slip faces are created by slope adjustments to oversteepening (i.e., landslides) created in part by an influx of saltating sand to the brink of the dune slip face from upwind. Grain fall from suspended sand may also contribute to the slip face surface. Transverse dunes have slip faces that dip downwind, and longitudinal dunes often have slip faces that are oriented at an angle to their crests but that dip downwind of the last wind to influence them (in this work, the classification of dune morphology follows the terms defined by *McKee* [1979].) Even oblique dunes, which are produced in a bidirectional wind regime that forces the dunes to move in a direction different from predominating winds, have slip faces oriented downwind from the winds that shape them [*Hunter et al.*, 1983]. Barchan dunes are the main exception to this rule in that they have crescentic slip faces, the central axis of which is oriented downwind, although this axis is simple to identify. Thus slip faces are a reliable marker of wind direction in that they almost always face downwind. In this work, slip faces were identified by their crescentic-shaped slip face brinks if the dunes are barchans (i.e., Figure 2b), and by long sharp slip face brinks on steep slip faces that reach from the brink to the crater floor if they are transverse dunes (i.e., Figure 2f). The large reversing crests are not considered slip face brinks because the slopes on either side are not obviously recent slip faces and therefore may not directly reflect wind directions (i.e., Figure 2c). Only the clearest cases are considered slip faces. To provide the best "ground truth" possible for comparison with the mesoscale model experi-

Figure 2. (opposite) The dark dunes of Proctor Crater. (a) Context for Figures 2b–2g. (b) Barchans at the eastern edge of the dune field containing two differently oriented slip faces (see arrows) (MOC NA M19-00307). (c) Large dark sand ridges (in this case, covered in frost), with an appearance similar to reversing transverse dunes because neither side is obviously a slip face. Note the lack of superimposed secondary dunes (MOC NA M23-01221). (d) Dunes near the eastern edge of the dune field, with accumulations of bright sand on their eastern slopes (MOC NA M07-02777). (e) Unusual slope adjustment resembling a typical landslide, indicating some amount of dune induration (MOC NA E03-01039). (f) Transverse dunes dominating the northwest edge of the dune field. This example is partially defrosted (MOC NA M15-01278). (g) A star dune with three arms, near the eastern edge of the dune field (MOC NA M07-02777).

ments, the orientations of as many slip faces as possible were measured. Measurements were made by hand, and directions were marked only for obvious slip faces and where the orientation was clear. Care was taken to avoid marking dune crests rather than slip face brinks, which are not necessarily colocated.

3.3. Dune Field Volume and EST

[23] The volume of the Proctor Crater dune field is a useful parameter for comparison to other dune fields on Earth and Mars. *Wasson and Hyde* [1983] define the equivalent sand thickness (EST) of a dune field as ''the thickness of a continuous sheet of sand which results from the hypothetical spreading out of dunes over a specified area.'' They used this parameter as an estimate of net sand supply to a dune field to show that dunes of differing morphology form in areas where sand is accumulating or migrating. If the volume of the dune field is known, the EST can be calculated by dividing the volume by the area covered by the dune field. Below is a discussion of two different techniques for estimating volume and EST using MOLA elevations.

[24] The first method uses tools built into ArcView to directly estimate the volume of a three-dimensional figure. A ''triangulated irregular network'' (TIN), or a three-dimensional construct of the dune field, was created using MOLA elevations. Using this topographic model, the amount of dune sand was calculated using a volume defined to be above the local crater floor (at a height of 541 m) and within a perimeter defined by the edge of the dark dunes as observed in MOC wide-angle and narrow-angle images. One difficulty with using the TIN to estimate volume is that although most of the large dunes are resolved along each MOLA track, the distance between tracks is usually too large to fully construct a proper model of the dune field (i.e., the dunes are aliased). The volume calculation only accounts for the volume beneath the modeled TIN, and it is subject to inaccuracies caused by the aliasing.

[25] The second method of determining the dune field volume uses each MOLA track that crosses the dune field, but only considers along-track estimates of dune height. Many of the dunes are well resolved along each MOLA track, allowing for an accurate determination of sand area beneath each track, or an integration of the area below the curve for each track. Once this value is determined, the average height of sand for each track can be calculated by dividing the integrated area by the length of that MOLA track across the dune field. This leads to an estimate of the equivalent sand thickness (EST) for each track. Forty-eight MOLA tracks are distributed uniformly across the dune field, and thus the mean EST from all of the tracks provides a reasonable estimate of the average EST of the entire dune field. This mean dune field EST value multiplied by an estimate of the surface area beneath the dunes leads to a sand volume estimate. The second method is considered to be more reliable because it relies only on the along-track MOLA distances in which most of the dunes are resolved, rather than on a three-dimensional construct in which cross-track surfaces are calculated using aliased data.

3.4. Composition From TES Spectra

[26] In this work, the deconvolution method described in *Bandfield et al.* [2000] and *Smith et al.* [2000] has been applied to summertime TES spectra to determine the composition of the Proctor Crater dune sand and the surrounding crater floor. A total of eight end-members were used in this analysis: four atmospheric components and four surface components. The atmospheric spectral end-members included dust at both high and low dust opacity, and water ice at two particle size distributions. The surface end-members included the surface types 1 and 2 from *Bandfield et al.* [2000], hematite [*Christensen et al.*, 2000b], and a blackbody spectrum to account for differences in spectral contrast.

[27] The concentration of surface type 2 (andesite/weathered basalt) is strongly influenced by the presence of atmospheric dust. The spectral signatures of andesite and dust are similar enough that under nonideal conditions, the surface component and the atmospheric component are not properly separated. Thus it is important to consider only the clearest spectra, to minimize contamination by dust. Because Proctor Crater is located in a known dust-raising area, the air is dusty in the summer when the signal is strongest and most reliable. However, full spatial coverage of the study area, and therefore the use of as many viable orbital tracks as possible, is desirable in order to seek out sand deposits and transport pathways. Therefore data from a single orbit, that were obtained over a warm surface with a clear atmosphere, are discussed first to provide a basis for comparison with the rest of the data. The discussion then extends to all orbits crossing the study area.

3.5. Thermal Inertia From TES

[28] To study the thermal properties of the floor of Proctor Crater, we have used thermal inertia values calculated from TES thermal bolometer measurements [*Jakosky et al.*, 2000; *Mellon et al.*, 2000]. They matched single nighttime (2 AM) temperature measurements from TES to a large lookup table of temperatures produced by a thermal model. The lookup table includes several parameters required for the model calculations, such as albedo, dust opacity, time of day, season, surface pressure, latitude, and thermal inertia. The thermal dust optical depth is assumed to be 0.1, scaled to the mean pressure level at 6.1 mbar. *Jakosky et al.* [2000] and *Mellon et al.* [2000] use a thermal model based on that of *Haberle and Jakosky* [1991], with additional considerations of seasonal and latitudinal variations. Although the thermal inertia values used here were calculated using brightness temperatures from the TES bolometer rather than from a single spectral band (as was previously done with the 20 μm channel of the IRTM data set), *Jakosky et al.* [2000] showed that the difference between the two surface temperature measurements had little effect on thermal inertias in the range of 50 to 300 J m^{-2} $s^{-0.5}$ K^{-1}.

[29] In this work, thermal inertia measurements were converted into particle size estimates using the empirical relation determined by *Presley and Christensen* [1997a]. This calculation employed a surface atmospheric pressure of 5 mbar, a typical value for summer nights at the latitude of Proctor Crater. In order to choose the most reliable values, we used only thermal inertias measured during southern summer (L_s = 240°–360°), with emission angles less than 10°, and with the best data quality ratings (values of 0 or 1).

[30] It must be emphasized that the particle sizes discussed here do not necessarily represent actual particle

sizes, but rather the effective particle sizes for unconsolidated particulate materials in each TES pixel. One challenge in interpreting thermal inertia measurements is that each TES pixel represents a thermal response from a 3 km × 6 km area on the surface, which could easily contain any combination of dust, outcrops, boulders, sand, and consolidated materials, each with its unique thermal signature. A further complication is that consolidated fine material produces the same thermal effect as larger but unconsolidated particles. Thus thermal inertia maps are most valuable for studying either places containing unconsolidated fine materials, which produce the lowest and least ambiguous values, or areas where the particle size range of the surface has been previously constrained.

[31] Dune fields are one of the few geological structures in which the degree of consolidation and range of particle sizes is predictable. By definition, active sand dunes are composed of unconsolidated sand grains, relieving the thermal ambiguity introduced by consolidated materials. In addition, sand dunes consist almost entirely of particles in a narrow size range that are lifted into saltation by the wind, thereby doing away with another complication of thermal inertia caused by poorly sorted materials. Thus dunes are among the most ideal features to study using thermal inertia. It is for these reasons that dunes have been consistently targeted as a control for new thermal inertia calculations of Mars.

4. Observations and Interpretations

4.1. Dark Dunes

4.1.1. MOC Narrow-Angle Images

[32] Close examination of MOC narrow-angle images of the dark dune field in Proctor Crater has led to many observations regarding the aeolian environment on the surface of Mars. Figure 2a shows the dune field with MOC narrow-angle images superimposed on a MOC wide-angle mosaic. At the scale of the wide-angle mosaic, the dunes display their characteristic northwest-to-southeast trend, which has led to the interpretation that these dunes are transverse to either a southwesterly wind [*Cutts and Smith*, 1973] or a northeasterly wind [*Ward et al.*, 1985].

[33] Closer inspection of the dunes leads to a new interpretation of dune morphology. Figures 3b and 2b shows widely spaced dunes at the eastern edge of the dune field. The edges of dune fields are useful locations to study dune morphology, because here the sand deposits tend to be thinner than in the center of the dune field [*Porter*, 1986], often leading to barchanoid dunes [*Wasson and Hyde*, 1983] with smaller and simpler slip faces that are easier to interpret. The smaller dunes are about 300 m across and, as determined from MOLA elevations, they are ~50 m high. On the basis of their overall crescentic shape, these dunes appear to be barchans created by ENE winds (e.g., wide arrows). However, these dunes also have slip faces oriented to the NNE, indicating another dune-influencing wind from the SSW (e.g., thin arrow). Thus, even at the edge of the dune field where a thin sand cover limits dune morphology, the situation is not as simple as originally thought. It seems that both previous estimates of directionally opposed dune-forming wind orientations may have been correct [*Cutts and Smith*, 1973; *Ward et al.*, 1985].

[34] A sample of the interior of the dune field is shown in Figure 2c. The large dunes have a spacing of up to 2 km and heights determined by MOLA elevations of up to 300 m. The appearance of these dunes is not consistent with that of transverse dunes, but they do resemble reversing transverse dunes, as inferred by *Lancaster and Greeley* [1987]. Star dunes are present in a few locations in the dune field (see Figure 2g), but the tall ridges interpreted as reversing transverse dunes dominate. Reversing dunes are produced by two winds oriented roughly 180° apart, leading to a slip face that reverses direction depending on whichever wind is dominant at the time of observation. The constant slip face reversal generally leads to steep inclines on both the stoss and lee slopes (e.g., the reversing crests of the Kelso Dunes, California [*Sharp*, 1966]). In the case of the Proctor Crater dunes, it is difficult to determine which slip face is active in these images. Star dunes are produced by more than two dune-influencing winds of differing orientations, leading to at least two overlapping transverse slip faces that create a star-like form in plan view. The dunes in Figure 2c appear most like reversing transverse dunes (e.g., the large ridges are symmetrical, indicating that slip faces form on either side of the crest), implying that at least two wind directions affect the morphology of the dunes.

[35] Perhaps more important even than the new morphological dune classification is the observation that there are no secondary dune structures on the slopes of these features. On Earth, large dunes (>~500 m) nearly always have smaller, superimposed dunes, either of the same type (i.e., small barchans on a large barchan), or of a different type (i.e., small star dunes on a large linear dune) [*Lancaster*, 1988]. By the classification of *Breed and Grow* [1979], the former system is termed a ''compound'' dune, and the latter is termed a ''complex'' dune. Dunes with no superimposed dune structures, such as those in Proctor Crater, are called ''simple''. The transition from simple dunes to compound and complex dunes is not well understood. The difference has been attributed to changes in climatic wind strengths [*Kocurek et al.*, 1991], a shift in bed form type akin to that between ripples and dunes [*Wilson*, 1972], and variations in transport rates on the larger dunes, as though dune slopes grow to approximate a small desert floor that accumulates their own small dunes in turn [*Lancaster*, 1985]. Regardless of what causes the shift between simple and compound/complex dunes, this transition is not seen on Mars, even at the 1–2 km scale of the Proctor Crater dunes. It may be that the scale at which this transition occurs on Mars is much larger than that on the Earth. It is tempting to dismiss this lack of superimposed dunes to a simple difference in atmospheric conditions on Mars and Earth, but previous studies comparing dune length, width, and spacing have shown that Martian dune dimensions in general correlate well with those of Earth dunes [*Breed et al.*, 1979]. Many of the terrestrial dune fields used in the study by *Breed et al.* [1979] consisted of compound and complex dunes that correspond well to the simple Martian dunes, suggesting that secondary bed forms likely have little effect on the overall structure of large primary dunes. There is no obvious reason why large Martian dunes should fail to produce secondary dunes. *Breed et al.* [1979] note the lack of secondary dunes from images at Viking resolutions, proposing that any secondary features that might have once existed have since eroded away. However, recent slip face

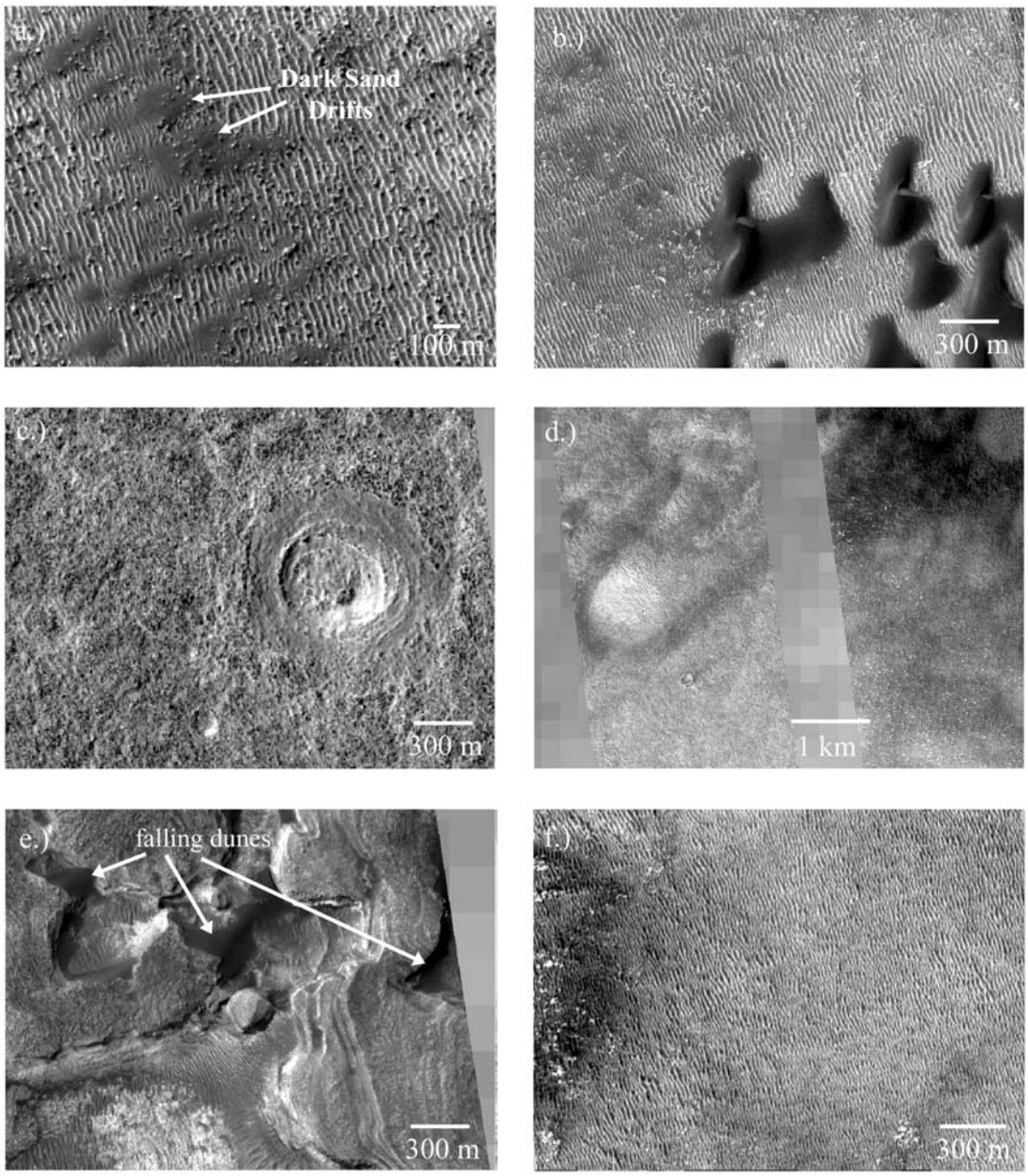

Figure 3. Examples of MOC narrow-angle images on the Proctor Crater floor: (a) Boulders and sand drifts (MOC NA M23-01221); (b) boulders, dark barchans, and bright dune forms (MOC NA M03-03088); (c) degraded craters on the Proctor Crater floor (MOC NA M02-01510); (d) dark erosional wind streaks (MOC NA M02-01510, M03-06827); (e) strata of basin fill and dark falling dunes in the western pit (MOC NA M03-00338); (f) uniform coverage of bright dune forms (MOC NA M03-06827); (g) dark sand trapped against a northeast facing hill slope, spawning dust devils as revealed by dark tracks (MOC NA M11-03806); (h) mosaic of three MOC narrow-angle frames over part of a concentric ridge (MOC NA M02-01510, M03-01614, M03-06827); and (i) wide-angle context for Figures 3a–3h.

adjustments (as discussed in section 4.4.2) demonstrate that the Proctor Crater dunes are still active, and so secondary features, by the standards of terrestrial dunes, should form under the current wind regime. This observation may bring into question all currently understood theories of bed form climbing. Alternatively, it may simply be that conditions that would produce secondary dunes on terrestrial structures do not exist on Mars at the observed scales.

[36] The interpretation of images of any surface involves discriminating the cause of brightness variations. These are most often created by changes in shading (e.g., topography) and by inherent albedo patterns (e.g., patches of ice on a dark surface). In some cases the interpretation requires careful consideration. Note that in the image analysis in this work, the terms "bright" and "dark" refer to relative brightness differences, and that no attempt is made to

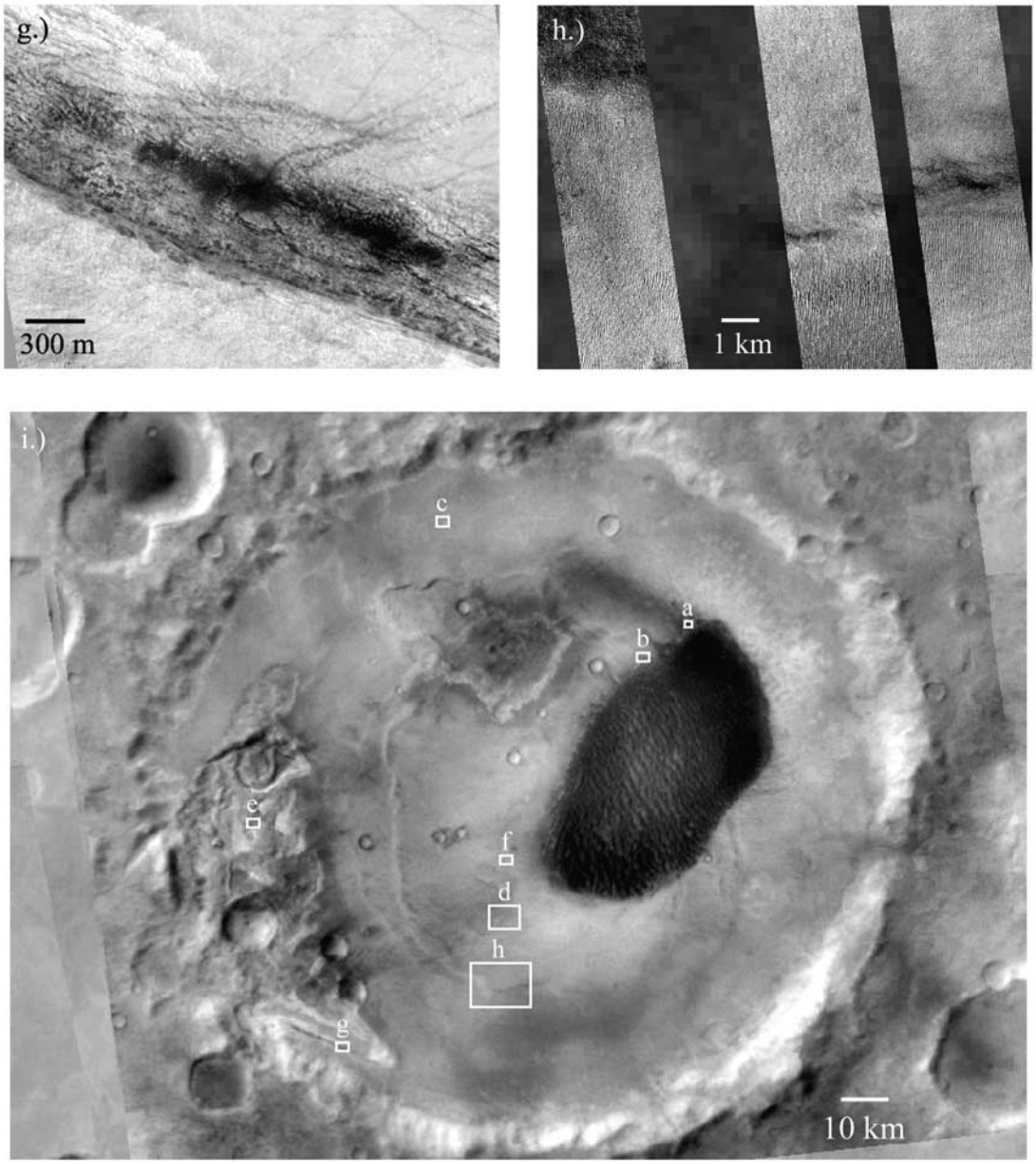

Figure 3. (continued)

measure absolute brightnesses. Figure 2d shows several dark dunes at the northeastern edge of the dune field. This image was taken during the summertime, when no frost cover was present. Like all of the narrow-angle images in this area, the sun azimuth angle is NNW-NW. From this perspective, the sun should reflect strongly off all slopes with a component facing roughly north or west. Therefore the west-southwest facing slopes of the dark dunes are interpreted to be bright because of reflected sunlight. The east-northeast facing dune slopes, however, have both a dark and a bright line. The dark stripe is interpreted as shady slope, most likely a slip face, oriented away from the sun. The bright stripes on the ENE slopes are less easy to interpret. They seem to lie on broad plinths of dark sand that underlie the top portion of the dunes. In places near the slip faces, the plinths become thin, exposing the underlying surface beneath the dark dunes. Even along these places where the plinth is gone and the top part of the dune rests on the bright dune forms that comprise this layer of the crater floor, the bright stripe is still present. These bright stripes are interpreted as accumulations of bright material. They only appear on dunes near the eastern edge of the dune field. It is possible that this bright material is accumulated dust. However, bright dust is easily kicked into suspension from the impact of saltating sand, which is easily cleaned off the majority of the dark dunes, and would also strip away this bright layer if it were composed of dust. It is more likely that the bright stripe is an accumulation of (relatively) bright sand that has been blown onto the ENE facing slip faces. It is possible that this bright material is composed of grains of a different size or density, becoming concentrated on the dune surface through differential sorting of particles by the wind. The source of the bright sand on the Proctor Crater dunes may be the tops of the bright dune forms

rounded from erosion shown in Figure 11c. In a similar study of the White Rock structure, *Ruff et al.* [2001] also propose that lighter material concentrated at the tops of dark ripples comes from the nearby eroding bright massifs that comprise White Rock. If this is the case, this bright stripe of material may be evidence that the bright dune forms are composed of sand rather than granules, because the bright material has saltated up the dune to accumulate at the base of a slip face.

[37] There are variations in the morphology of slip face adjustments on dunes in the center of the dune field. In Figures 15f–15h, the persisting dark lobes of material have no apparent topography. Most likely they are typical of slip face adjustments in loose sand, in that slender lobes of sand propagate downhill, only slightly disturbing the surface and leaving only a thin layer of loosened sand behind. Figure 2e shows a very different type of slip face adjustment. This feature has an appearance similar to a terrestrial landslide. Sublimating frost clings to the edges of the lobes on the lower part of the slope. Near the crest of the dune there is a scar indicating where material has been removed. At the bottom of the slope (i.e., at the toe of the landslide) there is an accumulation of sand that formed from material excavated from the scar uphill. Avalanche scars such as the example shown in Figure 2e are not stable in unconsolidated sand because they cannot retain their sharp edges, and thus they are not generally found on active sand dunes.

[38] The presence of an avalanche scar in the Proctor Crater dunes indicates some amount of sand cohesion. Because the more typical slip face adjustments are more common in the dune field, such cohesion is not likely to be typical in the Proctor Crater dunes. It may be that trapped volatiles freeze the dune, allowing landslide-like structures to form and maintain their shape. However, this feature is also visible in an image from the previous winter, indicating that its structure survived a volatile-free summer. It is possible that parts of the dune field are effectively stabilized from further activity by some cementation process. The question then arises as to how the dunes remain free of dust if no loose sand is present to scour it off each year. It may be that there is a very thin layer of active sand that is free to clear off dust under saltation, but that underneath this layer the dune sand is more consolidated.

[39] The northwestern edge of the dune field (see Figure 2a) contains a series of dune structures oriented obliquely to the NW-SE trend of the bulk of the dune field. Closer inspection (Figure 2f) shows that *Cutts and Smith* [1973] correctly interpreted these features as large transverse dunes with slip faces indicating winds from the southeast. These slip faces correspond to yet another wind direction influencing dune morphology. Residual frost coats a few areas on the upwind sides of these dunes, and filamentary streaks that are probably dust devil tracks cover irregularly shaped sand sheets that fill in and cover the underlying small bright dune forms.

4.1.2. Slip Face Orientations

[40] Figure 4a shows part of the dune field with all slip face markings (lines are parallel to the wind directions that produce each slip face). Three main wind directions influence dune morphology. Figures 4b and 4c show specific examples of slip faces exhibiting each of the three orientations. Figure 5 shows wind roses of each of the three main slip face directions and the mean wind orientations that produce them. Almost all of the measured slip face brinks were crisp, suggesting that they have not undergone erosion since they were last modified. Terrestrial dunes that experience more than one sand-moving wind tend to develop rounded brinks and subdued slip faces under modification from oblique winds [*Sharp*, 1966]. This rounding process is not so obvious in the Proctor Crater dune field, suggesting that these dunes may be partially cemented.

[41] In Antarctic dunes, snowfall buried by subsequent slip face activity has been observed to allow oversteepened cornices of sand cemented by snow to develop on lee slopes [*Calkin and Rutford*, 1974]. Similar lenses of snow have remained in terrestrial dunes throughout the summer season, such as those of Wyoming [*Steidtmann*, 1973] and the Antarctic dunes [*Calkin and Rutford*, 1974], and for a good portion of spring, Alaskan dunes [*Koster and Dijkmans*, 1988]. Like the sides of the landslide scar shown in Figure 2e, these sharp brinks in the Proctor Crater dunes may indicate the presence of seasonal frost trapped within the dunes. Although it is unlikely that frost would remain throughout the summer, it may persist long enough to allow old slip face brinks to retain their crispness.

[42] The first slip face orientation, shown in yellow (see Figure 4), is pervasive throughout the dune field, producing barchanoid dunes near the edges and contributing to the large reversing dunes that dominate the central portion of the dune field. Because they are so pervasive, these slip faces are referred to as the primary slip faces. The average orientation of 354 measured primary slip faces (see Figure 5a) indicates formative winds from 239° ± 18° (mean ± standard deviation), or WSW. (In this system, 0° indicates winds from the north). The spread in slip face orientations is caused by a gradual shift from WSW in the western and central portions of the dune field to SW on the eastern edge of the dune field (e.g., compare arrows in Figures 4b and 4c). These slip faces are consistent with the southwesterly wind regime proposed by *Cutts and Smith* [1973]. They also match the trend of most filamentary streaks interpreted as dust devil tracks (see Figure 12), most bright dune forms (see Figure 10), and many small dark sand streaks extending off the southeast edge of the dune field (see Figure 1a).

[43] A secondary wind, shown in turquoise in Figures 4a and 4b, has an average wind orientation from 150 measurements of 110° ± 18° (see Figure 5b), or from the ESE. This secondary wind is found in all but the easternmost portions of the dune field. This wind produces the transverse dunes on the northwest edge of the dune field, shown in Figure 2f. It is also partly responsible for creating the large reversing dunes found in the center of the dune field, in conjunction with the primary WSW winds. This ESE wind also produces the large dark sand streak that extends to the west-northwest from the northernmost tip of the dune field (see Figure 1a). Finally, it matches the orientations of the secondary set of bright dune forms that cover the crater floor (see Figure 10).

[44] The third wind orientation found is shown in magenta in Figures 4a and 4c. Unlike the primary and secondary winds, it appears to affect only the eastern portion of the dune field, although here this wind is dominant. On the basis of 154 measurements, this tertiary wind has an orientation of 75° ± 9°, or ENE (see Figure 5c), consistent with the dune orientations mapped by *Ward et al.*

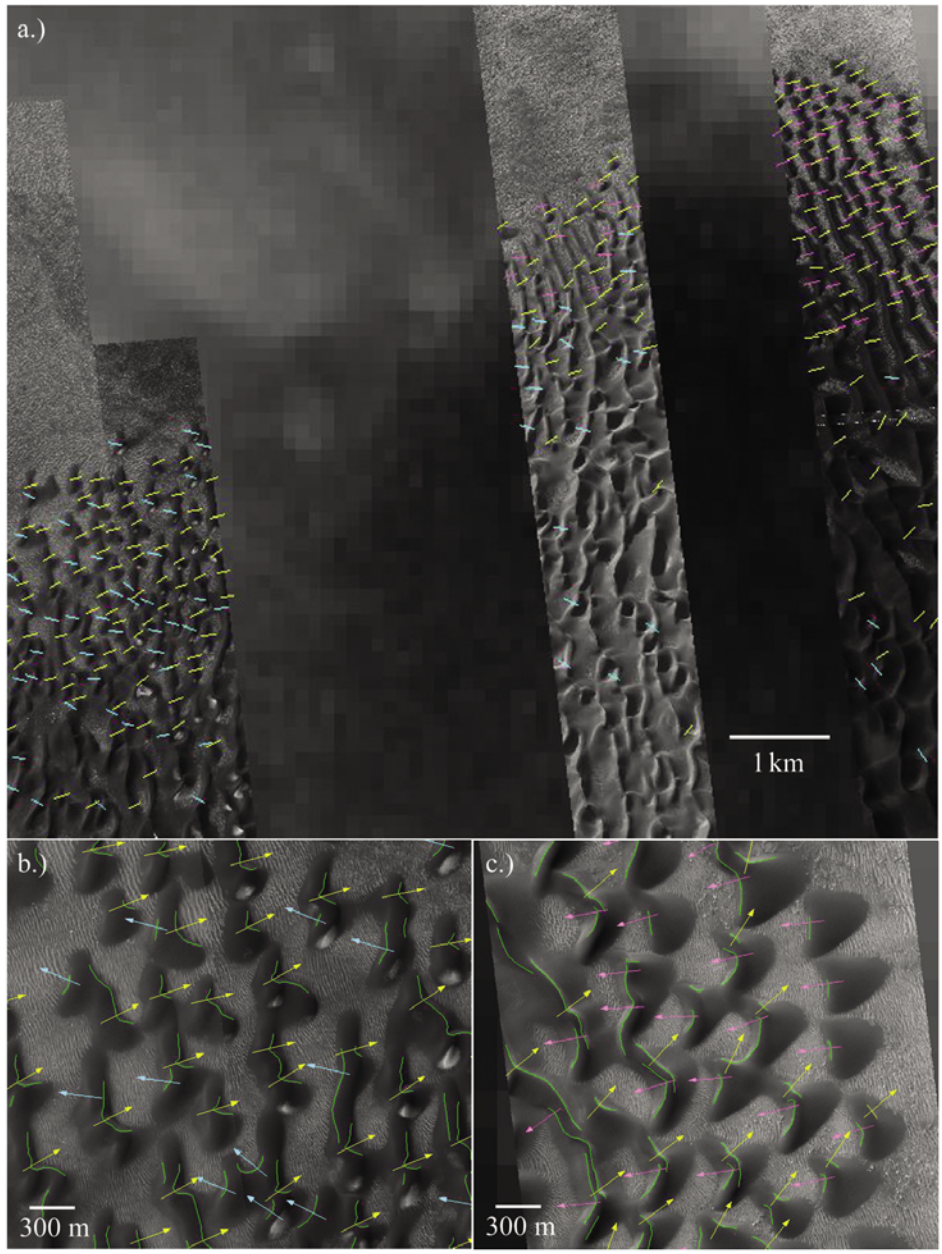

Figure 4. (a) The northern part of the dark dune field, with markers on measured slip faces. Colors correspond to the wind direction: Primary winds (yellow) are from the WSW, secondary winds (blue) are from the ESE, and tertiary winds (magenta) are from the ENE. (b, c) Examples of the three different slip face orientations.

[1985]. Both the secondary and the tertiary winds are oriented obliquely to almost 180° with respect to the primary winds, leading to the observed mixture of reversing transverse dunes and star dunes at the center of the dune field. The tertiary wind is oriented roughly 180° from the primary wind, which may mean that dust devil tracks and bright dune forms that appear to align with the primary wind in fact correspond to this wind. However, this third wind only appears on the eastern portion of the dune field, and thus it is likely only present over the northern and eastern portion of the crater floor. North and east of the dune field, dust devil tracks are conspicuously absent and bright dune forms are either rounded from erosion or absent. Thus there are no surface features other than dune slip faces and a small area of rounded bright dune forms that reveal this wind in the MOC NA images.

[45] The dunes as seen today correspond well to the orientations of not only bright dune forms, which are older and less mobile than the dark dunes, but also dust devils, which are reformed and erased on an annual basis and thus are much younger than the dunes (see section 4.4.1). It appears that the wind regime that built the dune field is still active today. Given the three opposing winds, the dunes are clearly located in an area where winds converge. This is expected of reversing transverse and star dunes. *Christensen* [1983] proposed that the intracrater dunes in the southern

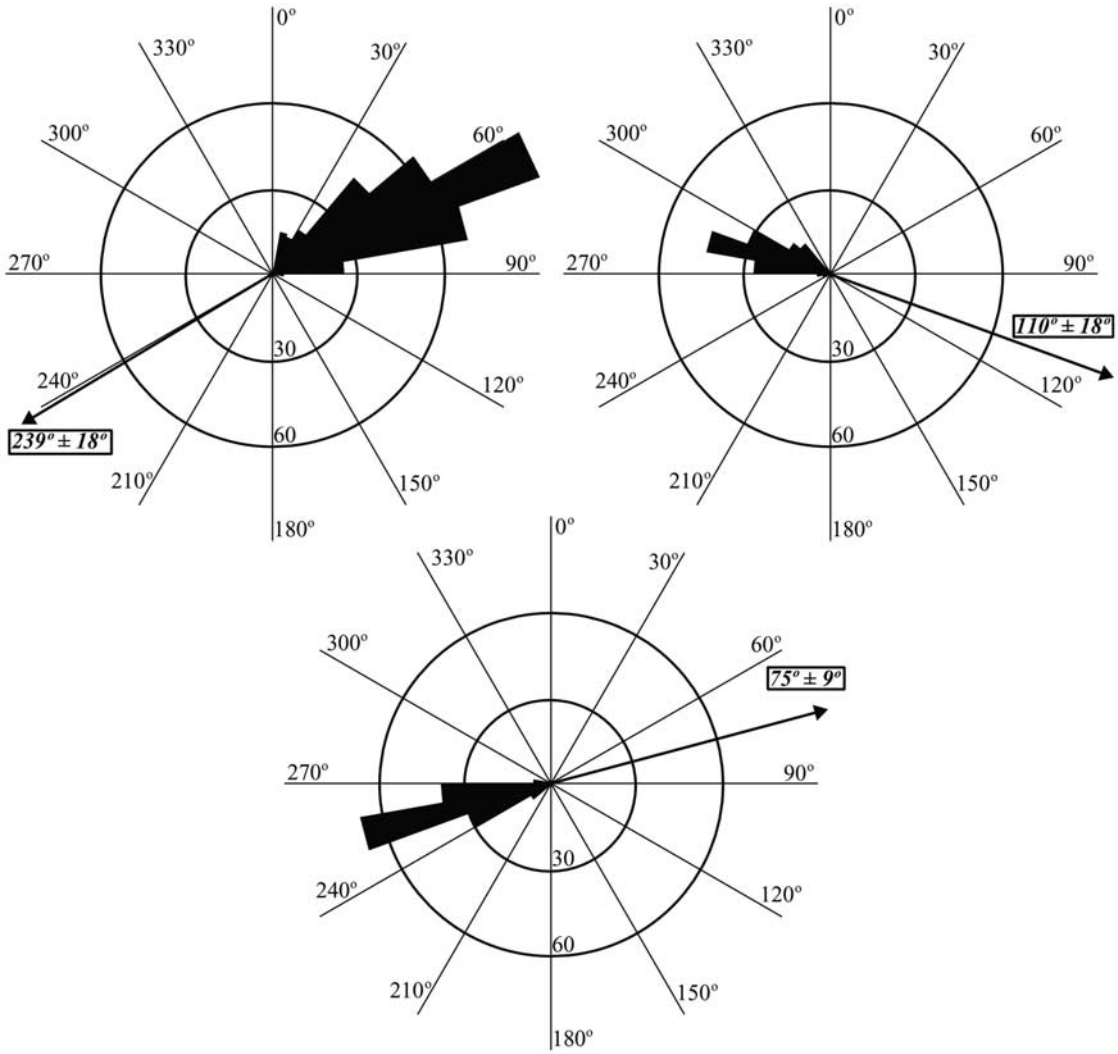

Figure 5. Rose diagrams of the three dune slip face orientations shown in Figure 4. Boxed numbers and bold arrows indicate the mean and standard deviation wind direction of the primary, secondary, and tertiary winds. In this system, 0° represents winds from the north.

highlands are trapped because the winds are strong enough to saltate sand downhill into the crater, but not strong enough to saltate sand uphill out of the crater. Here, the measurement of wind directions shows that the dune field is located where winds are balanced, leading to net sand deposition. If the sand were truly trapped by topography alone then the dunes would be located in the lowest places on the crater floor, the western and central pits (see Figure 1b), but this is not the case.

4.1.3. Dune Field Volume, Structure, and EST (Equivalent Sand Thickness)

[46] Using the first method to estimate dune field volume (see section 3.3), the resulting volume is 140 km^3. The estimated planimetric surface area defined by the perimeter at the edge of the dune field is 1728 km^2. Using a planimetric measurement of dune field surface area calculated in ArcView, the estimated volume of the dune field using the second method is 180 km^3. This value is larger than the first method, which was calculated by a built-in script in ArcView. The second method is probably more accurate than the first, so here 180 km^3 is considered the best estimate volume for the Proctor Crater dune field. *Lancaster and Greeley* [1990] estimated that the northern polar sand seas on Mars have a total volume of 1158 km^3. If their calculations are correct, then the volume of dune sand in Proctor Crater is more than one sixth of that in the northern polar sand seas. Given that several other craters in Noachis Terra have dune fields that are of similar size as that in Proctor Crater, it is probable that the volume of dune sand in the craters of the southern highlands is greater than that in the northern polar sand seas.

[47] The first volume estimate method described above leads to an EST of 80 m, and the second leads to an EST of 105 m. Both estimates are very high values, larger than those for most dune fields on the Earth. It is consistent with a convergent wind regime in which the sand transport into the dune field is greater than that out of the dune field. *Wasson and Hyde* [1983] found that star dunes form in areas with large EST values and a high variability of wind direction. The reversing and star dunes of Proctor Crater are certainly located in an area of convergent and variable winds, as evidenced by the three different slip face orientations described in section 4.1.2. The northern polar sand

dunes have a mean EST of only 1.8 m, consistent with the barchanoid and transverse dunes that are observed in these ergs [*Lancaster and Greeley*, 1990]. It seems that while the dune fields of Mars can be directly compared to those of Earth both morphologically and dynamically, the variations among dune fields on Mars is at least as great as that on Earth.

[48] Figures 6a and 6b show MOLA reflectivities and elevations, respectively, for a traverse across the dark dune field in Proctor Crater. This is a nighttime ground track, thus avoiding any complications caused by reflected sunlight. Each MOLA footprint is 170 m wide, and the along-track shot spacing is 300 m [*Smith et al.*, 2001]. The location of the traverse is shown in a MOC wide-angle mosaic in Figure 6d and in the 400 m resolution shaded relief DEM in Figure 6e. Although most of the track crosses the dark dune field, only the large dunes in the southern two thirds of the track are fully resolved. The northern third of the ground track crosses dunes that are smaller than the spacing of the MOLA shots. Although the larger dunes are barely resolved, several observations can be made based on MOLA data alone. First, the largest dunes are superimposed on a mound that reaches up to 50 m thick. The large dunes themselves range from 100 m to 250 m high, or phrased another way, 50 m to 200 m on the 50 m high mound. In places where net deposition of sand occurs, sand seas accumulate. If the deposition outpaces the rate of migration, then eventually bed forms will migrate over one another, causing dune fields to accumulate strata of sand beneath the current overriding dunes [*Rubin and Hunter*, 1982]. Because the dunes are located in a convergent wind regime, indicating net deposition, we interpret the 50 m high mound to be made of sand strata. The presence of this mound is consistent with the idea that the dunes of Proctor Crater are and have been located in an area of net deposition since the dune field began accumulating.

[49] One way of determining the location of the underlying sand mound within the dune field is to use MOC NA images. Features interpreted as boulders (see section 4.3.1) are strewn over the entire area surrounding and underlying the dune field, but only appear where the sand is thin enough to reveal their presence. The area in which MOC NA images do not show any boulders is outlined in Figures 6d and 6e. Boulders visible in MOC NA frames in Proctor Crater are 5–20 m wide, and presumably as high, so where the boulders disappear the sand cover must be at least 5 m thick. The boulders are barely resolved, and so it is difficult to tell from inspection whether they are partially buried or fully exposed. Because of the incomplete coverage of NA images over the dune field, the border of the sand deposit is highly uncertain. Stars have been marked on Figure 6b where the border of the sand deposit intersects with the MOLA track. These locations match fairly well where the sand deposit begins to thin out in the MOLA track. The bulk of the sand accumulation is in the central and western portions of the dune field. This suggests that in the eastern and northern portions, where the dunes are smaller (and poorly resolved by MOLA as a result), either the wind regime leads to less net deposition than in the rest of the dune field, or that the northern and eastern portions are simply younger and have not had the time to accumulate as much underlying sediment.

[50] A second observation from Figure 6b is that the large dunes resolved by MOLA are fairly symmetrical. In general, transverse dunes have a long shallowly angled stoss (upwind) and a short, steep lee (downwind) slope. The fact that this is not the case on the large ridges in the dark dune field indicates that these dunes cannot be simple transverse ridges. A symmetrical cross section is more consistent with reversing transverse dunes, as suggested by MOC NA images, or with longitudinal dunes.

[51] Another observation made using the MOLA track is that MOLA reflectivity correlates inversely with elevation. That is, the dune peaks are dark and the troughs between dunes are bright. This is well illustrated in a scatterplot of elevation versus reflectivity in Figure 6c, in which high elevations always have low reflectivities but some low areas have relatively high reflectivities. This correlation of bright material in interdune areas is not surprising given the appearance of bright dune forms in these areas. However, arrows in Figures 6a and 6b indicate that this relationship appears to hold true for every dune and trough that is resolved by MOLA, even over the 50 m accumulation of sand in the center of the dune field where bright dune forms are not present. Given this inhomogeneity and the multidirectional wind regime, the central deposit of sand is not likely to be a stratigraphically simple unit. In most cases on terrestrial dunes, grains decrease in size from the base of a dune to its crest [*Lancaster*, 1995], and so this change in reflectivity may reflect a shift in average grain size. If this is the case then there may be two populations of sand: one that is finer grained and dark, and one that is coarser and relatively bright. This violates the classic interpretation of Martian aeolian grains in that dark particles are considered to be sand sized while the bright grains are considered to be finer dust-sized particles. However, interdunes contain sediments that are much more poorly sorted than adjacent dunes [*Lancaster*, 1995], and so the brighter interdunes may merely reflect a higher concentration of bright dust that has not been stripped by saltation. Like many terrestrial dune fields, the interdune areas in the Proctor Crater dune field may serve as a depositional location for fines.

4.1.4. Dune Field Composition From TES Spectra

[52] Figure 7a shows original and modeled spectra averaged from eight TES pixels centered on the dark dune field in Proctor Crater. The TES pixels were chosen from a warm summertime orbit (L_s = 282.6°) with a relatively dust-free atmosphere (ock or orbit 5498, see Figure 7b). The original spectrum measured by TES, in magenta, shows the strong 667 cm^{-1} (15 μm) absorption due to CO_2 gas, a broad absorption between 800 and 1200 cm^{-1} (8–12 μm), and a relatively shallow absorption with small, sharp spectral features below 500 cm^{-1} (>20 μm) due mostly to water vapor. The model produced by the linear least squares fit of the end-members described in section 3.4 is shown in blue. The modeled spectrum closely matches the original spectrum, indicating that the fit is good. The spectral RMS error for the fit is 0.002, a low value for this data set [*Bandfield et al.*, 2000]. The dust opacity for this orbit is 0.12, and the ice opacity is 0.0. Figure 7a also shows the original spectrum with the modeled atmospheric components removed (red) and the modeled surface components only (green). Both of these spectra closely resemble surface type 1 from *Bandfield et al.* [2000], providing a qualitative identification of a

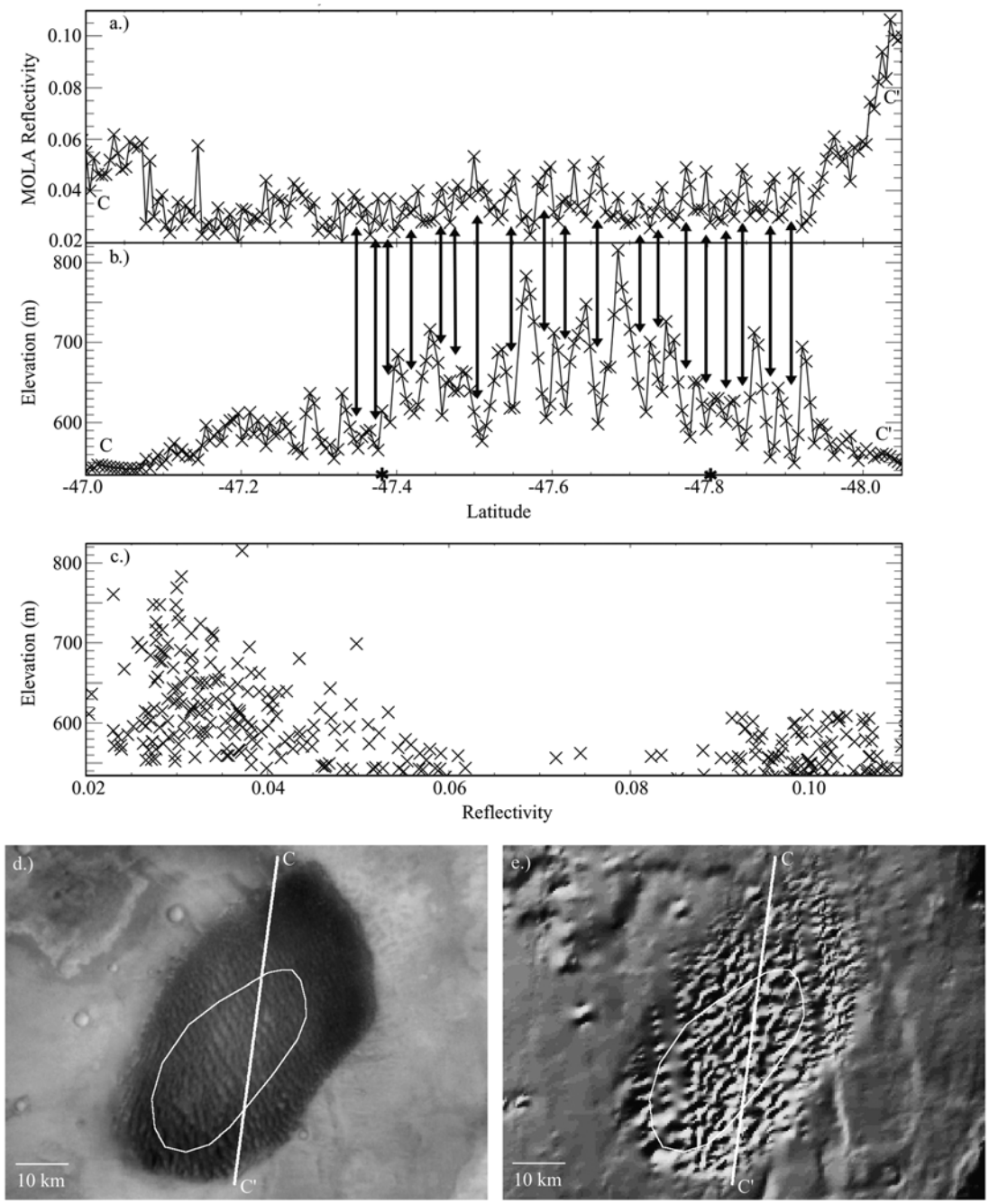

Figure 6. (a) MOLA reflectivities and (b) MOLA elevations for traverse CC′ (shown in Figure 6d.). Bold arrows between Figures 6a and 6b connect the low-lying areas between dunes, all of which correspond to higher MOLA reflectivities. Stars along the latitude axis indicate the edges of the 50 m high sand mound beneath the dunes. (c) Scatterplot of MOLA elevations versus reflectivity, showing that only the low elevations are bright (i.e., are not purely dark sand). (d) MOC wide-angle image of the dune field. (e) Shaded relief based on a 400 m resolution MOLA DEM. In both Figures 6d and 6e the traverse CC and an outline of the sand mound is shown.

composition consistent with basaltic sand. Concentrations from the end-member fit are 66.1% for the type 1 component (basalt) and 7.5% for the type 2 component (andesite/weathered basalt). The concentrations represent the amount of spectral contrast relative to the other end-members used in the deconvolution. The spectral contrast present in the Proctor Crater dune spectra is consistent with that of terrestrial basalt sands [*Christensen et al.*, 2000a; *Bandfield et al.*, 2000; *Bandfield*, 2002].

[53] Figure 7b shows the location of the TES orbit for ock 5498. Concentrations for surface types 1 and 2 along this track are plotted in Figure 7c. The concentrations have been averaged into bins of six pixels to account for any differences in the calibration of the six detectors on TES. Dashed

lines mark the edges of Proctor Crater in Figure 7c, and the edges of the combined dune field and the dark sand streak on its north edge are marked by dotted lines. Because the TES ground track crosses both the dune field and the dark sand streak at an oblique angle, there is an area of transition in Figure 7c from the crater floor to the sand deposits, marked as the light yellow area between dotted lines. The concentration of surface type 1 (basalt) increases over the dunes and the large dark streak, although it appears to be present in lower quantity along the rest of the track across the floor of Proctor Crater. Surface type 2 (andesite/weathered basalt) generally remains at or below the detection limit of ~0.15, indicating that it may not be present at all, although there are a few spots where the concentration climbs to 0.3, suggestive of a small local accumulation or outcrop. Unlike the basaltic component, the surface type 2 profile has no trend along the TES track, indicating that if any such material is present, it does not correspond with the location of the dark dune field or any other surface structure.

[54] Another measurement of use is a simple band index from original TES spectra in a useful wavelength range. *Bandfield* [2000] shows that band indices of spectral types 1 and 2 are simply calculated and compare well to maps produced from the linear deconvolution method. Band indices are affected by changes in elevation and atmospheric interference, and they provide only a qualitative estimate of composition. However, because the calculation for the band index is not subject to sensitive discrimination between different end-members, unlike the compositions derived from deconvolution, the resulting values are less variable from point to point. *Bandfield et al.* [2000] discuss an absorption in type 1 (basalt) spectra from ~200 to 500 cm^{-1}. Although this feature is present in both surface types 1 and 2, the low concentrations of surface type 2 along the single clear track (see Figure 7c) indicate that little if any of this end-member is present in Proctor Crater. In addition, dust accumulations have very low spectral contrast throughout the TES spectral range, which would elevate the emissivity in this wavelength range. Therefore low emissivities in this band index are used as an indicator of surface type 1 (basaltic material) only, and high emissivities are used as an indicator of bright dust. The band index used here to distinguish this feature is the average emissivity of uncorrected spectra between 350 and 450 cm^{-1}. It is this parameter that is mapped in Figure 7b and plotted in Figure 7d. The long wavelength emissivity mirrors the surface type 1 track in Figure 7c, lending weight to the argument that this band index is diagnostic for material having spectra consistent with basaltic sand in this area. In Figure 7b the dune field is well marked by low emissivity (i.e., stronger absorptions). On either side of the dune field there are moderately low emissivities (in violet and blue), indicating an intermediate amount of surface type 1 material in the middle and northern part of the crater floor.

4.1.5. Thermal Inertia of Dark Dunes, Broad View

4.1.5.1. Results

[55] TES thermal inertias over Proctor Crater are shown in Figure 7f. Colors are chosen to represent standard divisions in the Wentworth (phi) scale. The dark dune field displays a distinctive and fairly uniform thermal inertia relative to the surrounding terrain. The mean and standard deviation thermal inertia of the dunes is 305 ± 22 J m^{-2} $s^{-0.5}$ K^{-1}. Using the relation of *Presley and Christensen* [1997a] with a surface atmospheric pressure of 5 mbar, the thermal inertia converts to grain sizes of 1.1 ± 0.3 mm, in the range of coarse to very coarse sand (see Table 1). This thermal inertia is fairly consistent, if on the high end of, previous thermal inertia estimates of the dune sand.

[56] However, uncorrected atmospheric effects must first be considered. In their model, *Mellon et al.* [2000] include thermal radiation from a dusty, CO_2 atmosphere and latent heat from seasonal condensation of CO_2. However, they assume that the atmospheric dust optical depth remains at a constant value of 0.1, normalized to a 6.1 mbar pressure level. During the southern summer, in which the relevant TES data in Proctor Crater were obtained, the dust opacity easily climbs higher than this value, leading to a potential overestimate in thermal inertia values and therefore in effective particle sizes. At the elevation of the dune field, ~700 m above the datum, the dust opacity scales to 0.094. *Liu et al.* [2003] have calculated thermal infrared dust opacities using TES spectra, and so it is possible to investigate the effect of atmospheric dust on thermal inertia calculations from *Mellon et al.* [2000]. *Liu et al.* [2003] calculated 9 μm dust optical depths for TES data for comparison with Viking and Mariner 9 data. Figure 8a shows 9 μm dust opacities provided by J. Liu (personal communication, 2002) over the floor of Proctor Crater during the summer season in which thermal inertia values are available. The optical depths slowly drop throughout the summer season, only reaching values near 0.094 at the end of the summer. Six nighttime tracks of TES crossed the dune field during this season. Their respective thermal inertias are shown in Figure 8b. Of the six tracks, ocks (i.e., orbits) 4425 and 5079 only cross the northernmost part of the dune field. The remaining four traverse the entire dune field, as shown in Figure 7f. Like the dust opacities in Figure 8a, the thermal inertia values drop as the summer season progresses, reflecting the influence of uncorrected atmospheric dust on surface temperatures. The track with the closest correspondence to dust opacities near 0.094 is the last one, ock 5406. Thus the thermal inertias from the

Figure 7. (opposite) Composition and thermal inertia from TES. (a) Results from the deconvolution of TES spectra over the dark dunes. The dune spectra are consistent with basalt spectra. (b) Plot of long wavelength emissivity for a nondusty traverse across the dark dunes. (c) Concentrations of spectral end-members type 1 (basalt) and type 2 (andesite or weathered basalt) across the traverse shown in Figure 7b. (d) Long wavelength emissivity for the traverse across the dark dunes shown in Figure 7b. In both Figures 7c and 7d, dashed lines mark the inner edge of the crater rim, and yellow shaded regions mark the obliquely oriented edge of the dark dune field. (e) Long wavelength emissivity for all summertime ground tracks over Proctor Crater. Variations from orbit to orbit are caused by changes in atmospheric dust content. (f) Thermal inertia of summertime ground tracks over Proctor Crater, binned by effective grain size. The dark dunes have a thermal inertia consistent with coarse to very coarse sand.

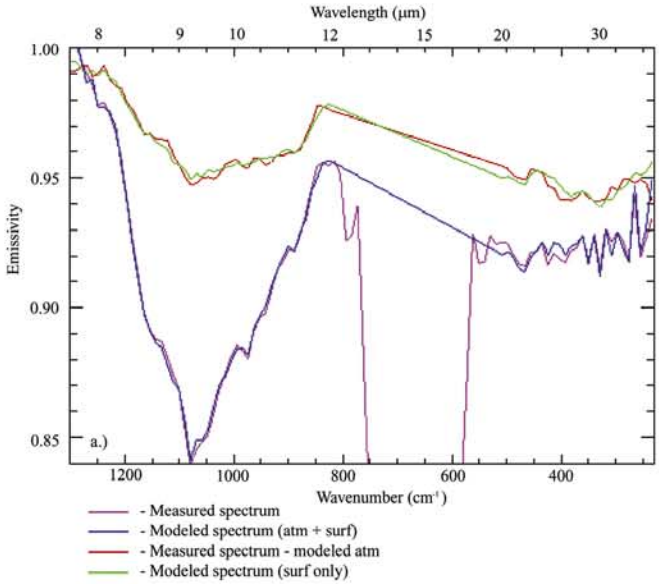
Wavelength (μm)
8
9
10
12
15
20
30
1.00
0.95
0.90
0.85
Emissivity
a.)
1200
1000
800
600
400
Wavenumber (cm-1)
- Measured spectrum
- Modeled spectrum (atm + surf)
- Measured spectrum - modeled atm
- Modeled spectrum (surf only)

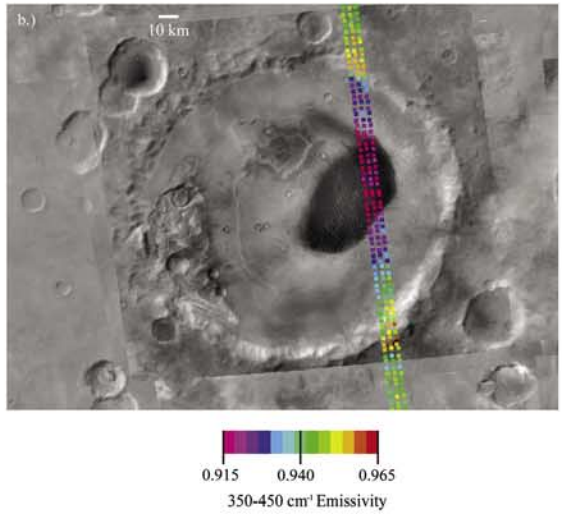
b.)
10 km
0.915
0.940
0.965
350-450 cm-1 Emissivity

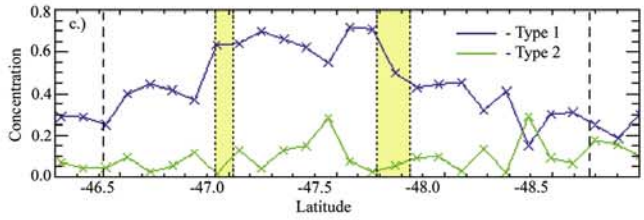
c.)
0.8
0.6
0.4
0.2
0.0
Concentration
- Type 1
- Type 2
-46.5
-47.0
-47.5
-48.0
-48.5
Latitude

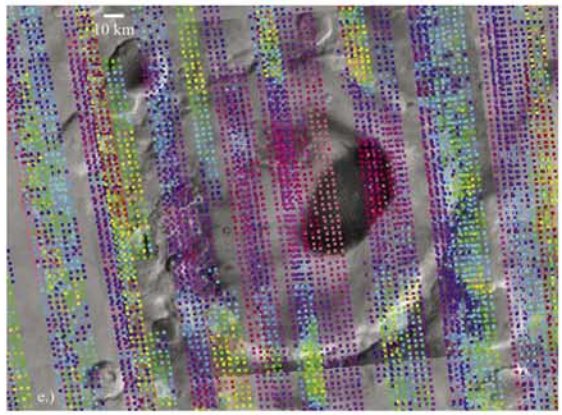
10 km
c.)
0.875
0.915
0.940
0.965
0.985
350-450 cm-1 Emissivity

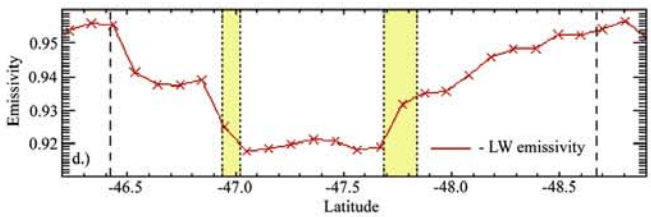
0.95
0.94
0.93
0.92
Emissivity
d.)
- LW emissivity
-46.5
-47.0
-47.5
-48.0
-48.5
Latitude

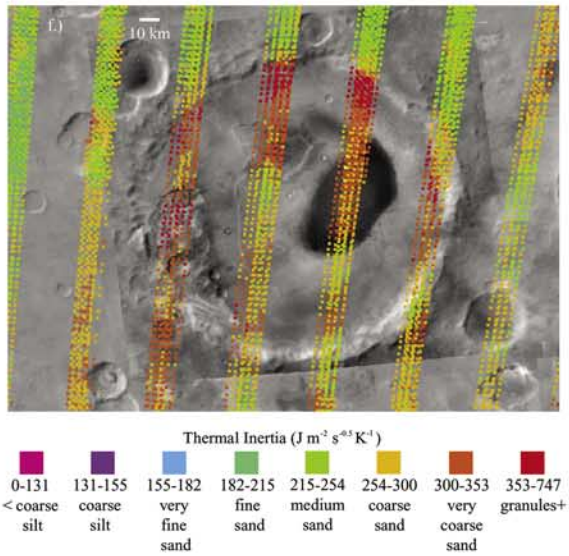
f.)
10 km
Thermal Inertia (J m-2 s-0.5 K-1)
0-131
< coarse silt
131-155
coarse silt
155-182
very fine sand
182-215
fine sand
215-254
medium sand
254-300
coarse sand
300-353
very coarse sand
353-747
granules+

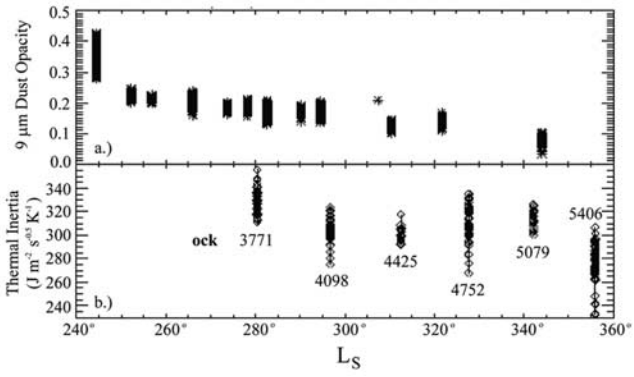

Figure 8. (a) Thermal infrared dust optical depths as a function of season inside Proctor Crater. Note the slow decay as fall approaches. (b) Measured thermal inertias from over the dark dune field as a function of season. Note how the highest thermal inertias roughly correlate with higher dust opacity.

last track are considered the most accurate of the six. The average thermal inertia of ock 5406 over the dune field is 277 ± 17 J m^{-2} s$^{-0.5}$ K^{-1}, leading to a grain size estimate of 740 ± 170 μm. This is in the range of coarse sand (500–1000 μm), which is more consistent with previous work and less surprising than the original estimate of 1.1 ± 0.3 mm.

[57] A second simplification of most previous thermal inertia calculations, including that of *Mellon et al.* [2000], is that they do not account for the effect of slope on surface temperatures. However, dune fields are by definition comprised of slopes of varying degrees and azimuths. Depending on the orientation of the average slope within a TES pixel, the effective surface may be either more or less heated by the sun during the day. Slopes facing away from the sun (southward) will receive less direct sunlight for a shorter time during the day than will sunward facing (northward) slopes. In addition, the excess surface area created by topography will lead to more radiative cooling at night than is accounted for by the current assumption of a flat, horizontal surface. The effect of daytime heating will vary depending on the geometry of the dune field; the effect of nighttime cooling is to slightly lower the measured thermal inertia. At the scale of TES pixels this effect is difficult to estimate, but daytime heating is considered in detail in section 4.1.6.1.

[58] Another possible error may come through the conversion from thermal inertia to effective particle size. The relation of *Presley and Christensen* [1997a] involves surface air pressure, for which we selected a constant value of 5 mbar, chosen from typical summertime values predicted in Proctor Crater by the Mars Mesoscale Model 5. It may be that the model predictions are incorrect, or that the assumed constant value is unrealistic. However, the dependence of thermal inertia on air pressure is not strong. If the air pressure were lower by as much as 1 mbar, which is unlikely, then *Presley and Christensen* [1997a] predict an average grain size of 820 μm corresponding to the measured thermal inertia of 277 J m^{-2} s$^{-0.5}$ K^{-1}. At an air pressure as much as 1 mbar higher, the equivalent grain size is 640 μm. In either case, the estimated particle sizes are still in the range of coarse sand. Thus an incorrect air pressure does not greatly change the estimated particle size.

[59] The packing *Presley and Christensen* [1997a] used in their samples is described as "medium dense", like that of loose sediments on a surface, and not unlike that expected for dune sand. Thus grain packing differences between Martian dunes and their samples do not seem to be an issue. *Presley and Christensen* [1997b] discuss the effect of bulk density on thermal inertia. In their samples, they used spherical glass beads that pack more tightly than angular grains of the same size distribution. A lower bulk density from more poorly packed grains, likely more representative of real dune sand than their glass spheres, produces a lower thermal conductivity and therefore a lower thermal inertia estimate than spherical particles. Thus the measurement of 740 ± 170 μm sized spherical grains may also be explained by even larger angular grains with a lower bulk density, although the transport of larger grains into the dune field would be difficult to explain.

[60] *Presley and Christensen* [1997b] discuss the effect of particle size sorting on thermal inertia. Preliminary studies may indicate that thermal inertia measurements reflect only the largest particles in a sample. If this is indeed the case, then it may well be that the majority of the dune sand is smaller than the observed coarse sand fraction estimated from the thermal inertia measurement. Further work is necessary to determine if this effect is real.

4.1.5.2. Interpretation

[61] A further challenge of the thermal inertia measurement is in its interpretation. *Edgett and Christensen* [1994] point out that the surface grains of dunes may be coarser than the average grains of the dune volume because ripples composed of larger grains tend to form on the surface of dunes. Additionally, it is possible that the thermal inertia measurement of 277 ± 17 J m^{-2} s$^{-0.5}$ K^{-1} actually indicates that the dunes are composed of grains, smaller than the estimated size of 740 ± 170 μm, that are partially cemented. This is consistent with two observations made in MOC narrow-angle images, in which unexpectedly sharp slip faces and landslide scars on the dunes may indicate some amount of induration (see discussion in section 4.1.1). However, the lack of seasonal dust accumulations on the dunes would seem to indicate that the dunes are regularly cleaned of any dust deposits, and therefore that they are active. As suggested in that section, it is possible that a thin top layer of uncemented sand is present and sweeps the dunes clean, while not providing enough of a thermal signal to block an underlying cemented layer of grains. Alternatively, the dune sand may truly be in the range of 740 ± 170 μm, or coarse sand. If this is the case, then interpretations can be made on the nature of the source material. Because of the downwind isolation of a particular grain size in dunes, it is a challenge to determine the size distribution of the source material of the dunes.

4.1.6. Thermal Inertia of Proctor Crater Dunes, Spatial View

4.1.6.1. Results

[62] We have discussed the mean thermal inertia of the Proctor Crater dunes. However, close inspection of particle sizes across a dune field can reveal a pattern that has implications for the history of the dune field itself. On Earth, the finest sand grains are those most easily moved by

the wind. Thus the coarser grains generally remain behind as the finer grains are transported downwind, often leading to a subtle trend across a dune field [e.g., *Lancaster*, 1995]. The Proctor Crater dune field on Mars shows a tantalizing trend in thermal inertia that may be indicative of a progression in particle size.

[63] Figure 9a shows thermal inertia versus latitude for the six nighttime passes over the dune field for which bolometric thermal inertias are available (shown spatially in Figure 7f). For each orbit, each of the six detectors is plotted separately to reduce any confusion caused by calibrational inconsistencies from one detector to another. Two of the passes only cover the northernmost edge of the dune field. The TES tracks cross the dune field at an oblique angle, causing differences in the latitude of the dune field edges. In addition, the tracks vary in length because they cross the dune field at different longitudes.

[64] Figure 9a demonstrates that there is a wide spread in calculated thermal inertia values over the dunes, varying from ~233 to ~355 J m^{-2} $s^{-0.5}$ K^{-1}. This effect is also shown in Figure 8b. The variation from orbit to orbit is far greater than that between detectors within a single orbit. As discussed in section 4.1.5.1, the dominant cause of these variations is in differences in atmospheric dust opacity from one orbit to another. As before, we consider the measurements of ock 5406 to provide the thermal inertias most representative of actual surface properties. These values are replotted on a different scale in Figure 9b.

[65] The thermal inertias of ock 5406 show a clear downward trend from north to south across the dune field, ending in a steep drop at the southernmost edge. The plot also shows effective particle sizes estimated using the empirical relation from *Presley and Christensen* [1997a], assuming a surface atmospheric pressure of 5 mbar. If this trend is real, rather than an artifact of the data or data processing, then it may indicate a change in effective particle size or cementation across the dune field. However, first it must be shown that this trend is a real effect on the Martian surface.

[66] The trend in thermal inertia may be caused by a shift in daytime temperature across the dune field. As discussed section 4.1.5.1, irregularities in the geometry of the dune field could lead to differential daytime heating. One pass over the dune field is shown in Figure 9c. This orbit is the one spatially closest to the nighttime orbits, but it crosses

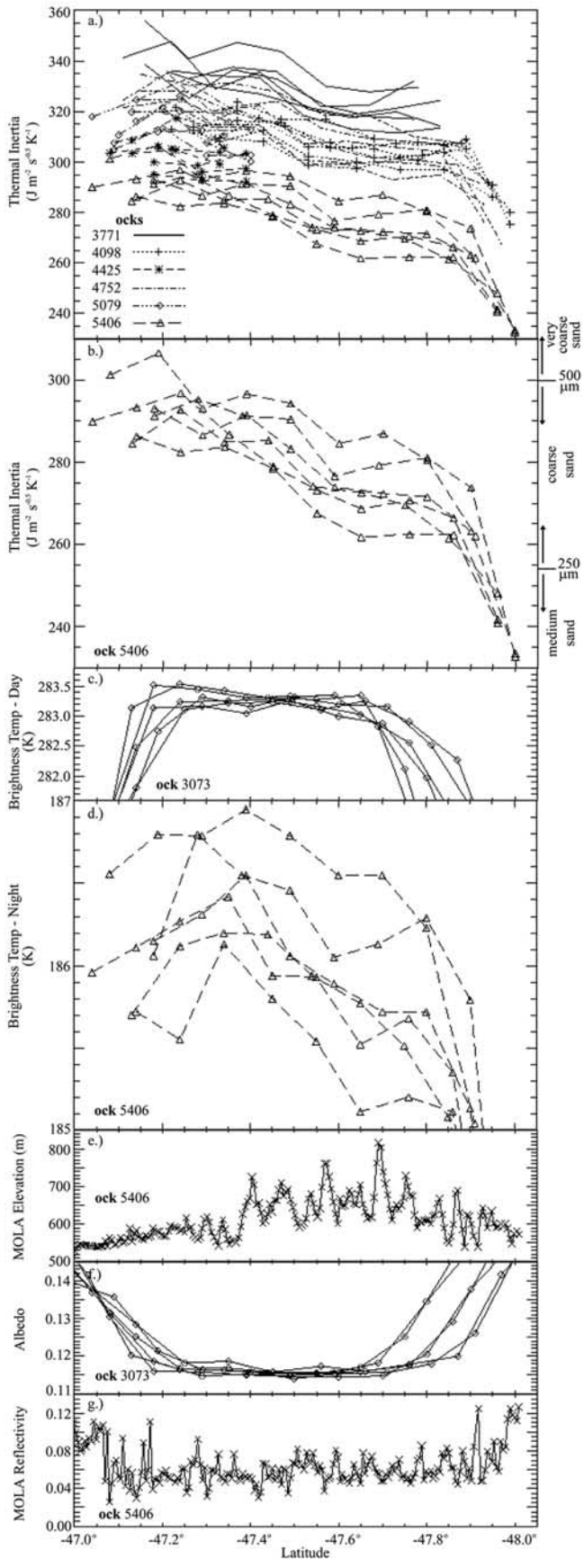

Figure 9. (opposite) Trends in thermal inertia across the dune field. (a) All summertime thermal inertia measurements for each of six orbits (see Figure 8b) and each of six detectors. Note the general downward trend to the south. (b) Thermal inertias from ock 5406 only. Ock 5406 is considered to have dust opacities closest to those used in the thermal inertia calculation, and thus ock 5406 has the most accurate thermal inertia values. (c) Daytime brightness temperatures from ock 3073. (d) Nighttime brightness temperatures from ock 5406. (e) MOLA elevations from ock 5406. (f) TES albedos from ock 3073. (g) MOLA reflectivities from ock 5406. Note that the downward trend in thermal inertia in Figures 9a and 9b do not correlate with any measured parameter other than nighttime brightness temperature, from which the thermal inertias are calculated.

the dune field farther east and at a different angle, leading to a shorter and more northerly track across the dunes than is shown in the nighttime tracks. The daytime temperature clearly peaks over the dunes, which have a low albedo and thus absorb a higher percentage of incident solar energy. At the edge of the dune field the temperatures fall off to reflect the brighter surface of the crater floor. However in the center of the track, from latitude 47.3°S to 47.7°S, the daytime temperatures show little variation. Thus at the scale of TES, there are no observable effects on the surface temperature from any features on the surface.

[67] Nighttime temperatures, on which the thermal inertia values are based, do show a change across the dune field. Figure 9d shows measurements from ock 5406, which clearly shows the downward trend in temperatures to the south. Note that the southernmost measurements are cut off in this plot to emphasize the trend along the remainder of the track. Thus the shift in thermal inertia originated in the surface temperatures in the original measurements from the bolometer. In addition, the southward shift in thermal inertia appears in all tracks crossing the dunes with an L_s range spanning the southern summer (see Figure 9a). This repeatability indicates that the shift is not caused by uncorrected atmospheric effects or a calibration problem in TES, but rather that it is a real phenomenon on the Martian surface.

[68] It is possible that physical factors other than particle size or degree of cementation are affecting the surface temperatures and thus the thermal inertias across the dune field. Figure 9e shows MOLA elevations across ock 5406. Because *Mellon et al.* [2000] correct for elevation using a $1° \times 1°$ MOLA map, the majority of the dune field is assumed to be at a single elevation in thermal inertia calculations. However, the central and southern region of the dune field is actually about 150 m higher than the northern end of the dune field. A lapse rate of −2.5 K/km [*Zurek et al.*, 1992] indicates a mean decrease in air temperature of 0.4 K with an increase in height of 150 m, a value similar to the drop seen in each detector in Figure 9d. Thus it might appear that the gradient in thermal inertias is simply due to a change in altitude. However the sensible heat flux from the surface to the atmosphere on Mars is so small [e.g., *Sutton et al.* [1978], particularly at night, that surface temperatures should not be expected to reflect the ambient air temperature. Therefore the change in air temperature with elevation will not affect thermal inertia calculations.

[69] Thermal inertia is also directly affected by changes in air pressure, and thus with elevation [*Presley and Christensen*, 1997a]. However, the 150 m of elevation change leads to a drop in surface pressure of 1.4%, or 0.07 mbar. A change in air pressure this small has little effect on calculated thermal inertias, and therefore does not explain the change in thermal inertia across the dune field.

[70] It is also possible that a change in surface albedo could cause differences in daytime surface heating and thus create the observed downward trend in thermal inertias. For example, a relative increase in brighter interdune areas toward the southern end of the dune field could lead to lower daytime temperatures, which would in turn lead to the slightly lower nighttime surface temperatures measured by TES. Figures 9f and 9g show surface reflectivity from the broadband visible TES bolometer and from MOLA at 1.064 μm, respectively. The TES track in Figure 9f shows measurements from the same orbit in which daytime surface temperatures were measured (Figure 9c). In the TES track the dune field appears as a consistently dark area with a visible albedo ranging from 0.115 to 0.12. There is no trend across the dune field that corresponds to the nighttime surface temperatures. Likewise, MOLA reflectivity, taken from the nighttime pass corresponding to ock 5406 in Figure 9b, shows a uniform low value across the dune field, save for a few bright interdune spots. The frequency of bright interdune spots remains low and constant, except at the edges of the dune field where the spots become larger and more common. It is clear from both TES and MOLA reflectivities that the drift in thermal inertia is not influenced by a spatial variation in albedo across the dune field. Even if there were some effect from albedo, it should be reflected in daytime surface temperatures, and no such trend appears in Figure 9c.

4.1.6.2. Interpretation

[71] Thus far, effects from dust opacity, atmospheric temperatures, changes in air pressure with altitude, daytime surface temperatures, and both TES and MOLA albedo have been ruled out as influencing the trend of thermal inertias across the Proctor Crater dune field. Therefore the trend in thermal inertia, directly reflected in nighttime surface temperatures, does reflect differential cooling rates of surface materials within the dunes. Several situations could lead to the observed trend.

[72] First, there may be bright interdunes that are unresolved at the scale of both TES and MOLA. These areas may be composed of material that is more indurated and thus effectively has a higher thermal inertia than loose sand. The northern part of the dune field (between −47.0° and −47.4°S) has smaller dunes that are largely unresolved in MOLA profiles (see Figure 9e). This area of the dune field is not superimposed on the broad 50 m thick layer of sand discussed in section 4.1.3, and it may well have a higher percentage of indurated interdune areas. However, south of latitude −47.4°S, where the dunes are superimposed on the layer of sand and where interdune areas are nonexistent, the gradient in thermal inertia continues. In any event, the surface of the crater floor just outside the dune field has lower thermal inertias relative to the dune field (see Figure 7f). Since the interdunes are small exposures of the same lower thermal inertia surface surrounding the dune field, then a higher frequency of interdune areas should decrease the average thermal inertia of a TES pixel, rather than increasing it as is observed.

[73] Second, the degree of dune cementation may vary across the crater. This could be the case if one side of the dune field experienced more frequent winds above the saltation stress threshold relative to the other side. However, the entire dune field seems to be swept clean of bright fines that might otherwise collect on more cemented and thus less active dunes. Furthermore, there is no obvious change in dune morphology across the dune field that reflects any change in cementation (i.e., erosional slumps or sandblasting on solidified dunes). Therefore a change in cementation across the dunes seems unlikely.

[74] Finally, the thermal inertia gradient may be caused by a steady decrease in grain size to the south. If this is the case then this trend has implications for the history of the dune field. Because any such implications on Mars are

almost entirely unknown at this time, studies of terrestrial dune fields will be used as a basis for comparison. In terrestrial sand seas where there is a single upwind sand source and a dominant prevailing wind direction, the sand tends to become both finer and better sorted downwind, reflecting the transportability of smaller grains [e.g., *Lancaster*, 1989]. The dominant wind in Proctor Crater blows from the west-southwest, but the wind regime reflected in slip faces indicates convergent wind orientations. Sand accumulations interpreted in section 4.3.1 as falling dunes and eroded bright dune forms to the southwest of the dune field suggest that the majority of the dune sand was transported into its current position by the dominant west-southwesterly winds. On the basis of terrestrial studies, one would then expect the coarsest grains to be located in the western and southern parts of the dune field.

[75] However, thermal inertias suggest a general fining of grains to the south, which is inconsistent with a possible transport from the west or south. It may be that the secondary (east-southeasterly) and tertiary (east-northeasterly) winds have recently been more dominant, causing the finer grains to move back toward the west and south. MOC narrow-angle images show recent slope adjustments indicative of winds from the east-northeast (shown in Figure 15f–15h, and discussed in section 4.4.2). If these slope adjustments show more than just a seasonal trend that is erased by reversing winds each year, then these winds may have sent the finer grains downwind. It is unclear how readily a shift in prevailing winds could affect the grain size distribution across an entire dune field, but only the top layer of sand is represented in a thermal inertia calculation and thus only this layer need be affected.

[76] Other possibilities explaining a trend in grain size must be considered. In the dunes of the northern Sahara, it has been found that the grain size and dune size are directly correlated [*Wilson*, 1973]. However, measurements from several other dune fields have shown that this relation does not generally hold true [e.g., *Wasson and Hyde*, 1983]. If this translates to Martian conditions, then there is no correspondence between the increasing dune size in the southern part of the dune field and the finer estimated grain size in that area. In any case, *Wilson* [1973] proposed a positive correlation between dune size and grain size, opposite of the effect indicated in the Proctor Crater dunes. Thus the effective grain size across the Proctor dunes likely has little bearing on the pattern of dune size and spacing.

4.2. Bright Dune Forms

4.2.1. MOC Narrow-Angle Images

[77] The locations and orientations of bright bed forms within Proctor Crater have been identified and mapped (see Figure 10a). White boxes outline the locations of narrow-angle images. The bright bed forms are generally only visible in narrow-angle images, and so inferring the distribution of bright bed forms is an interpretation dependent on the spatial coverage of the MOC NA frames. The bright dune forms cover most of the floor of Proctor Crater (e.g., see Figure 3f), including the western and central pits. As described by *Malin and Edgett* [2001], the bed forms are more common in low-lying areas such as small craters and local troughs. This is true on a larger scale as well, because these features are less common on the nearby intercrater plains than they are on the floor of Proctor Crater, which can itself be regarded as a low-lying area with respect to the surrounding highlands (see Figure 1b). The bright bed forms appear to be absent along the northernmost and southernmost rim of the crater floor, although coverage is too poor to determine if this is a trend that spans the entire outer edge of the crater floor.

[78] To determine the average orientation of the bright bed forms, the along-crest directions of 961 bed forms within 22 MOC NA images were measured. The resulting rose diagram is shown in Figure 10b. The bed forms appear symmetrical at this scale, with no obvious upwind or downwind slopes, and thus there is a directional ambiguity of 180°. All directions are therefore constrained to greater than 270° or less than 90°. There are two modal directions that appear in the wind rose: a primary one at 330°–350° and a secondary one at 5°. If these bright dune forms are oriented transverse to the winds that most recently shaped them, as would be the case if they are granule ripples or small transverse dunes, then they reflect winds oriented ENE-WSW and ESE-WNW, respectively. The first of these matches the orientations of dark streaks interpreted as dust devil tracks (discussed in section 4.4.1), and both directions correspond to measured dune slip face orientations (discussed in section 4.1.2).

[79] The bright bed forms on the floor of Proctor Crater display a wide variety of morphologies. Several examples are shown in Figure 11. Figure 11a shows an area southwest of the main dune field in which the bright dune forms appear to be either eroding away or being buried. Arrows point to an example of a crest that appears intermittently. The appearance of this bed form crest could indicate that it has been either degraded by erosion or buried in low places, an ambiguity that is resolved by considering the density of small positive features, interpreted in this work as boulders, in the area (these features are discussed in greater detail in section 4.3.1). Boulders should preferentially disappear under any mantle that might also bury the bright dune forms, but this is not the case in Figure 11a. Rather, these features become more prevalent in areas where the bright bed forms appear less crisp, indicating that the process influencing the bright dune forms is erosion, not burial. It is unclear what process causes the erosion of the bright dune forms, but the fact that not all regions of the Proctor Crater floor show this degradation suggests that this process is local rather than regional.

[80] Figure 11b shows an area south of the main dune field in which two sets of bright dune forms can be seen (indicated by large and small arrows). Figure 11a also shows two sets of dune forms, although they are less obvious. Both sets of bed forms in Figure 11b have sharper crests than those in Figure 11a. Each set of bed forms has a distinct wavelength and orientation. These two sets of dune forms in Figure 11b were produced at different times, possibly under different wind conditions. The smaller set of dune forms must postdate the larger, because they crosscut these larger, more degraded bed forms. The smaller bed forms were likely formed from material eroding off the larger bed forms. Assuming these features are transverse, the larger bed forms were created by winds coming from either the east or west, and the smaller bed forms were produced from winds from either the southwest or the

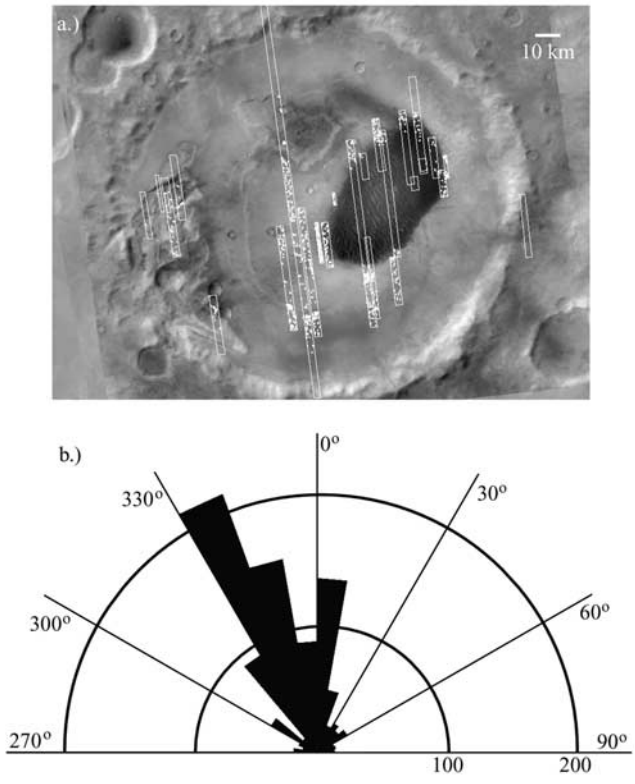

Figure 10. (a) MOC wide-angle mosaic of Proctor Crater. Boxes outline the location of narrow-angle images. White dots locate the bright dune forms on the floor of Proctor Crater, which are generally only visible at narrow-angle resolutions. (b) Rose diagram of bright dune form along-crest orientations. If these features are transverse, the winds that form them are orthogonal to these directions. An orientation of 0° indicates a north-south alignment, while orientations of 90° or 270° indicate an east-west alignment. Because of an upwind versus downwind measurement ambiguity, all orientations are restricted to an orientation of 90°–270°. Note two concentrations of orientations at 330°–350° and 0°–30°.

northeast. This may represent a change in dominant wind directions with time. Alternatively, if the bright dune forms are indeed granule ripples then the difference in characteristic bed form size may indicate either a change in grain size or a change in wind strengths. It is possible that the two sizes of bed forms were created in the same wind regime, even though they are of different ages. In this scenario, the smaller, younger bed forms are composed of smaller grains, and therefore may be formed by relatively weaker winds than the larger bed forms. The larger bed forms may have been created by much differently oriented but stronger wind gusts that were less frequent, but that were strong enough to move the larger grains that form the larger bed forms.

[81] Figure 11c shows bright dune forms just off the eastern edge of the dark dune field. These features appear to be much more rounded than the sharp-crested features of Figure 11b. We interpret this rounding to be from erosion of the bed form crests, in a process distinct from that shown in Figure 11a. It may be caused by wind deflation or abrasion, either of which could preferentially erode crests, leaving behind rounded remnants. The rounded crests also suggest some amount of cohesion in these bright bed forms in that some part of their structure has remained resistant to the process that has eroded them. *Malin and Edgett* [2001] found stabilized dark dunes in the Herschel Basin that also display wind erosion in what may be a process similar to that acting on the bright dunes east of the dark dune field in Proctor Crater.

[82] Previous work by *Malin and Edgett* [2000a, 2001] has demonstrated that the large dark sand dunes on Mars stratigraphically overlie the small bright bed forms where they are found together. In Proctor Crater there is a similar relationship wherever dark dunes and bright bed forms coincide. Figure 11d shows dark sand accumulations (interpreted in section 4.3.1 as falling dunes) overriding bright dune forms in a depression in the western pit. Arrows point to areas where the dark sand, appearing to migrate to the northwest, has piled dark sand against the upwind side of bright dune forms. This demonstrates not only that the dark dunes lie stratigraphically above the bright dune forms, but also that they have been active more recently than the bright dune forms. Figure 11e shows a similar relationship between bright dune forms on the northwestern edge of the main dune field. Here, barchans traveling to the northeast ride over the smaller, bright features. White arrows point to places where dark sand can be seen burying bright dune forms. In the wake of the dark dunes (i.e., upwind of the dunes), the bright features are no longer present, indicating that the passage of the dark barchans disturbs the bright dune forms and erodes them. Similar erosion in the wake of dunes occurs on the eastern side of the dark dune field, demonstrating that at some point dark sand existed to both the east and southwest of the current dune field perimeter. In Figure 11e, a few small darker ripple-like dune forms have reformed on the upwind side of some of the barchans (see dark arrows), suggesting that the process that forms the small bed forms is still active when the proper materials are present. The fact that dark dunes in one part of the crater floor erode bright dune forms as they migrate over them, but in another area have little effect, indicates that there is a spatial variation in either the amount of cohesion of the bright dune forms or the strengths of the winds that saltate dark sand and abrade the bright dune forms.

[83] Within the main dark dune field, the relationship between dark dunes and bright bed forms is more complex. Figure 11f shows both types of features near the eastern edge of the dune field. On the right, dark dunes pass over bright dune forms without influencing their orientations. Farther into the dune field, on the left, the large dark dunes clearly affect the orientations of the small bright dune forms. *Malin and Edgett* [2001] describe the refraction of bright bed forms around topographic obstacles. The same pattern appears to be in effect here, even illustrating Huyguen's Principle by creating hemispherical waves in the wake of two closely spaced dark dunes (see arrows). It seems that at the edge of the dune field, bright bed forms are unaffected, older and possibly more stabilized than the dark sand. However, farther into the dune field the bright bed forms are clearly affected by wind flow around the dark dunes, indicating that the dunes and bright bed forms are coeval. It is possible that inside the dune field, wind gusts accelerate when channeled between dark dunes, causing

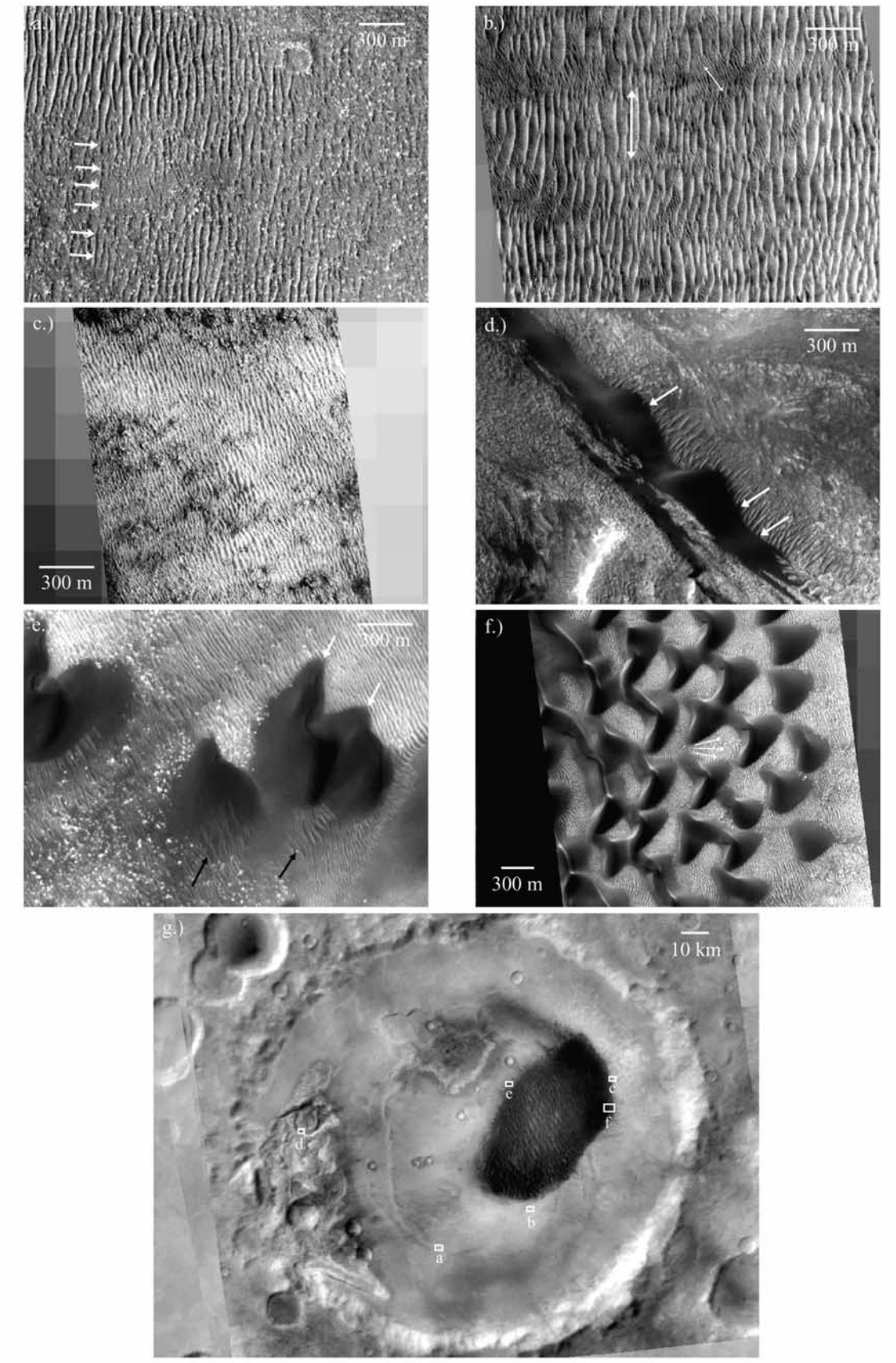
a.)
300 m
b.)
300 m
c.)
300 m
d.)
300 m
e.)
300 m
f.)
300 m
g.)
10 km
a
b
c
d
e
f

winds that are strong enough to reactivate the bright bed forms. This suggests that the bright dune forms, although stable relative to the dark dunes, are not so cemented that they cannot be reactivated by strong winds.

4.2.2. Composition of Bright Dune Forms

[84] The long wavelength emissivities of the Proctor Crater floor, including that of the bright dune forms, are shown in Figure 7e. The regions on the crater floor with bright dune forms are located in areas with low to moderate emissivities, indicative of moderate to strong components of surface type 1 (basalt-like spectra). Most of these areas have a weaker basalt-like component than the dark dune sand. Possible interpretations are discussed below with the thermal inertia results (section 4.2.3.2).

4.2.3. Thermal Inertia of Bright Dune Forms

4.2.3.1. Results

[85] Where bright dune forms predominate, the average thermal inertia (see Figure 7f) appears to be that of medium to coarse sand. In addition, the areas where these bright dune forms are most plentiful correspond to the lowest thermal inertias measured on the floor of Proctor Crater (compare Figures 10a and 7f).

4.2.3.2. Interpretations

[86] High-resolution images of these areas show boulders that could raise the average thermal inertia and dust devil tracks revealing the presence of bright dust accumulations that would lower the average thermal inertia of these areas. The complications caused by these other features make thermal inertia interpretations of the small bright dune forms difficult. As discussed above, the bright dune forms are most likely either small, cemented dunes composed of sand-sized particles or the granule ripples. However, neither their indurated nor their granular nature is demonstrated in thermal inertia measurements, which indicate an effective particle size finer than that in the dark dunes.

[87] Because the bright dune forms are probably not composed of medium to coarse sand, other factors must be considered that would lead to this thermal inertia result. It may be that a layer of seasonal dust fallout partially obscures the surface of the bright dune forms, thereby effectively lowering their thermal inertia. Such a dust layer would be intermediate in the *Pelkey et al.* [2001] terms ''thermally thick'' and ''thermally thin''. If this dust layer is present then the correspondence of bright dune forms with the lowest thermal inertia measurements in Proctor Crater suggests that the bright dune forms preferentially retain accumulated dust relative to the surrounding terrain, perhaps by sheltering dust in the cracks between granules or pebbles. A good test for the preferential accumulation of dust would be to seek progressive seasonal shifts in thermal inertia with increasing concentrations of dust devil tracks. TES and MOC data are too sparse for such a study, but the THEMIS data set could provide such information.

[88] The compositional analysis discussed in section 4.2.2 indicates that many bright dune forms are located in areas with a moderate basalt-like signature. This result is surprising given that it is in an area we have interpreted as partially thermally obscured by dust accumulations. However, dust devil tracks are prevalent over the bright dune forms, exposing parts of the underlying bright dune forms. It is possible that these swaths of uncovered material contribute to the basaltic signature in these areas.

4.3. Proctor Crater Floor

4.3.1. MOC Narrow-Angle Images

[89] High-resolution MOC NA images provide unprecedented detail of the Martian surface that is often surprising when compared with the lower-resolution view. Here, some examples of the various types of terrain on the Proctor Crater floor are shown to emphasize the diversity of surface features in the study area.

[90] Figure 3 shows several high-resolution views of the floor of Proctor Crater. Many characteristics of the surface become evident at this scale. Much of the floor is strewn with small ''bumps'' ranging in size up to 20 m and down to the limit of resolution at 5 m (Figures 3a and 3b). In Figure 3a, the larger ''bumps'' have shadows visible at the MOC NA resolution, indicating that they are blocky, positive features on the landscape. We interpret these ''bumps'' as boulders. Figure 3a also shows drifts of dark sand (see arrows) that partially bury some of these boulders, indicating that the boulders are older than the sand drifts, and that the boulders are taller than the sand drifts are deep.

[91] There is little evidence for extensive fluvial or glacial activity in the crater, and the Proctor Crater walls are generally too far from most of the crater floor to have produced these boulders from mass wasting. Thus we propose that these boulders were emplaced by impact events on the Proctor Crater floor. Boulders produced by crater formation indicate that the surface is consolidated enough to produce coherent blocks that do not shatter or crumble upon landing. Small crater ejecta blankets typically extend out to one to two crater radii, far less than what is necessary to explain the ubiquitous boulder fields on the crater floor given the paucity of small craters present both on the floor of and outside the crater. Thus these boulders could not all have come from outside Proctor Crater. Their high abundance on the floor of Proctor Crater must indicate some process by which boulders accumulate relative to other features, and is considered below with regards to the numerous eroded craters on the crater floor.

[92] There are many small craters in varied states of erosion on the floor of Proctor Crater (Figure 3c). It is

Figure 11. (opposite) Bright dune forms on the Proctor Crater floor. (a) Degraded crests of bright dune forms, with arrows delineating one example (MOC NA M0301614). (b) Two sets of bright dune forms, differing in wavelength and orientation (MOC NA M0802629). (c) Rounded crests of bright dune forms east of the dark dune field, possibly indicating gradual abrasion or deflation (MOC NA M1002249). (d) Dark falling dunes overriding smaller bright dune forms (MOC NA M0300338). (e) Dark barchans overriding bright dune forms. As the barchans pass by, they erode away the bright dune forms, but small ripple-like features reform in the wake of the barchans (MOC NA M1001334). (f) In the interior of the dark dune field, bright dune forms reflect local winds influenced by the large dark dunes. This is not generally the case at the edge of the dune field (MOC NA M1900307). (g) Context for Figures 11a–11f.

tempting to conclude that the subdued appearance of these craters is caused by burial alone, but the ubiquitous boulder fields on the crater floor suggest the situation may be more complex. Dust or sand mantles that bury craters should also bury boulders unless there is a constant supply of boulders. The lack of fresh craters implies that the impact-driven supply of boulders is very slow. Thus we interpret this to mean that the crater floor has undergone extensive erosion and perhaps minor mantling, leaving behind boulders as finer material is blown away, and leading to the highly degraded state of craters observed today. Only deflation by the wind is capable of removing so much material so uniformly across the flat crater floor. Except for the accumulated dunes and bright dune forms, the Proctor Crater floor currently appears to be a landscape dominated by aeolian erosion.

[93] Figure 3d shows an area to the southwest of the main dark dune field, showing dark wind streaks draped downwind of a small crater and a larger relatively bright topographic low that may be a highly degraded crater. Dark streaks such as these may be caused by either the deposition of dark material, such as the dark sand that comprises the dune field, or by the preferential erosion of relatively bright material, such as the material within the bright dune forms. The streaks are aligned with southwest winds, much like the slip faces on dark dunes, suggesting that these features are not only aeolian but they may be produced by the same winds that influence the dune field. If the small bright bed forms in Figure 3d are transverse bed forms, then they are also aligned with this wind. A greater concentration of boulders within the dark streaks relative to the immediate vicinity is consistent with preferential erosion, and so we consider the dark streaks in this area to be caused by erosional stripping of a relatively bright material over a darker, bouldered surface, as opposed to deposition of dark sand.

[94] A close view of the large western pit (Figure 3e) shows that erosion of the pit has revealed terraced material that appears to be layered, sedimentary strata. Some surfaces appear rough and may be exhumed volcanic flows, although any source of lava from within Proctor Crater has since been buried by successive infill of sediments. The layers exposed in the pit may comprise all or part of the ~450 m of crater fill. To first order the strata appear to be horizontal beds, indicating that little deformation or faulting has taken place. In the pits the basin fill material has undergone erosion, possibly by wind action, to expose these strata. This erosion occurred after a period of cratering on the surface of the layered unit, but prior to the passage of dark sand through the area.

[95] Superimposed on the erosional surface are small ripple-like bed forms and larger accumulations of dark sand. The dark sand is mostly piled against cliffs facing north and east, although some sand stretches across the valleys to reach the opposing wall. We interpret the dark sand accumulations as either ''climbing dunes'' or ''falling dunes''. Studies of climbing dunes, falling dunes, sand sheets, and dune fields in the terrestrial deserts such as the Mojave of North America [*Zimbleman et al.*, 1995] and the Sahara [*Wilson*, 1971; *Mainguet and Cossus*, 1980] have led to an understanding of sand transport pathways from the original sand source to the final sand sink. For the first time, satellite imagery of Mars is of high enough resolution to allow a similarly detailed pursuit on another planet. If these sand accumulations are falling dunes, then they are consistent with the prevailing winds from the southwest observed in the dark dunes (see section 4.1.2) and dark streaks (see section 4.4.1). Many areas in the large western pit of Proctor Crater have similar dark sand accumulations. These features may indicate traces of a sand transport path. Perhaps the sand in the large dark dune field in the center of Proctor Crater has traveled from at least as far away as the western pit. If so, then the western pit may be regarded as a potential sand source for the dune material. However, the westernmost edges of the western pit also have accumulations of dark sand, suggesting that the dune sand may have originated from farther away than the western pit. The eastern edge of the western pit is not steep enough to inhibit sand from moving up onto the central crater floor, and so it would not prevent such a transport pathway from existing.

[96] Figure 3h is a mosaic of MOC wide-angle and narrow-angle images that shows a close view of one of the concentric ridges that rings the crater floor. Little of the original structure is obvious at this scale. Small bright dune forms are ubiquitous in this image, although they become larger and sharper immediately south of the concentric ridge. To the north of the ridge, dark patches indicate small accumulations of dark material [*Malin and Edgett*, 2001], possibly the same dark sand that comprises the dark dune field and the falling dunes in the western pit. Both the bright dune forms and the dark sand deposits postdate the emplacement of the ridge; however, the different areas and modes of deposition reflect different conditions under which these features formed. The single deposit of dark sand, trapped downwind of the ridge, suggests that this is a remnant of material that previously swept through the region, originating elsewhere. However the commonness of the bright dune forms indicates that the materials forming these features has not moved on downwind, and in fact they may have formed in place.

4.3.2. Proctor Crater Floor Composition

[97] Figure 7e shows the long wavelength emissivity for all daytime, nadir-looking TES pixels in Proctor Crater with a surface temperature above 250 K. Figure 7e is shown with an extended version of the scale used in Figure 7b. There is a great deal of variation in the long wavelength band index in this data set. Within each orbit, each of which is three pixels wide, there is little variation in dust opacity, so along-track variations in emissivity reflect actual changes in surface composition. However, differences in emissivity from orbit to orbit show the effects of uncorrected atmospheric parameters, especially atmospheric dust. The changes in emissivity from one orbit to another make interpretation difficult, however features persisting from one track to the next are considered real even if their relative emissivities are different.

[98] As with the single orbit shown in Figure 7b, the strongest signals in Figure 7e are those over the dune field and the dark streak of sand emerging northwestward from the northernmost tip of the dune field. There is a general concentration of basalt-like material west of the dune field and in the bottoms of both the western and the central pits, reflected by fairly low emissivities (blue and violet). MOC NA images show that the low-lying floors of the pits

contain some amount of dark dune sand, which are likely responsible for the low emissivities there (i.e., see Figure 3e), although the concentrations may also be indicative of exposed outcrops of more cohesive material in the western and central pit walls. Outside the crater walls, the emissivity rises, indicating the presence of finer, brighter particles. The transition from low to high emissivity is rather sharp along the northern rim of the crater floor, suggestive of a contact between floor materials and intercrater and rim materials. The transition across the northwestern and southern parts of the crater floor is not as well defined.

[99] Much of the area surrounding the dune field, especially to its west, has a fairly low emissivity, indicating a moderate level of basalt on the crater floor. Bright dune forms are absent northeast of the dark dune field but present south of the dune field, and this lack of correlation with composition indicates that these features are not likely responsible for these moderately low emissivities. Boulders are present almost everywhere on the crater floor outside the dune field, including areas of both high and low emissivity, so they also are not responsible for the variation in emissivity. No obvious landform contributes to this emissivity trend.

4.3.3. Proctor Crater Floor Thermal Inertia, Results and Interpretations

[100] Figure 7f shows thermal inertia values across Proctor Crater. The northern region of the crater floor has a high thermal inertia, indicative of a gravelly or well-consolidated surface. The northern rim of Proctor Crater may experience strong drainage air flows during the night during part of the year. It may well be that these areas are scoured clean of loose sediments, as suggested by *Christensen* [1983] for crater floors in Noachis Terra, exposing a rocky or consolidated surface. Indeed the bright dune forms in this area, nearly ubiquitous across the rest of the crater floor, appear to be highly eroded or absent (see Figures 10a and 11c, section 4.2.1). The moderate basalt-like signature in this area, shown in Figure 7e, indicates that this scoured surface could contain some amount of material with spectra consistent with basalt.

[101] Outside the crater rim to the north, the thermal inertia sharply drops to a value consistent with medium sand. This sharp contact may indicate a fundamental change either in the surface or in the wind regime at the edge of the crater. Strong winds would carry any loose sediments across this contact from the intercrater plains to the crater floor, and yet there appears to be no thermally distinct evidence for such transport. Perhaps the most plausible explanation for the sudden change in effective particle size is a change in surface roughness inside the crater. If winds sweeping down the crater rim abruptly encounter a smoother, flatter surface with a lower roughness height, then loose particles will be much more easily lifted into saltation, in turn kicking any dust into suspension, and leaving behind a scoured surface of immobile material that will have a relatively high thermal inertia. These strong drainage flows will also serve to keep new dust from settling onto the surface, which might otherwise obscure this contact.

[102] In contrast with the northern rim, the southern edge of the crater floor grades into the rim and intercrater plains, much as the long wavelength emissivity does in this area. This area has a weaker basalt-like signature than on the rest of the crater floor (see Figure 7e) and no bright dune forms (see Figure 10). The southern rim may be a terrain much like that on the northern edge of the crater floor, only this area does not experience strong nighttime drainage winds that would scour the surface clean. Thus some amount of dust can settle out on the surface here, partially obscuring the higher thermal inertia of the indurated sediments and almost completely obscuring their basaltic signature.

[103] The floor of the large western pit, like the northern part of the crater floor, also has a fairly high thermal inertia. There are known dark sand accumulations, bright dune forms, and abundant features interpreted as boulders in the pit (see Figure 3e), none of which appear to contribute to such high thermal inertia values on the rest of the crater floor. A possible explanation is that the western pit floor is composed of consolidated materials, like that on the northern crater floor. Thus the thermal inertia may indicate that the pit surfaces are largely exposed outcrops of the eroded sediments of the pit walls. The central pit has a slightly lower thermal inertia than that of the western pit, suggestive of more accumulated fines. Much of the exposed materials in the western pit are the terraced sediments comprising its walls and local relief. The surfaces in the western and central pits and along the north edge of the crater floor may be the same sedimentary unit, indicating that the ~450 m of basin fill in Proctor Crater is composed of indurated material. Given the relief and steep slopes evident in Figure 3e, this result is hardly surprising. Combined with the basalt-like signature in the pits discussed in section 4.3.2 and shown in Figure 7e, the correlation of composition with high thermal inertias suggest that the sediments may have a basalt-like component.

4.4. Ephemeral Features

4.4.1. Dark Filamentary Streaks

[104] Of the 26 MOC NA images taken of Proctor Crater before the end of the mapping mission, nine contain dark filamentary streaks that we interpret as dust devil tracks. One summertime image in Proctor Crater (MOC NA E1101316, not shown) shows a small bright spot ~50 m across that is not present in an earlier, overlapping image. This bright spot has been interpreted as an active dust devil by K. Edgett (personal communication, 2003).

[105] Like the features described by *Malin and Edgett* [2001], the dark filamentary streaks are long and thin, up to at least a few kilometers long and 10–50 m wide. *Grant and Shultz* [1987] mapped many similar features on the floor of Proctor Crater, attributing them to "tornado-like tracks". Dust devils are local vortices produced in unstable atmospheric conditions. The Martian surface, which warms up significantly more than the overlying atmosphere, is an ideal place for the forming of dust devils, particularly during the summer when surface heating is at its peak.

[106] These streaks are very similar to the "long dark filaments" first described by *Cutts and Smith* [1973], although they did not attribute them to dust devils. *Grant and Shultz* [1987] mapped these features in a portion of the Proctor Crater floor in both Mariner 9 and Viking images, noting that they appear in midsummer and disappear in the fall, and that their positions change from one year to another. These tracks almost certainly provide information on the orientations of winds of moderate strength. Weaker

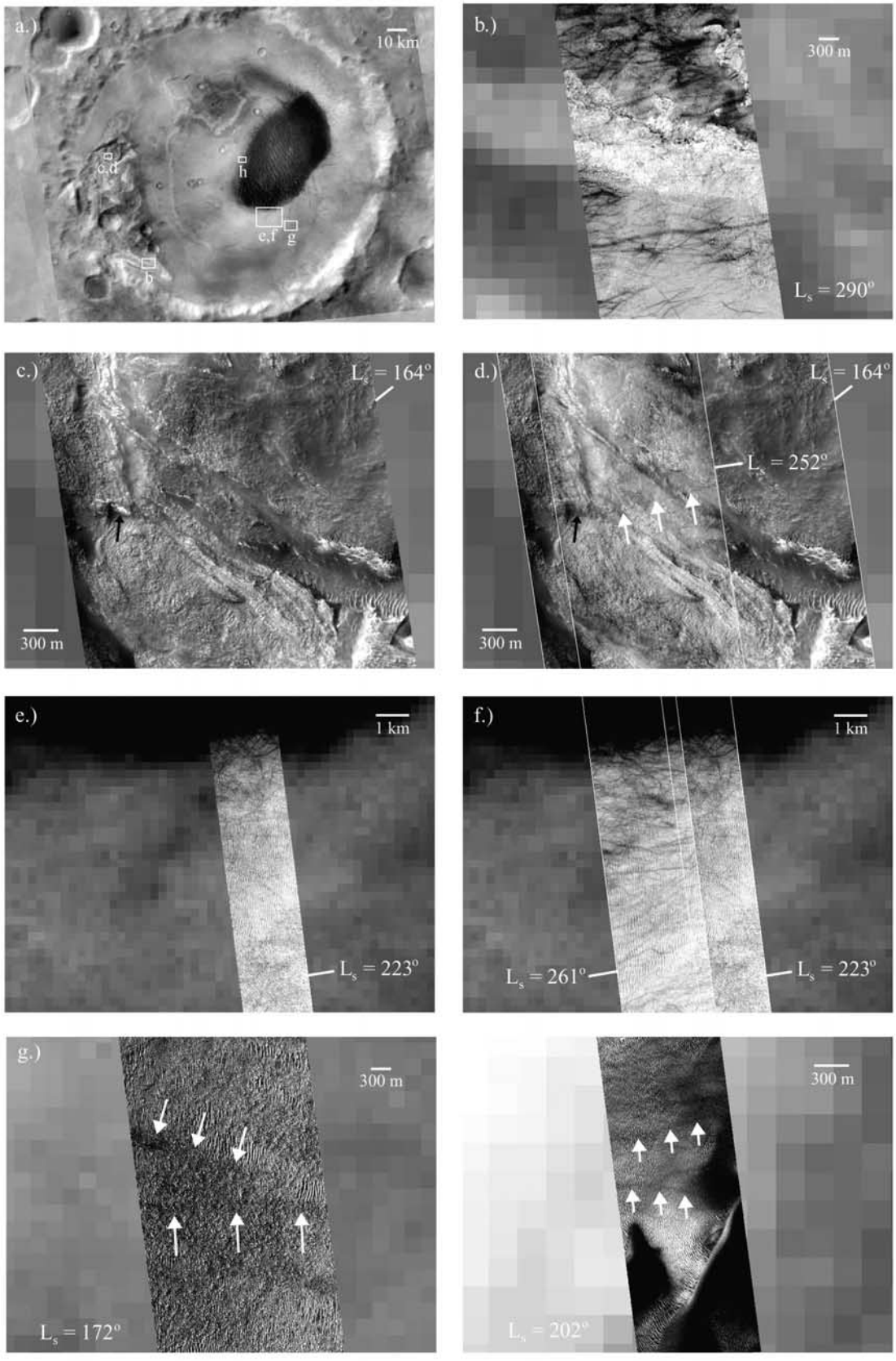
a.)
10 km
c,d
h
e,f
g
b
b.)
300 m
L_s = 290°
c.)
L_s = 164°
300 m
d.)
L_s = 164°
L_s = 252°
300 m
e.)
1 km
L_s = 223°
f.)
1 km
L_s = 261°
L_s = 223°
g.)
300 m
L_s = 172°
300 m
L_s = 202°

winds would not have the strength to move dust devils downwind [*Metzger et al.*, 1999], and very strong winds remove kinetic energy from the boundary layer, preventing dust devils from forming.

[107] All the dark filamentary streaks in Proctor Crater are dark features. If they are dust devil tracks, then their lower albedo indicates that the dust devils that formed them removed or disrupted a relatively bright material from the surface as they passed by. The tracks cross dark sand, bright dune forms, and seemingly bare surfaces. Although there are tracks on dark sand sheets at the edge of the dune field, most dark dunes are free of these features, even in images where the tracks are dense just off the edge of the dune field. This suggests that if dust devils do pass over dark dunes, there is little bright dust present on the surface of the sand to be removed by a passing dust devil. With two exceptions (described below), the tracks are found in images ranging in season from $L_s = 223°–354°$, or from mid spring through late summer. This is the same time of year that they were observed by *Grant and Shultz* [1987] in Mariner 9 and Viking Orbiter images. As discussed in section 4.4.2, seasonal frost begins to appear in Proctor Crater partway through autumn, and remains on shady slopes until late winter. Thus dust devils appear to form and create erosive tracks during the warmest time of year when surface heating is at a maximum and frost is absent.

[108] Figure 3g shows an example of the dark tracks on the wall of the western pit. In this image the lower left corner is high ground. The layers are visible in a steep wall that crosses the frame from the upper left to the lower right. The upper right corner is low ground, and largely covered in bright dust that has been removed in places by dust devils. The dark splotches on the hillside are interpreted as accumulations of dark sand that has been transported into the region from the southwest (lower left), much like the falling dunes of Figure 3e. Some of the dust devil tracks appear to originate in the dark sand, and then to move downwind to the ENE. The surface heating over dark sand will be greater than that over bright dust, and so it is probably easier for dust devils to form over dark sandy surfaces than elsewhere. Further discussions below of dust devils in the vicinity of the dark dune field are consistent with this idea.

[109] Figure 12 shows several examples of dust devil tracks in Proctor Crater. Figure 12a shows the locations of each example. Figure 12b shows several dust devil tracks that are quite apparent when crossing over a featureless surface, but appear only faintly over a nearby outcrop. A few possible scenarios can explain this observed difference. The outcrop may be relatively free of a dust cover that is being removed elsewhere by passing dust devils. Alternatively, the outcrop may be comprised of material with an albedo similar to that of a regional dust cover, so that any removal of dust leaves behind no obvious trail.

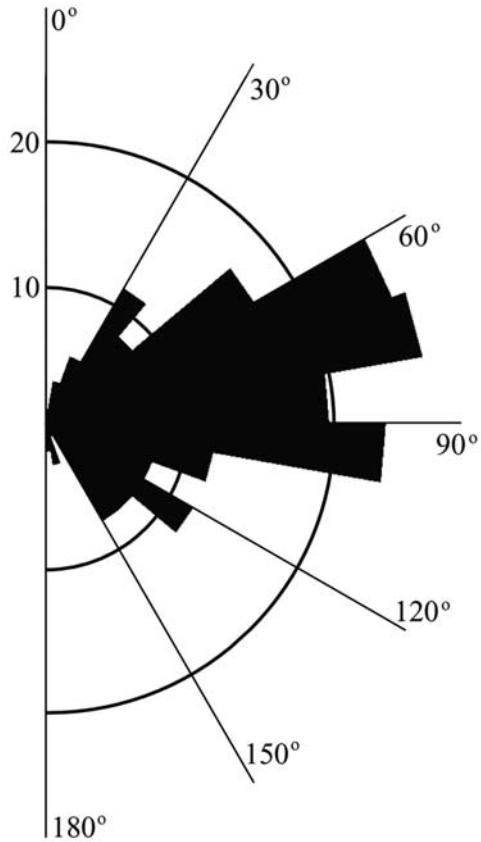

Figure 13. Rose diagram of dust devil track orientations. Orientations of 0° or 180° indicate a north-south alignment, while an orientation of 90° indicates an east-west alignment. Because of an upwind versus downwind measurement ambiguity, all orientations are restricted to an orientation of 0°–180°. Note the two concentrations of orientations at 60°–80° and 90°–100°.

[110] There are two examples of MOC NA frames that overlap, allowing for a study of dust devil development through the spring and summer. Figures 12c and 12d show an example from inside the western pit. In Figure 12c, an image from late winter, there are no signs of dust devil tracks. In Figure 12d, there is one faint track marked by white arrows. It is oriented ENE-WSW. The black arrow shows a remnant patch of seasonal ice on a shady slope that has disappeared by late spring, when the second frame was taken.

[111] The second set of overlapping images is shown in Figures 12e anf 12f, which are located just south of the edge of the dark dune field. In late spring, in Figure 12e, the dust devil tracks are not very abundant and seem to be concentrated near the edge of the dune field. Later in the summer,

Figure 12. (opposite) Dust devil tracks on the Proctor Crater floor. (a) Context for Figures 13b–13h. (b) Tracks crossing a featureless plain but not across a bright outcrop (MOC NA M11-03806). (c, d) Overlapping images in the late winter and late spring, demonstrating the appearance of a dust devil track (MOC NA M03-00338, M09-06250). (e, f) Overlapping images from the late spring, showing a growing number of dust devil tracks (MOC NA M08-02629, M10-01334). (g, h) Images showing potential dust devil tracks in the winter time (MOC NA M03-03087, MOC NA M07-01445), although the faintness of the tracks (images have been greatly stretched) may indicate that these tracks are remnant features from the previous summer season.

in Figure 12f, the dust devil tracks are much more prevalent. Most of the tracks in the overlapping portion of the springtime image are still present in the summertime image, indicating that they are not often erased by strong summer winds. The average orientation of dust devil tracks does not appear to change from one frame to the next, indicating no net seasonal shift in wind direction. This growth in density from spring to summer suggests that the dust devil tracks develop each year and do not persist from season to season. In addition, the dust devils that form early in the season may be more common on the dark dunes than on the rest of the crater floor because the low albedo of the dune sand increases surface heating, possibly encouraging dust devil formation as well. The fact that springtime tracks are not erased by summer winds may indicate either that summertime winds are not strong enough to erode away spring tracks, or that the winds may indeed be strong, but that there is no loose sand available to erode older tracks.

[112] There are two examples of dark streaks observed before the start of the dust devil season, shown in Figures 12g and 12h (white arrows). In each case the image contrast was stretched a great deal to show these features. Both sets of streaks are aligned with most of the other dust devil tracks (see discussion below). Because of the time of year at which these images were taken and the faintness of the features, we suggest that these streaks are old dust devil tracks from the previous summer. If this is the case then they have recently become defrosted. It may be that over the course of the year, dust fallout obscures dust devil tracks so that each spring, the surface presents a ''blank slate'' for dust devils to erode. Perhaps such a process is not always complete, sometimes leaving old tracks incompletely obscured. Alternatively, dust fallout may continue after the time at which these images were taken, obscuring them before the summer season commences.

[113] Only one summertime image on the crater floor contains no dust devil tracks (not shown). This is in the same area north and east of the dune field in which the small bright dune forms appear rounded and eroded (see Figure 11c). It is not clear why dust devil tracks are not produced in this area. If this is a place of constant wind erosion, then there may be no thin layer of settled dust to be lifted by a passing dust devil. Either this is a place where dust is prohibited from settling, perhaps from strong winds, or it is quickly remobilized with a mechanism other than dust devils, such as saltation in local sand sheets. Another explanation may be that there is dust on the surface here, but that there is little contrast between it and the underlying surface. However, thermal inertia calculations, discussed in section 4.3.3, are high enough that there can be very little dust on the surface in this area, supporting the proposal that this area does not accumulate fines. Not surprisingly, the effectiveness of wind action appears to vary spatially across the crater floor.

[114] To determine the daytime wind regime during the summer, the orientations of the most prominent dust devil tracks were measured using an application in Arcview. Figure 13 shows a rose diagram (i.e., a histogram on a polar plot) of the mean orientation of 196 measured dust devil tracks. Because determining the upwind versus downwind direction is impossible from observing most dust devil tracks, all directions shown have been restricted to 0° to 180°. Tracks oriented at 0° or 180° are oriented north-south, and tracks measured at 90° are oriented east-west. One modal direction is evident in Figure 13, with a spread from 60°–100°, or generally ENE-WSW. This is the same main orientation of dust devil tracks mapped by *Grant and Shultz* [1987] in both Mariner 9 and Viking Orbiter images. Because of the dust devil tracks appearing to initiate on the sand patch shown in Figure 3g, we consider these dust devil tracks to be formed by winds from the WSW. This direction also corresponds to the dune orientations observed by *Cutts and Smith* [1973], as well as those measured in this work, as discussed in section 4.1.2.

[115] The orientation measurements of dunes and dust devil tracks have several implications. The persistence of dust devil track orientations from one mission to another indicates that daytime summer winds are very consistent in direction. Because the dunes in Proctor Crater are so large, they have a long memory, and thus reflect the prevailing winds over at least several decades, and possibly over the last million years (assuming that they are active). The correspondence of dust devil tracks to dune slip face directions indicates that these wind directions have been very typical of this area in the summer for some time. Furthermore, dunes require winds above the saltation threshold to shape them, but dust devils may move under lighter winds (*Metzger et al.* [1999] estimates that ~5 m/s winds will move dust devils), and so this alignment indicates that both strong and moderate winds blow in this direction.

4.4.2. Frost Features

[116] *Malin and Edgett* [2001] studied the frosting and defrosting of dunes at both poles. They found that the dunes are generally the first features to develop frosted surfaces during autumn, and they are the last features to lose frost in the spring. They suggest that Martian dunes may trap volatiles, much as *Sharp* [1966] found that the Kelso Dunes of the Mojave Desert trap water. In addition, *Malin and Edgett* [2001] found that defrosting tends to begin with small dark spots commonly located at the dune margins, which enlarge slowly and coalesce until the entire dune surface is defrosted. They proposed that dark sand beneath thin bright frost accumulations warms more quickly than in other areas, causing the frost to sublimate in patches. Little is known about the relationship between frost and dune sand on Mars, but the MOC narrow-angle images indicate that the interactions are complex and certainly worth further study.

[117] Although Proctor Crater is located in the midlatitudes (47°S), rather than near the poles, the region is covered in seasonal frost each winter. Thus the numerous images of the dune field provide an opportunity to compare how these dunes frost and defrost relative to the polar dunes. MOC narrow-angle images show that frost cover begins in mid southern autumn, at approximately $L_s = 50°$, and remains in patches on the dunes until late winter at approximately $L_s = 165°$. Because Proctor Crater is located in the midlatitudes, the seasonal frost cover does not last as long as it does closer to the poles. Image coverage during the southern fall is too sparse to determine if the dunes acquire frost before the remainder of the Proctor Crater floor does, as is expected. However, poleward facing slopes on the dunes are certainly the last surfaces to defrost in late

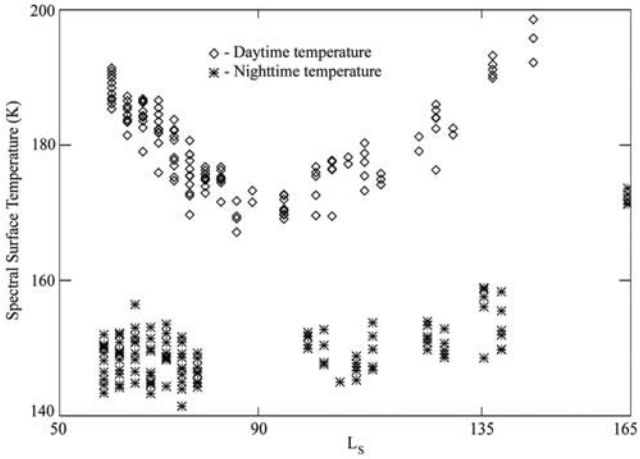

Figure 14. Spectrally derived surface temperatures from TES over the Proctor Crater dune field. The temperatures are separated into day and night measurements, and they are plotted as a function of season during the winter. Nighttime temperatures indicate the presence of CO_2 frost, but daytime temperatures are too warm for CO_2 frost. Thus the seasonal frost visible in MOC NA images is interpreted as H_2O frost that survives during the day.

winter, consistent with the observations of *Malin and Edgett* [2000b].

[118] It is not clear from MOC NA images whether the seasonal frost is CO_2 or H_2O ice, or some combination thereof. Figure 14 shows spectrally derived surface temperatures from TES over the Proctor Crater dune field within the solar longitude range that frost is apparent in MOC NA images. *Bandfield and Smith* [2003] show that these temperatures in a fairly nondusty atmosphere should be no more than ~2 K lower than the actual surface temperature. Nighttime temperatures in Figure 14 remain close to the CO_2 frost point until about $L_s = 135°$, indicating that CO_2 frost probably forms on the surface of the dunes during the winter night. However, the daytime temperatures only drop down to 170 K, right at the winter solstice ($L_s = 90°$), indicating that CO_2 frost is unstable on the dunes during the daytime. We interpret these data to indicate that the frost that is visible in the MOC NA images, which were obtained during the warmest time of day, most likely show a thin veneer of H_2O frost that persists throughout the day, while CO_2 frost forms at night and sublimates the following day.

[119] Figures 15a and 15b show overlapping images during the late winter from two consecutive years. Each image shows partially defrosted dunes within the Proctor Crater dune field with dark spots similar to those found by *Malin and Edgett* [2000b]. Interpreting images with partial frost cover can be tricky, because features can appear bright from either frost albedo or incident sunlight. Determining whether an area is inherently bright or only apparently so from shading differences requires experience with viewing several MOC images, preferably over different seasons and under different lighting conditions. Figure 15c shows an interpretation of the features shown in Figure 15b, built from such a knowledge base. Dune crestlines refer to linear peaks of dunes. Slip faces generally begin from these crestlines, but not all slopes that reach to the crest are necessarily slip faces. Bright dune forms are located in the interdune flats and thus represent low-lying areas. Slope or slip face adjustments, as defined here, are avalanches of sand that has been oversteepened by the wind at the brink of a dune. Such slope adjustments are generally oriented downhill and are good indicators of the local gradient. The patchy seasonal frost remains in low-lying areas and on the southern and western sides of dunes. Shadows are located southeast of dune crests, created by a low winter afternoon sun to the northwest.

[120] The Proctor Crater dunes develop dark spots as they defrost that persist in location from year to year (e.g., compare Figures 15a and 15b). The repetitiveness of dark spot locations indicates that their position is dependent on some relatively stable aspect of the dune surface. Unlike the dark spots on polar dunes, the dark spots on the Proctor Crater dunes are concentrated on steep slopes, rather than along the dune margins. In addition, these features rarely appear on hills facing any direction but toward the pole. The largest spots in Figures 15a–15c contain bright cores, which have not been observed in polar dunes. The cores are brighter than frost on the surrounding slope, indicating that this material is not simply a remnant frost patch from the previous uniform cover. *Bridges et al.* [2001] found that dark spots located in small gullies on Mars, similar to the spots on the dunes, are aligned with the local dip and channel trend (i.e., downhill along the channel). In contrast, the spots in the Proctor Crater dunes appear to be aligned either along the strike of the south facing dune slope or parallel to the crest.

[121] There are a few possible explanations for the presence and location of the dark spots. The spots may be associated with granule ripples that can form on dune slopes. However, in areas where there is summertime coverage of slopes that form dark spots while defrosting, there is no evidence for any features on the smooth dune slopes. Furthermore, there is no physical reason why granule ripples would preferentially form on pole-facing slopes, as the dark spots do. Another idea is that the dark spots are small avalanches over the seasonal frost cover, although no known mechanism causes slope adjustments to form in the same locations in the middle of dune slopes year after year. Finally, it may be that the dark spots are concentrated along interfaces between exposed dune strata. Wind erosion on terrestrial dunes often exposes the internal dune strata. Furthermore, water ice tends to accumulate along strata interfaces in terrestrial dunes. Snowfall can form icy strata within the dune that persists from year to year [e.g., *Calkin and Rutford*, 1974]. A similar process could occur on Mars with either H_2O or CO_2 ice. If this occurred, then insolation would warm the exposed sandy strata more than the nearby exposed icy strata. This could easily cause reprecipitation of sublimating frost onto the exposed icy strata, creating the bright cores of the dark spots seen in Figure 15b. This mechanism is similar to that proposed by *Malin and Edgett* [2000b] to explain bright frost halos around dark sublimation spots.

[122] Alternatively, the dark spot cores could brighten as wind blows frost from elsewhere into small cracks that are exposed by defrosting, such as the process described for polar "spiders" by *Piqueux et al.* [2003], although summertime

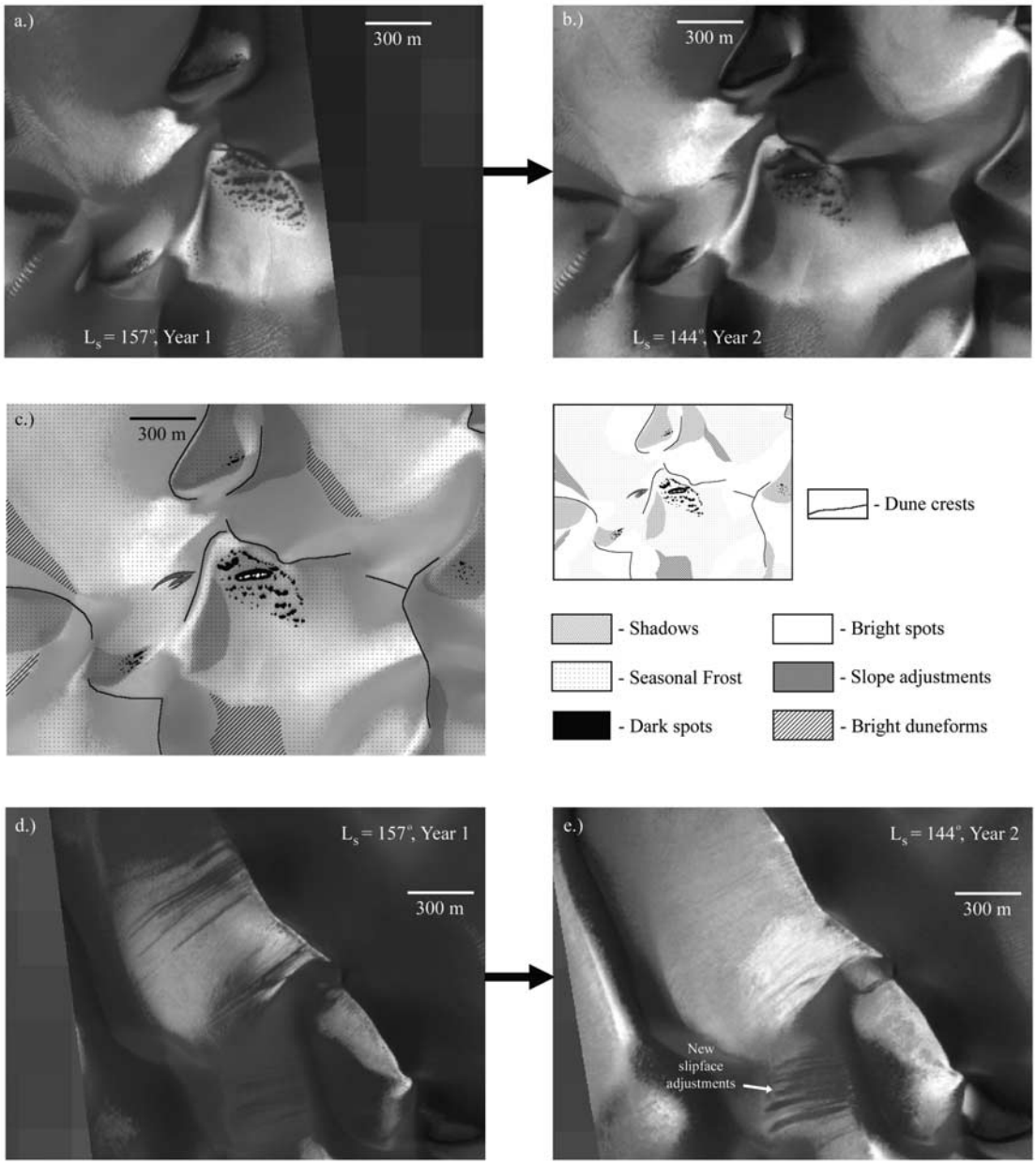

Figure 15. Frost in the dark dune field. (a, b) The same area nearly 1 Martian year apart. Defrosting spots occur in the same locations, suggesting that they are produced by some underlying persistent aspect of the dunes (MOC NA M02-02711, E03-01039). (c) A diagram of the features in Figure 15b. (d, e) The same region nearly 1 year apart, with new slip face adjustments formed within the year (MOC NA M02-02711, E03-01039). (f–h) Sequence of images over the same area of the dune field, each showing slope adjustments that persist for at least 1 year. Figure 15f is a late winter image of year 1, where such adjustments appear to be superimposed on seasonal frost, giving the impression that they are fresh features (MOC NA M02-02711). Shortly after the frost has disappeared from the slope (Figure 15g), the same adjustment scars are still visible (MOC NA M03-03088). Nearly a year after the first frame (Figure 15h), when the frost has reformed, the slope adjustment scars are still visible, giving the impression that they are recent movements over the seasonal frost. Rather, they must be somewhat older features that inhibit frost formation or allow frost to sublimate more easily (MOC NA E03-01039).

images of dune slopes show a surface devoid of any obvious roughness that could trap windblown ice grains. The melting of snow lenses trapped in terrestrial dunes is known to create unusual surface features, such as small sinkholes and tensional cracks [*Koster and Dijkmans*, 1988]. However, there is no such known process on Mars, where ice trapped in dunes may never melt.

[123] Since these dark spots mostly form on the shaded slopes and manage to persist much longer into the season than on other slopes, the frost may have enough time to

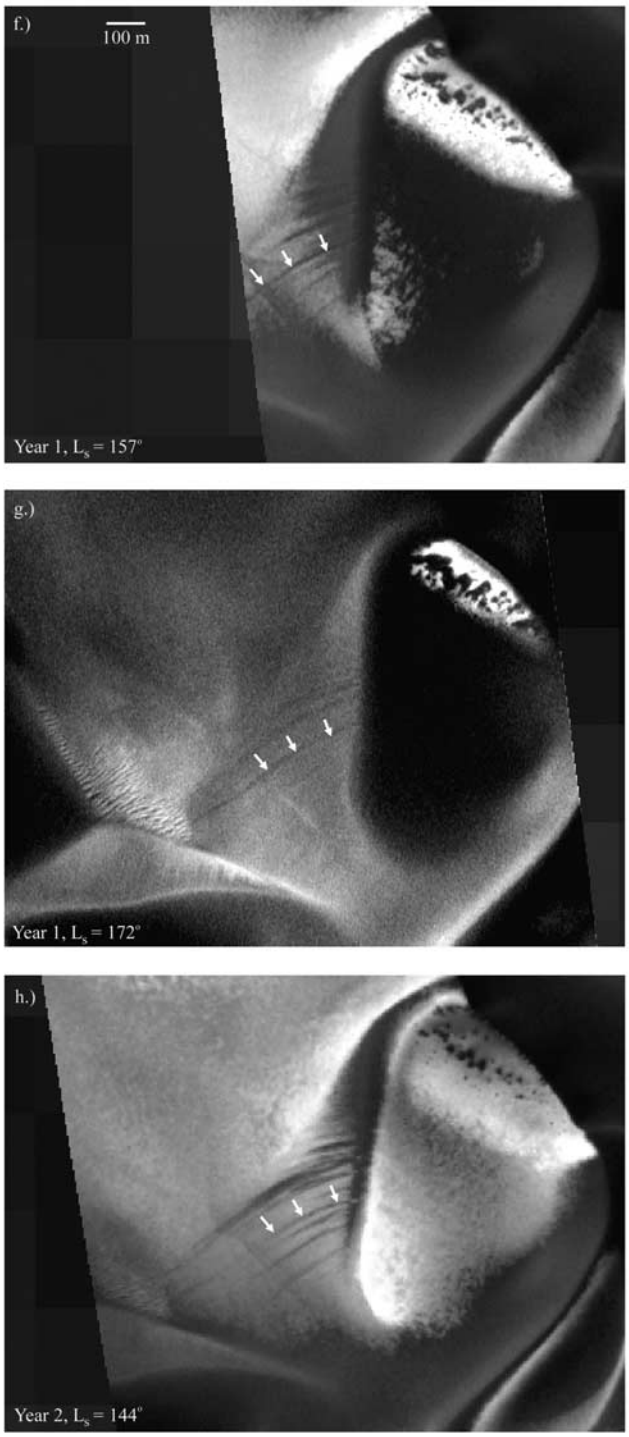

Figure 15. (continued)

undergo sintering caused by compaction and grain growth in a process modeled by *Eluszkiewicz* [1993]. Thus preferential sublimation may occur from differential ice grain growth, in which transparent areas absorb more heat from insolation and sublimate faster than opaque areas. This process may in turn be influenced by ice trapped in underlying exposed dune strata. For example, the weight of frost overlying an exposed icy layer between sandy strata may compact some of the upper icy layer enough that it sinters into larger grains, which become more transparent to sunlight as they grow. As the frost slowly thins from sublimation, this relatively transparent layer becomes more and more exposed to daily heating until enough heat is collected to begin localized sublimation. There is no reported terrestrial analog for this process, or for defrosting spots on sandy surfaces such as these. This process is similar to that suggested by *Malin and Edgett* [2000b] and *Bridges et al.* [2001] to explain dark sublimation spots. In the case of the Proctor Crater dunes, sintering in icy dune strata may explain the alignment of dark spots along the slope of the dune. The presence of ice strata may also explain the bright cores, as icy strata may be cold enough to cause reprecipitation of locally sublimating frost, once the initial wave of defrosting has occurred and swept outward from the center of the spots.

[124] *Edgett and Malin* [2000] show slip face adjustments in Proctor Crater dunes and propose that they are fresh movements over seasonal frost. However, as they consider, and as discussed below, such slope adjustments may not be as fresh as they appear. Fortunately, there is evidence suggesting that the dunes in Proctor Crater are active from year to year, although the season in which these movements occur is not constrained. Figures 15d and 15e show the same area roughly 1 year apart. Figure 15d is the same area shown in Figure 17 of *Edgett and Malin* [2000]. In the first frame a frost-covered slope shows superimposed dark tongues of sand that are typical of dune slip face adjustments from easterly winds. In the second frame, taken nearly 1 year later, seasonal frost has since sublimated away and reformed on the dune field. The slip face features of the previous year are barely discernable beneath the recent year's frost accumulation. However, new dark tongues of sand have formed farther south, overriding some older scars that are faintly visible in the first frame. In both cases the sand-moving winds come from the east. These dunes are without question active with fresh slip face scars forming each year. However, these movements do not appear to be very common, as not all of the slope adjustments of the previous year are buried by subsequent activity.

[125] There is enough coverage over enough time to show that some slip face adjustment scars remain for at least a year, and that they therefore may superimposed on annual frost cover as suggested by *Edgett and Malin* [2000]. Figure 15f–15h show the same area at three different times, each showing the same set of slip face adjustments. Figure 15f was taken during the time of partial frost cover, in late winter. Arrows point to a prominent dark slope adjustment lobe that appears to have formed over the frost. Figure 15g shows the same area later that year, when most of the frost has sublimated away. In this frame, most of the bright surfaces are sunlit slopes, whereas in Figure 15f most of the bright surfaces are frosted slopes. Even though the frost is gone, the dark stripes from slip face adjustments are still visible. The following winter, in Figure 15h, the same dark slope adjustments are still visible, although a new larger and darker scar has formed nearby in the intervening year. It appears that although these features appear to be superimposed on seasonal frost, they are not. Some aspect of the nature of these scars inhibits frost from forming, and/or allows frost to sublimate more easily than on the surrounding slopes, making them appear dark relative to the ice-covered slopes. Slip face adjustments loosen the

surface material, and it may be that these less densely packed surfaces expose more surface area to the air and thus allow frost to sublimate more quickly than on a more densely packed surface. The assessment of frost features on the Proctor Crater dunes reveals more about the nature of the dunes than it does about the frost that covers them.

5. Discussion and Proposed Geomorphic Sequence

[126] This study has led to an understanding of the sedimentary history of the interior of Proctor Crater. Each of the different data sets incorporated into the GIS has provided a unique set of information about the surface of the Proctor Crater floor. Here are speculations on the implications of the observations, presented in chronologic form so that results from each data set are integrated into a single consistent history.

5.1. Crater Formation and Basin Fill

[127] Proctor Crater was formed during the period of heavy bombardment. It is 150 km in diameter, in the size range of peak ring basins. Wall slumping is expected in a crater this size, although currently no such features are visible.

[128] After the crater was formed, up to 450 m of layered sediments filled the crater basin. These deposits have a thermal inertia consistent with indurated material and a partially basaltic composition. Much of the material is hard enough to produce boulders upon impact, but friable enough to be eroded by the wind. The sediments could be lake deposits or fallout of aeolian material, possibly volcaniclastic. Some volcanic flows may be interfingered with the aeolian deposits, although evidence for them is difficult to establish in the images.

[129] After the sediments were emplaced, further small impacts bombarded the Proctor Crater floor, producing small craters with associated boulder fields. Today these craters are in varying states of erosion, some of which are barely discernable. Ubiquitous boulder fields with no apparent source crater hint at a large quantity of long erased craters, indicating that a great deal of the fine sediment on the crater floor has been stripped away by the wind.

5.2. Origin of the Basin Fill

[130] The high thermal inertias of the pits and northern crater floor coupled with their moderate basalt-like signature may have implications for the origin of the sedimentary deposits filling Proctor Crater. *Malin and Edgett* [2000a] proposed that sedimentary layers deposited elsewhere were produced by one of two processes: either they collected as lake sediments in low-lying basins, or they were transported by the wind through suspension to their current location. Either hypothesis may be considered for the layered materials in Proctor Crater.

[131] If a lake ever stood in Proctor Crater, then it would have been ~150 km in diameter, and it would have to have survived long enough to deposit ~450 m of sediments. If the sedimentary layers in Proctor Crater were deposited as lakebeds then some amount of the basaltic material may have been aqueously altered. *Wyatt and McSween* [2002] reinterpreted the "andesitic" surface type 2 of *Bandfield et al.* [2000] as low-temperature aqueously altered basalts. However, very little of Surface type 2 is found on the crater floor (see Figure 7c). Rather, the areas on the crater floor and in the pits interpreted as swept clean of fines have a signature consistent with some amount of unaltered basalt. If these interpretations are correct, then they lend weight to the perspective that at least some of the layered sediments on Mars were not emplaced aqueously. However, it should be emphasized that such alteration rates are not yet well constrained.

5.3. Formation of the Western and Central Pits

[132] Two large pits have been eroded out of the sedimentary layers filling the floor of Proctor Crater. The larger of the two, the western pit, covers approximately one tenth of the crater floor and reaches to a depth of 1 km. The pits were likely eroded by aeolian abrasion and deflation, although there may have been weakening from below, for instance from underground water, that contributed to the erosion of these features. Large craters on the western side of the Proctor Crater floor may also have initiated the weathering process that produced the western pit, although this hypothesis seems unlikely because no such craters are present near the central pit.

[133] Layers exposed in the walls of the western pit provide evidence for the former accumulation of sediments. Steep slopes in the walls and thermal inertias consistent with consolidated material suggest that the sediments are highly indurated. Indeed, the presence of boulders most likely produced by impact onto the surface of these strata indicates that highly consolidated material and possibly clasts are present. The composition of the floor of the western pit has a basalt-like component. Although accumulations of sand are present, they do not dominate the interior of the pit, and therefore this compositional signature is probably indicative of basalt-like material in the ~450 m of sedimentary layers.

5.4. Bright Dune Forms

[134] After and perhaps during the erosion of the pits, small bright bed forms appeared throughout the crater floor. These features are superimposed on pits and craters, and thus postdate them. They are much more common on the Proctor Crater floor than the surrounding intercrater plains.

[135] Although many aspects of the bright dune forms are unresolved, it is possible to speculate on the origin of these features. The widespread presence of these dune forms throughout the crater floor, their apparent difficulty of mobilization, as well as the lack of transport pathways of bright material into the crater, suggests that these features were produced from local material. The numerous boulders and degraded craters on the floor of Proctor Crater indicate that a large amount of material has been stripped off the surface, some of which accumulated into these bright bed forms. In contrast, the dark dune field is localized in the center of the crater floor, with indications of a transport pathway from the southwest. Because some of the bright dune forms are eroded by the passage of the dark dunes, the bright dune forms must have accumulated and become relatively immobile before the dark sand accumulated in Proctor Crater.

[136] These dune forms may be either small dunes composed of bright sand, or ripples composed of larger grains. Thermal inertias of these features are consistent with medium sand, but their eroded nature and lack of movement with respect to much larger, dark dunes suggests that if they are dunes then they must be at least partially cemented. It is possible that dust fallout, etched by the plentiful dust devil tracks that form every summer season, obscures the true thermal response of the material comprising the bright dune forms. It is also possible, that, if these features are granule ripples, they are composed of a mixture of fine and coarse materials that can produce a thermal inertia consistent with medium sand.

[137] Some of the bright dune forms have rounded crests and eroded structures, indicating that in places they may have become cemented. However, in the interior of the dark dune field, the orientations of these bed forms are strongly influenced by the presence of the large dunes. In addition, they can reform after a dark dune has passed by, as the dark dune slowly destroys the older bright dune forms it encroaches on. Thus the processes and materials that produce bright dune forms are probably still active today. These recently influenced or newly created bed forms are less likely to be cemented than their older, eroded counterparts. However, these young bright bed forms also move more slowly than the large dark dunes, like the older bright bed forms, which is not expected if any of the bright bed forms are dunes as well. Therefore the bright dune forms are probably granule ripples rather than dunes.

5.5. Origin of the Dark Dune Sand

[138] Some time after the bright bed forms were established on the Proctor Crater floor, dark basaltic sand accumulated in the center of the crater floor. Several other craters in Noachis Terra also contain large dune fields of dark sand, which may have been emplaced concurrently with the sand in Proctor Crater. It is possible that the dark sand dunes may be contemporaneous with the bright dune forms, and that these two types of bed forms may have eroded from a single sedimentary source material. However, there is a trail of dark sand accumulations and eroded landforms leading from the southwest on the Proctor Crater floor, and there is no evidence of any other dark sand movements leading to the dark dune field. In contrast, the bright dune forms cover most of the floor of Proctor Crater, with no indications of any prior material transport. Furthermore, there is ample evidence that the dark dunes are superimposed on the bright dune forms. We interpret this disparity to indicate that the bright bed forms formed in place with material eroded from the Proctor Crater floor, and that at a later time, the dark sand comprising the dune field accumulated in the center of the crater after transport from the southwest.

[139] The range of particle sizes that are observed in a dune field must also be present in its source material. In order to put constraints on potential sources of sand in Proctor Crater, all possible sources must be considered. Experimental work intended as a study of the lunar surface showed that roughly 5% of the impact ejecta from a basalt surface is composed of grains in the range of coarse sand (500–1000 μm) [*Gault et al.*, 1963]. Actual lunar soil samples, created by impacts and subsequent bombardment ranged in mean particle sizes from 380 μm down to 32 μm [*Lindsay*, 1976]. He proposes that soil grains decrease in size with age as continual impacts pulverize the surface material into increasingly smaller and well-sorted particles. Recent calculations of impact gardening on Mars indicate that since the Noachian era several tens of meters of regolith should have been produced by the constant bombardment of small impactors [*Hartmann et al.*, 2001]. However, only the least exposed surfaces would have created particles in the size range of the coarse sand grains in the Proctor Crater dunes, because according to the reasoning of *Lindsay* [1976], surfaces exposed to more bombardment would accumulate successively finer soils less likely to contain the coarse sand now present in the Proctor Crater dune field. However, before reaching this steady state of soil fining, such surfaces may have been buried and later exhumed, exposing the preserved sand-sized grains to the wind and allowing them to become source of sand for the dunes. Thus, although unlikely, impact gardening cannot be completely ruled out as a source of Martian dune sand.

[140] Measurements of volcanic ash from phreatomagmatic eruptions of the Kilauea volcano show a broad distribution of particle sizes [*Gooding*, 1982], indicating that this is one possible source of coarse sand. *Edgett and Lancaster* [1993] have proposed that Martian dune sand could be created by the fluvial erosion of lava flows or by the aeolian reworking of pyroclastic materials. Recent studies of MOC narrow-angle images have revealed structures morphologically similar to rootless cones, volcanic structures found in Iceland that are produced by the explosive interaction of lava with ground water [*Lanagan et al.*, 2001]. Such eruptions produce beds of glassy ash and scoria that could easily be a source of the coarse basaltic grains such as those in the Proctor Crater dunes. Phreatomagmatic eruptions may in fact be (or have been) prevalent on Mars, although the extent of the material they would have produced is at this time unquantifiable. *Williams et al.* [2003] have identified a feature in the central pit on the floor of Proctor Crater that they interpret as a cinder cone, although more investigation is required to confirm this discovery. Given that loose volcaniclastic material may be abundant on the Martian surface, and that its composition can be similar to that of the Proctor Crater dune sand, volcaniclastic material cannot be ruled out as a sand source.

[141] Meteoritic material may also be considered as a potential source of dune sand. *Flynn and McKay* [1990] calculated that, given the mass influx of meteorites to Mars and their chance of surviving entry into the atmosphere without being melted or vaporized, the meteoritic component of 60–1200 μm particles in the Martian soil is expected to be between 2 and 29% by mass. However, the basalt-like composition of the Proctor Crater dunes is inconsistent with most meteoritic material. The dominance of the surface type 1 material in the dune field suggests that other materials are only present in trace quantities. Furthermore, it is likely that any sand-sized meteoritic particles in the Martian soils are too fragile to withstand sustained saltation (see Figure 3 of *Flynn and McKay* [1990]), and thus fragment into smaller grains before they reach the large dune fields. Thus we consider meteoritic material to be an unlikely sand source for the Proctor Crater dunes.

[142] Of the three source materials considered (impact ejecta, volcaniclastic grains, and meteoric material), only meteoric material may be ruled out based on compositional differences. Alternate grain sources, such as dust aggregates [*Greeley*, 1979], may be ruled out on a compositional basis. It is possible that dune material may have multiple sources, particularly if it has traveled a great distance from its source. It is possible that a sand transport path may cross various sources, each of which adds to the saltating material as it progresses downwind. Thus the most likely source, volcaniclastic grains, and the potential secondary source, impact ejecta, may both be responsible for various accumulations of basaltic sand on Mars, although to what extent each process plays a role in Martian aeolian history remains to be determined.

[143] Regardless of the source of sand, its presence in craters in the southern highlands indicates that a large quantity of basalt sand was available for transport, possibly in a single event, and that it was subsequently redistributed by the wind into dunes now trapped on crater floors.

5.6. Sand Transport Pathways

[144] Proctor Crater is located in the southern midlatitudes, a zone in which the surface gradually transitions from a strongly basaltic signature to the north, to a type 2 surface to the south [*Bandfield*, 2002]. *Bandfield* [2002] also points out that TES spectra only sample surficial, particulate materials and that this latitudinal compositional transition does not appear to have distinctive boundaries. The zonal shift may well be caused by a regional sorting of sand grains by the wind, potentially from midlatitude westerlies that produce the primary slip faces in the Proctor Crater dune field. Compositional sorting of sand by the wind has been studied in terrestrial basaltic dunes by *Bandfield et al.* [2002] and, as discussed above, proposed in dune fields on Mars by *Wyatt et al.* [2001]. The lack of evidence for sand of surface type 2 in Proctor Crater implies that, if there is any such material in this particular region of the compositional transition, it is most likely obscured by dust deposits. However, sand with spectra consistent with basaltic material dominates the dune field and much of the floor of Proctor Crater, indicating that no such mantling has occurred on the surface type 1 sand.

[145] Transport pathways for basaltic sand outside Proctor Crater, if they ever existed, have been since buried, eroded away, or both. In this situation, compositional information is not very useful in locating sand sources or transport pathways, save for providing the information that they are not easily discernable at the surface. It is possible that the western pit is the source of the basalt-like sand that now comprises the dune field. The presence of sand accumulations interpreted as dark falling dunes on east facing cliffs within the western pit (i.e., see Figure 3e), as well as the large swath of eroded bright bed forms southwest of the dark dunes (see Figure 3d), suggests that the sand originated from the southwest, and possibly from beyond the western rim of Proctor Crater. Several other craters in Noachis Terra also have large dune fields (e.g., Rabe and Kaiser Craters), and not all of these have pits that could have supplied such a quantity of dark sand. Since transport pathways in the vicinity of Proctor Crater are not apparent, it may be necessary to search for them on a larger scale.

5.7. Dune Field

[146] If the dune sand originated outside the crater, then it was most likely west-southwest winds that carried it in, leaving behind falling dunes and eroded bright dune forms as the remnants of an ancient transport path. Inside the crater, however, dune morphology suggests that the wind regime changes, producing a convergent airflow that traps the sand quite effectively. Topographic effects of the crater wall could produce this effect. The wind regime in Proctor Crater suggests that all of the intracrater dune fields in the southern highlands of Mars are features trapped, not by topography alone, but by convergent local winds that are influenced by topography.

[147] As sand accumulated in the dune field, a mound of sand in the center of the dune field grew to its current height of 50 m, with large dunes superimposed on top. This deposit indicates a long history of sand accumulation, and it is likely to contain interfingered dust deposits. The dune field location has probably not changed much since the dunes first accumulated, although slight deviations to the north and east have occurred as the dune-forming winds varied in strength relative to one another. The large dunes take the form of reversing and star dunes, consistent with a converging wind regime.

[148] The presence of barchans at the edge of the dune field indicates that the dunes, when last moved, were left in a state of disequilibrium with their environment. This could mean that the dune field has yet to reach its final resting location. A more likely conclusion is that the dune field is mostly in a state of equilibrium, and that these barchans at the edges of the dune field reflect small variations in relative wind strengths over the course of several centuries or perhaps millennia. Such barchans are typical of dune field perimeters on Earth, and they tend to be more mobile than the larger interior dunes because they contain less material. Thus they probably reflect more recent winds.

[149] The large dark dunes do not contain smaller superimposed secondary dunes as terrestrial dunes of this size do (i.e., they are simple dunes). This effect is not caused by the erosion of previously formed secondary dunes, because the dunes are still at least partially active and they should be continuously forming smaller dunes. However, slip face avalanches appear to flow down the entire slip face of either side of the large dune ridges. The reason for this difference between Martian and terrestrial dunes may be related to different atmospheric conditions between the two planets, or by some influence of trapped volatiles on Martian dune morphology.

[150] Parts of the dark dunes are clearly active today. Slip face adjustments that change in position from year to year are present, indicating that continual avalanching occurs. However, *Williams et al.* [2003] found no observable movement of dunes within a 2 year span during the Mars Global Surveyor mission. Because the dunes are influenced by winds from opposing directions, they will probably not migrate in any direction, but instead they will likely fluctuate around a mean position, with the amplitude of each fluctuation depending on the relative strengths of the winds in a particular year. The Kelso Dunes in the Mojave

Desert of California move in this fashion [*Sharp*, 1966]. In a few places on the dunes, slope adjustments take the form of small narrow landslides that are not erased by subsequent slope activity. The fact that these avalanche scars retain their form indicates that the underlying sand in these locations is at least somewhat indurated.

[151] The dune field displays a uniform and repeatable decrease in thermal inertia from north to south that is interpreted to be a real physical phenomenon. It is not caused by a shift in percentage of interdune flats or by any observable change in dune cementation. It may reflect a change in grain size, indicating a decrease in grain size to the south. However, the primary wind blows from the WSW, and logically this wind should preferentially blow finer particles northward. Nevertheless, the wind regime is complex, and an expected particle size distribution is therefore difficult to predict. Only a higher spatial resolution data set, and perhaps in situ measurements, will resolve whether or not it is grain size changes that cause this shift in thermal inertia.

[152] The observed wind pattern of all the aeolian features indicates that three main winds influence the floor of Proctor Crater. Dune slip faces indicate three formative winds. The primary wind blows from the WSW, and this is the wind originally responsible for transporting sand to the center of the crater floor. Slip faces oriented to this wind occur throughout the dark dune field. Both bright bed forms and dust devil tracks are aligned with this wind, indicating that this wind has blown since before the dark sand arrived and that it still blows today. Dust devil tracks are produced by spring and summer early afternoon winds, but these winds are most likely too light to produce movement on the dune slip faces. A secondary wind blows from the ESE. This wind is represented by slip faces throughout all but the easternmost portions of the dune field. A subset of the bed forms is oriented to this wind, indicating that these winds, like the primary winds, must blow strong enough to produce granule ripples. A tertiary wind blows from the ENE, but corresponding slip faces in the dunes only occur in the eastern portion of the dune field. Some sand movements in the center of the dune field may be formed by this wind, although the dune slopes here are not obviously slip faces. Dust devils tracks are not aligned with this wind, but some of the bright dune forms may be.

5.8. Erosion and Deposition on the Crater Floor

[153] One region of the crater, to the northeast of the dark dune field, is unique in several respects. The single MOC narrow-angle image of this area shows a surface devoid of boulders and bright dune forms, which is an unusual characteristic of the Proctor Crater floor. It is also the location of the only summertime image that does not contain dust devil tracks. This region has a thermal inertia typical of indurated materials and a composition with a moderate basalt signature. This area is probably a windy zone, such that dust deposits, bright dune forms, and even boulders do not remain. The boulders, which are created from impact into the sedimentary deposits filling the crater, may withstand ejection upon impact but erode away under the persistent action of the wind. This area may be subject to strong slope winds, perhaps even the same tertiary winds from the ENE that influence the eastern portion of the dune field.

[154] There is an indistinct thermal inertia and compositional border along northwest and southern edge of the crater floor that could be produced by a number of processes. It may be that this area is more sheltered from wind relative to the rest of the crater floor, where either fewer dust devils pass by or winds are not strong enough to saltate sand that would scour away seasonal dust fallout. Alternatively, the poorly defined change in long wave emissivity may be caused by surface features that preferentially retain dust, for example, by a surface texture that impedes the erosive effect of the wind.

[155] We propose that the moderate to low emissivities around the dune field indicate a lack of accumulated dust, and that they may indicate the presence of a material with spectra consistent with basaltic material in the crater floor. Thus the crater floor materials are potentially some combination of basalt-like grains plus fines that have become indurated over time.

5.9. Ephemeral Features

[156] The remainder of the geomorphic sequence of Proctor Crater includes seasonal features such as frost and dust accumulations. Dark dust devil tracks develop during the spring and summer, indicating that prior to this season some amount of dust has accumulated on the surface since the previous summer season. In the springtime tracks are most prevalent over dark sand, where the surface warms enough to produce dust devils. As the summer approaches the tracks expand to include most of the rest of the crater floor. Dust devil tracks change little during the summer season, indicating that few are erased over the summer, and thus little sand is present beyond the edge of the dark dune field that might otherwise saltate under strong winds and erase the tracks by removing nearby dust.

[157] Frost forms on dunes at $L_s = 50°$ (mid fall) and sublimates away completely by $L_s = 165°$ (late winter). At night, CO_2 and H_2O frost forms, but during the day, only the H_2O frost remains. The sun-facing slopes quickly lose their frost as spring approaches, but the pole-facing slopes retain frost for a much longer time. On these south facing slopes the frosts form dark spots as they slowly sublimate away. These spots persist in location from year to year, and they form lineations that may parallel exposed bedding structures from within the dunes. The largest sublimation spots have bright cores, which may simply be reaccumulated ice. Sintering potentially leads to increased transparency along bedding plains, which is one possible explanation for the coherent spacing of the dark spots.

6. Conclusions

[158] The sedimentary history of Proctor Crater is one of a complex interaction of accumulating and eroding sediments. This history began with the eventual accumulation of ~450 m of potentially aeolian material that has subsequently been indurated, impacted, eroded, and possibly reworked into bright dune forms. The sand in the dark dune field is but the most recent set of sediments to accumulate in the crater. All aeolian features indicate a very stable wind regime through-

out the observable aeolian history, which is reflected both in old and stabilized bright dune forms and in recent seasonal dust and frost accumulations. Thus from its earliest history onward, aeolian processes have played an important role in the story of Proctor Crater.

[159] **Acknowledgments.** I thank several people who made invaluable contributions to this paper. Trent Hare and Shane Byrne provided technical expertise with image processing and using ArcView and IDL. Anton Ivanov aided in assembling MOLA data. Junjun Liu provided optical depth calculations. In addition, Arden Albee, Mark Richardson, Andy Ingersoll, Jeff Plescia, Mike Mellon, Matt Golombek, Bruce Murray, and Shane Byrne aided with constructive discussions regarding the manuscript and various parts of the analysis. Thanks also to Ken Edgett and an anonymous reviewer for their perceptive and much needed suggestions. This work was supported by grants from the NASA MDAP and PG&G programs.

References

Arvidson, R. E., Wind-blown streaks, splotches, and associated craters on Mars: Statistical analysis of Mariner 9 photographs, *Icarus*, *21*, 12–27, 1974.

Bandfield, J. L., Isolation and characterization of Martian atmospheric constituents and surface lithologies using thermal infrared spectroscopy, Ph.D. thesis, 213 pp., Ariz. State Univ., Tempe, 2000.

Bandfield, J. L., Global mineral distributions on Mars, *J. Geophys. Res.*, *107*(E6), 5042, doi:10.1029/2001JE001510, 2002.

Bandfield, J. L., and M. D. Smith, Multiple emission angle surface-atmosphere separations of Thermal Emission Spectrometer data, *Icarus*, *161*, 47–65, 2003.

Bandfield, J. L., V. E. Hamilton, and P. R. Christensen, A global view of Martian surface compositions from MGS-TES, *Science*, *287*, 1626–1630, 2000.

Bandfield, J. L., K. S. Edgett, and P. R. Christensen, Spectroscopic study of the Moses Lake dune field, Washington: Determination of compositional distributions and source lithologies, *J. Geophys. Res.*, *107*(E11), 5092, doi:10.1029/2000JE001469, 2002.

Bell, J. F., III, P. C. Thomas, M. J. Wolff, S. W. Lee, and P. B. James, Mineralogy of the Martian north polar sand sea from 1995 Hubble Space Telescope near-IR observations, *Lunar Planet. Sci.*, *XXVIII*, abstract 1757, 1996.

Blount, G., M. O. Smith, J. B. Adams, R. Greeley, and P. R. Christensen, Regional aeolian dynamics and sand mixing in the Gran Desierto: Evidence from Landsat thematic mapper images, *J. Geophys. Res.*, *95*, 15,463–15,482, 1990.

Breed, C. S., Terrestrial analogs of the Helluspontus dunes, Mars, *Icarus*, *30*, 326–340, 1977.

Breed, C. S., and T. Grow, Morphology and distribution of dunes in sand seas observed by remote sensing, *U.S. Geol. Surv. Prof. Pap.*, *1052*, 253–304, 1979.

Breed, C. S., M. J. Grolier, and J. F. McCauley, Morphology and distribution of common "sand" dunes on Mars: Comparison with the Earth, *J. Geophys. Res.*, *84*, 8183–8204, 1979.

Bridges, N. T., K. E. Herkenhoff, T. N. Titus, and H. H. Kieffer, Ephemeral dark spots associated with Martian gullies, *Lunar Planet. Sci.* [CD-ROM], *XXXII*, abstract 2126, 2001.

Calkin, P. E., and R. H. Rutford, The sand dunes of Victoria Valley, Antarctica, *Geogr. Rev.*, *64*, 189–216, 1974.

Christensen, P. R., Eolian intracrater deposits on Mars: Physical properties and global distribution, *Icarus*, *56*, 496–518, 1983.

Christensen, P. R., J. L. Bandfield, M. D. Smith, V. E. Hamilton, and R. N. Clark, Identification of a basaltic component on the Martian surface from Thermal Emission Spectrometer data, *J. Geophys. Res.*, *105*, 9609–9621, 2000a.

Christensen, P. R., et al., Detection of crystalline hematite mineralization on Mars by the Thermal Emission Spectrometer: Evidence for near-surface water, *J. Geophys. Res.*, *105*, 9623–9642, 2000b.

Clark, R. N., T. Hoefen, and J. Moore, Martian olivine global distribution and stratification using spectral feature mapping of Mars Global Surveyor Thermal Emission Spectrometer data, paper presented at the DPS Birmingham Meeting, Am. Astron. Soc., Birmingham, U. K., abstract 3.06, 6–11 Oct. 2002.

Cutts, J. A., and R. S. U. Smith, Eolian deposits and dunes on Mars, *J. Geophys. Res.*, *78*, 4139–4154, 1973.

de Vaucouleurs, G. H., *Physics of the Planet Mars: An Introduction to Aerophysics*, Faber and Faber, New York, 1954.

Edgett, K. S., and P. R. Christensen, The particle size of Martian aeolian dunes, *J. Geophys. Res.*, *96*, 22,765–22,776, 1991.

Edgett, K. S., and P. R. Christensen, Mars aeolian sand: Regional variations among dark-hued crater floor features, *J. Geophys. Res.*, *99*, 1997–2018, 1994.

Edgett, K. S., and N. Lancaster, Volcaniclastic aeolian dunes: Terrestrial examples and application to Martian sands, *J. Arid Environ.*, *25*, 271–297, 1993.

Edgett, K. S., and M. C. Malin, New views of Mars eolian activity, materials, and surface properties: Three vignettes from the Mars Global Surveyor Mars Orbiter Camera, *J. Geophys. Res.*, *105*, 1623–1650, 2000.

Eluszkiewicz, J., On the microphysical state of the Martian seasonal caps, *Icarus*, *103*, 43–48, 1993.

Fenton, L. K., Atmospheric processes on Mars: Atmospheric modeling and GIS analysis, Ph.D. thesis, 215 pp., Calif. Inst. of Technol., Pasadena, 2003.

Fenton, L. K., and M. I. Richardson, Martian surface winds: Insensitivity to orbital changes and implications for aeolian processes, *J. Geophys. Res.*, *106*, 32,885–32,902, 2001.

Flynn, G. J., and D. S. McKay, An assessment of the meteoric contribution to the Martian soil, *J. Geophys. Res.*, *95*, 14,497–14,509, 1990.

Garvin, J. B., J. J. Frawley, S. E. H. Sakimoto, and C. Schnetzler, Global geometric properties of Martian impact craters: An assessment from Mars Orbiter Laser Altimeter (MOLA) digital elevation models, *Lunar Planet. Sci.* [CD-ROM], *XXXI*, abstract 1619, 2000.

Gault, D. E., E. M. Shoemaker, and H. J. Moore, Spray ejected from the lunar surface by meteoroid impact, *Rep. TN D-1767*, 39 pp., NASA, Washington, D. C., 1963.

Gooding, J. L., Petrology of dune sand derived from basalt on the Ka'u Desert, Hawaii, *90*, 97–108, 1982.

Grant, J. A., and P. H. Shultz, Possible tornado-like tracks on Mars, *Science*, *237*, 883–885, 1987.

Greeley, R., Silt-clay aggregates on Mars, *J. Geophys. Res.*, *84*, 6248–6254, 1979.

Greeley, R., and J. D. Iversen, *Wind as a Geological Process on Earth, Mars, Venus and Titan*, Cambridge Univ. Press, New York, 1985.

Greeley, R., A. Skypeck, and J. B. Pollack, Martian aeolian features and deposits: Comparisons with general circulation model results, *J. Geophys. Res.*, *98*, 3183–3196, 1993.

Haberle, R. M., and B. M. Jakosky, Atmospheric effect on the remote determination of thermal inertia on Mars, *Icarus*, *90*, 187–204, 1991.

Hartmann, W. K., J. Anguita, M. A. de la Casa, D. C. Berman, and E. V. Ryan, Martian cratering 7: The role of impact gardening, *Icarus*, *149*, 37–53, 2001.

Herkenhoff, K. E., and A. R. Vasavada, Dark material in the polar layered deposits and dunes on Mars, *J. Geophys. Res.*, *104*, 16,487–16,500, 1999.

Hess, S. L., R. M. Henry, C. B. Leovy, J. A. Ryan, and J. E. Tillman, Meteorological results from the surface of Mars: Viking 1 and 2, *J. Geophys. Res.*, *82*, 4559–4574, 1977.

Hunter, R. E., B. M. Richmond, and T. R. Alpha, Storm-controlled oblique dunes of the Oregon coast, *Geol. Soc. Am. Bull.*, *94*, 1450–1465, 1983.

Jakosky, B. M., M. T. Mellon, H. H. Kieffer, P. R. Christensen, E. S. Varnes, and S. W. Lee, The thermal inertia of Mars from the Mars Global Surveyor Thermal Emission Spectrometer, *J. Geophys. Res.*, *105*, 9643–9652, 2000.

James, P. B., H. H. Kieffer, and D. A. Paige, The seasonal cycle of carbon dioxide on Mars, in *Mars*, pp. 934–968, Univ. of Ariz. Press, Tucson, 1992.

Kieffer, H. H., T. Z. Martin, A. R. Peterfreund, B. M. Jakosky, E. D. Miner, and F. D. Palluconi, Thermal and albedo mapping of Mars during the Viking primary mission, *J. Geophys. Res.*, *82*, 4249–4291, 1977.

Kocurek, G., K. G. Havholm, M. Deynoux, and R. C. Blakey, Amalgamated accumulations resulting from climatic and eustatic changes, Akchar Erg, Maritania, *Sedimentology*, *38*, 751–772, 1991.

Koster, E. A., and J. W. A. Dijkmans, Niveo-aeolian deposits and denivation forms, with special reference to the Great Kobuk Sand Dunes, northwestern Alaska, *Earth Surf. Processes Landforms*, *13*, 153–170, 1988.

Lanagan, P. D., A. S. McEwen, L. P. Keszthelyi, and T. Thordarson, Rootless cones on Mars indicating the presence of shallow equatorial ground ice in recent times, *Geophys. Res. Lett.*, *28*, 2365–2367, 2001.

Lancaster, N., Variations in wind velocity and sand transport rates on the windward flanks of desert sand dunes, *Sedimentology*, *32*, 581–593, 1985.

Lancaster, N., Controls of eolian dune size and spacing, *Geology*, *16*, 972–975, 1988.

Lancaster, N., *The Namib Sand Sea*, A. A., Balkema, Brookfield, Vt., 1989.

Lancaster, N., *Geomorphology of Desert Dunes*, Routledge, New York, 1995.

Lancaster, N., and R. Greeley, Mars: Morphology of southern hemisphere intracrater dune fields, in *Reports of Planetary Geology and Geophysics*

Program, 1986, *Tech. Mem. 89810*, pp. 264–265, NASA, Washington, D. C., 1987.
Lancaster, N., and R. Greeley, Sediment volume in the north polar sand seas of Mars, *J. Geophys. Res.*, *95*, 10,921–10,927, 1990.
Lindsay, J. F., *Lunar Stratigraphy and Sedimentology*, 302 pp., Elsevier Sci., New York, 1976.
Liu, J., M. I. Richardson, and R. J. Wilson, An assessment of the global, seasonal, and interannual spacecraft record of Martian climate in the thermal infrared, *J. Geophys. Res.*, *108*(E8), 5089, doi:10.1029/2002JE001921, 2003.
Mainguet, M., and L. Cossus, Sand circulation in the Sahara: Geomorphological relations between the Sahara Desert and its margins, *Paleoecol. Africa Surrounding Isl. Antarc.*, *12*, 69–78, 1980.
Malin, M. C., and K. S. Edgett, Sedimentary rocks of early Mars, *Science*, *290*, 1927–1937, 2000a.
Malin, M. C., and K. S. Edgett, Frosting and defrosting of Martian polar dunes, *Lunar Planet. Sci.* [CD-ROM], *XXXI*, abstract 1056, 2000b.
Malin, M. C., and K. S. Edgett, Mars Global Surveyor Mars Orbiter Camera: Interplanetary cruise through primary mission, *J. Geophys. Res.*, *106*, 23,429–23,570, 2001.
McCauley, J. F., M. H. Carr, J. A. Cutts, W. K. Hartmann, H. Masursky, D. J. Milton, R. P. Sharp, and D. E. Wilhelms, Preliminary Mariner 9 report on the geology of Mars, *Icarus*, *17*, 289–327, 1972.
McKee, E. D., Introduction to a study of global sand seas, in *A Study of Global Sand Seas*, *U.S. Geol. Surv. Prof. Pap.*, *1052*, 1–19, 1979.
Mellon, M. T., B. M. Jakosky, H. H. Kieffer, and P. R. Christensen, High resolution thermal inertia mapping from the Mars Global Surveyor Thermal Emission Spectrometer, *Icarus*, *148*, 437–455, 2000.
Metzger, S. M., J. R. Carr, J. R. Johnson, M. Lemmon, and T. J. Parker, Sediment flux from dust devils on Mars—Initial calculations, *Lunar Planet. Sci.* [CD-ROM], *XXX*, abstract 2022, 1999.
Noe Dobrea, E. Z., and J. F. Bell III, Composition and mineralogy of the Martian north polar dune deposits: Constraints from TES and HST observations, *Lunar Planet. Sci.* [CD-ROM], *XXXII*, abstract 2099, 2001.
Pelkey, S. M., B. M. Jakosky, and M. T. Mellon, Thermal inertia of crater-related wind streaks on Mars, *J. Geophys. Res.*, *106*, 23,909–23,920, 2001.
Peterson, J. E., Geologic map of the Noachis Quadrangle of Mars, *U.S. Geol. Surv. Misc. Geol. Invest. Map, I-910*, 1977.
Piqueux, S., S. Byrne, and M. I. Richardson, The sublimation of Mars's southern seasonal CO_2 ice cap and the formation of "spiders," *J. Geophys. Res.*, *108*(E8), 5084, doi:10.1029/2002JE002007, 2003.
Porter, M. L., Sedimentary record of erg migration, *Geology*, *14*, 497–500, 1986.
Presley, M. A., and P. R. Christensen, Thermal conductivity measurements of particulate materials: 2. Results, *J. Geophys. Res.*, *102*, 6551–6566, 1997a.
Presley, M. A., and P. R. Christensen, The effect of bulk density and particle size sorting on the thermal conductivity of particulate materials under Martian atmospheric pressures, *J. Geophys. Res.*, *102*, 9221–9229, 1997b.
Ramsey, M. S., P. R. Christensen, N. Lancaster, and D. A. Howard, Identification of sand sources and transport pathways at the Kelso Dunes, California, using thermal infrared remote sensing, *Geol. Soc. Am. Bull.*, *111*, 646–662, 1999.
Rogers, D., J. L. Bandfield, and P. R. Christensen, Identification of small isolated basalt regions in the northern hemisphere of Mars, DPS Pasadena Meeting, Am. Astron. Soc., Pasadena, Calif., abstract 59.04, 23–27 Oct. 2000.
Rubin, D. M., and R. E. Hunter, Bedform climbing in theory and nature, *Sedimentology*, *29*, 121–138, 1982.
Ruff, S. W., P. R. Christensen, R. N. Clark, H. H. Kieffer, M. C. Malin, J. L. Bandfield, B. M. Jakosky, M. D. Lane, M. T. Mellon, and M. A. Presley, Mars' "White Rock" feature lacks evidence of an aqueous origin: Results from Mars Global Surveyor, *J. Geophys. Res.*, *106*, 23,921–23,927, 2001.
Sagan, C., J. Veverka, P. Fox, L. Quam, R. Tucker, J. B. Pollack, and B. A. Smith, Variable features on Mars: Preliminary Mariner 9 television results, *Icarus*, *17*, 346–372, 1972.
Schofield, J. T., J. R. Barnes, D. Crisp, R. M. Haberle, S. Larsen, J. A. Magalhaes, J. R. Murphy, A. Seiff, and G. Wilson, The Mars Pathfinder atmospheric structure investigation/meteorology (ASI/MET) experiment, *Science*, *278*, 1752–1757, 1997.
Sharp, R. P., Wind ripples, *J. Geol*, *71*, 617–636, 1963.
Sharp, R. P., Kelso Dunes, Mojave Desert, California, *Geol. Soc. Am. Bull.*, *77*, 1045–1074, 1966.
Smith, D. E., et al., Mars Orbiter Laser Altimeter: Experiment summary after the first year of global mapping of Mars, *J. Geophys. Res.*, *106*, 23,689–23,722, 2001.
Smith, H. T. U., Aeolian deposition in Martian craters, *Science*, *238*, 72–74, 1972.
Smith, M. D., J. L. Bandfield, and P. R. Christensen, Separation of atmospheric and surface spectral features in Mars Global Surveyor Thermal Emission Spectrometer (TES) spectra, *J. Geophys. Res.*, *105*, 9589–9607, 2000.
Steidtmann, J. R., Ice and snow in eolian sand dunes of southwestern Wyoming, *Science*, *179*, 796–798, 1973.
Sutton, J. L., C. B. Leovy, and J. E. Tillman, Diurnal variations of the Martian surface layer meteorological parameters during the first 45 sols at two Viking lander sites, *J. Atmos. Sci.*, *35*, 2346–2355, 1978.
Thomas, P., Present wind activity on Mars: Relation to large latitudinally zoned sediment deposits, *J. Geophys. Res.*, *87*, 9999–10,008, 1982.
Thomas, P., Martian intracrater splotches: Occurrence, morphology, and colors, *Icarus*, *57*, 205–227, 1984.
Thomas, P., and J. Veverka, Red/violet contrast reversal on Mars: Significance for eolian sediments, *Icarus*, *66*, 39–55, 1986.
Ward, A. W., K. B. Doyle, P. J. Helm, M. K. Weisman, and N. E. Witbeck, Global map of eolian features on Mars, *J. Geophys. Res.*, *90*, 2038–2056, 1985.
Wasson, R. J., and R. Hyde, Factors determining desert dune type, *Nature*, *304*, 337–339, 1983.
Williams, K. K., R. Greeley, and J. R. Zimbelman, Using overlapping MOC images to search for dune movement and to measure dune heights, *Lunar Planet. Sci.* [CD-ROM], *XXXIV*, abstract 1639, 2003.
Williams, S. H., J. R. Zimbelman, and A. W. Ward, Large ripples on Earth and Mars, *Lunar Planet. Sci.* [CD-ROM], *XXXIII*, abstract 1508, 2002.
Wilson, I. G., Desert sandflow basins and a model for the development of ergs, *Geogr. J.*, *137*, 180–199, 1971.
Wilson, I. G., Aeolian bedforms—Their development and origins, *Sedimentology*, *19*, 173–210, 1972.
Wilson, I. G., Ergs, *Sediment. Geol.*, *10*, 77–106, 1973.
Wyatt, M. B., and H. Y. McSween Jr., Spectral evidence for weathered basalt as an alternative to andesite in the northern lowlands of Mars, *Nature*, *417*, 263–266, 2002.
Wyatt, M. B., J. L. Bandfield, H. Y. McSween Jr., and P. R. Christensen, Compositions of low albedo intracrater materials and wind streaks on Mars: Examination of MGS TES data in western Arabia Terra, *Lunar Planet. Sci.* [CD-ROM], *XXXII*, abstract 1872, 2001.
Zimbleman, J. R., and S. Wilson, Ripples and dunes in the Syrtis Major region of Mars, as revealed in MOC images, *Lunar Planet. Sci.* [CD-ROM], *XXXIII*, abstract 1514, 2002.
Zimbleman, J. R., S. H. Williams, and V. P. Tchakerian, Sand transport paths in the Mojave desert, southwestern United States, in *Desert Aeolian Processes*, edited by V. P. Tchakerian, pp. 101–130, Chapman and Hall, New York, 1995.
Zurek, R. W., J. R. Barnes, R. M. Haberle, J. B. Pollock, J. E. Tillman, and C. B. Leovy, Dynamics of the atmosphere of Mars, in *Mars*, pp. 835–933, Univ. of Ariz. Press, Tucson, 1992.

J. L. Bandfield and L. K. Fenton, Department of Geological Sciences, Arizona State University, Mail Code 1404, Tempe, AZ 85287, USA. (joshband@imap3.asu.edu; lkfenton@asu.edu)

A. W. Ward, Astrogeology Branch, U.S. Geological Survey, 2255 North Gemini Drive, Flagstaff, AZ 86001, USA. (wward@usgs.gov)